UNIVERSITY OF OKLAHOMA

GRADUATE COLLEGE

UNDERSTANDING THE SEISMIC RESPONSE OF SINGLE HELICAL PILES IN DRY SANDS USING A LARGE-SCALE SHAKE TABLE TEST

A THESIS

SUBMITTED TO THE GRADUATE FACULTY

in partial fulfillment of the requirements for the

Degree of

MASTER OF SCIENCE

By

TATIANA MELISSA VARGAS CASTILLA
Norman, Oklahoma
2017

UNDERSTANDING THE SEISMIC RESPONSE OF SINGLE HELICAL PILES IN DRY SANDS USING A LARGE-SCALE SHAKE TABLE TEST

A THESIS APPROVED FOR THE
SCHOOL OF CIVIL ENGINEERING AND ENVIRONMENTAL SCIENCE

BY

_____
Dr. Amy B. Cerato, Chair

_____
Dr. Gerald A. Miller

_____
Dr. Kanthasamy K. Muraleetharan

TABLE OF CONTENTS

LIST OF TABLES

LIST OF FIGURES

ABSTRACT

Helical piles are deep foundations composed by a steel shaft and single or multiple helical plates welded at their tip or throughout their lead section, respectively, which allows them to be screwed into the ground during installation, producing minimum vibration and fewer soil disturbance compared with other type of deep foundations; moreover, their helixes provide extra resistance or bearing capacity to the piles, enhancing their uplift and compression behaviors. This type of pier has been widely implemented in seismically active areas of New Zealand. Nevertheless the use of screw anchors is restricted to non-earthquake prone areas within the United States territory, mainly due to the lack of a quantitative prof that demonstrates their performance under earthquake loadings or even more, that compares their seismic performance with other types of foundations. According to the United States Geological Survey statistics, the number of earthquakes within the US territory is increasing. Moreover the Federal Emergency Management Agency reported that the US annualized earthquake loss was $5.3 billion in 2008. A demand is then posed to improve current foundations' resilience or dynamic performance and to propose other alternatives to mitigate future earthquake damages. This research aims to determine the dynamic response of helical piles embedded in dry sand subjected to lateral seismic loadings using the largest U.S. shake table located at the University of California-San Diego. Furthermore, it attempts to identify the difference between the performance of a helical pile and an equivalent driven pile under earthquake events, in addition to quantifing the influence of the number of helices and shaft geometry on the overall seismic resistance of the helical pile. To that end, two full-scale tests were conducted in eight single helical piles (four with 5.5" outside diameter (O.D.) and four

3.5” O.D.), one double helical pile with 3.5” O.D. and one 3.5” O.D. driven pile, embedded in dense, dry sand up to a depth of 11 feet. Each pier was instrumented with strain gages throughout its shaft length to calculate bending moments and axial loading. Moreover the sand bed, laminar box and pile heads were instrumented with accelerometers. Two conditions were evaluated: piles with free head and piles supporting inertial weights on top, for each stage, two major earthquakes were replicated: the Takatori-Kobe of 1995 and the Northridge 1994, under 100%, 75% and 50% amplitudes. During each shake, videos and photos were taken to register the soil-pile interaction and a DCP test was conducted on the sand bed before and after shaking. The results show that the dynamic performance of the piles was primarily influenced by their natural frequency. For the frequency range tested (0.5 to 5 Hz) and up to a peak acceleration of 0.67g, it was found that the single helical pile presented a stiffer behavior compared with the double helical pile, which may be attributed to the higher soil disturbance produced during the installation of the double helical pile. In addition, under ground motions characterized by a low frequency content (up to 1.5 Hz), the square-shaft helical pile outperformed the response of the circular-shaft helical pile for all the accelerations tested. Finally, under seismic conditions, a hysteretic reduction of the damping response of single helical piles with respect to the depth of the soil was observed.

1. INTRODUCTION

Helical piles are deep foundations that are composed of a slender steel shaft and single or multiple plates welded throughout their lead section, typically at a spacing of three times the diameter of the lower helix plates and at a three- or six-inch pitch. Helical piles are screwed into the soil with a hydraulic torque motor and the plates help pull the pile into the ground. This installation method produces smaller vibrations and noises than other types of installation methods such as driving, making helical piles ideal for tight-quarter construction sites found in urban settings. Additionally, the bearing plates of this type of pile provide both compressive and tensile capacity and this pile capacity can be directly correlated to the installation torque through a torque correlation factor, K_t.

Alexander Mitchell invented the first screw anchor in 1833, and the first installation was executed by hand in 1836. By 1900, over 160 United States patents were established for different helical pile designs and installation methods, but most of them were implemented in the construction of lighthouses. Currently, helical piles are used in the United States in a wide range of applications due to their versatility. They are used with high-tension guyed anchor wires, pipeline anchors, transmission tower foundations and light to moderate residential and commercial construction. Most recently they have started to be used in multi-story, urban tower projects when tight quarters are encountered. Helical piles are also widely used to retrofit existing buildings and to build new structures in seismic active areas of New Zealand, where it has been anecdotally observed that helical piles provide superior resistance than other types of deep

foundations under seismic events. For example, after the 2011 Christchurch earthquake, all buildings located at the epicenter of this 6.3 Magnitude event that were founded on helical piers exhibited only minimal structural damage (Wood, 2015). Some of the nearby buildings in this area of downtown Christchurch that used other types of foundations, however, were structurally condemned; in one instance collapsing and killing 115 people, which represented 60% of the earthquake's total fatalities (New Zealand Police , 2012). However, a direct comparison between the performance of the buildings supported on helical piles and the buildings that implemented other types of deep foundations can not be made as other factors may have affected their performance (i.e. age of the building, building type, etc).

While helical piles are used throughout Japan and New Zealand, their use in seismic areas within the United States remains somewhat limited, the lack of overall acceptance of helical piles in seismically active zones by local building officials, is most likely due to a lack of quantitative data that demonstrates their damping characteristics and seismic performance, or a report that provides a direct comparison between their performance with the performance of other types of deep foundations during an earthquake event. The available data regarding their behavior is limited and could be attributed to differential behavior of foudnations. For instance, six years after the Northridge earthquake of 1994 (6.7 Mw), Perko (2009) reported that Rupiper (a California registered engineer) conducted assessments of different structures supported on helical piles. One of his findings was that a three-bedroom residence partially repaired with helical piles exhibited great damage, including concrete-cracks up to 2 inch, on the portion that was supported

with a slab-on-grade foundation, which was located on the left side of the front door. The area supported on helical piles, however, resisted the earthquake without any apparent damage (Perko H. , 2009).

In April of 2008, the Federal Emergency Management Agency (FEMA) 366 report stated that the United States annualized earthquake loss was $5.3 billion per year. This magnitude of monetary loss, as well as the increasing number and frequency of earthquakes throughout the state of Oklahoma, for example, is now generating a demand to evaluate and understand the resilience and damping characteristics of different types of foundations. The number of foundations and structures that require seismic retrofitting after earthquake events is also increasing, making it necessary to implement a foundation system that preserves the integrity of current structures. Quantifying the performance of helical piles under seismic loading represents a first step in the search for a solution to lessen and mitigate earthquake damage. The available qualitative data suggest that helical screws have high resistance under lateral and vertical dynamic loading because they tend to provide a ductile response. However, a quantitative study that truly simulates a seismic event has never been conducted.

The proposed research aims to determine the full-scale performance of helical piles under lateral dynamic loading generated in two major earthquakes: the 1994 Northridge and the 1995 Great Hanshin Earthquakes. To achieve this research objective, a test was planned to replicate these earthquakes at 50%, 75%, and 100% of their amplitudes. Each of these tests was conducted on ten piles with two different diameters and yield stresses (f_y): 3.5”

x 0.25" wall thickness (f_y=65 ksi) and 5.5" x 0.45" wall thickness (f_y=85 ksi). There were ten piles, divided as follows: six single helix pipe piles with a length of twelve feet (two piles with an f_y=65 ksi and four piles with a f_y=85 ksi) and one with a length of thirteen feet (f_y=65 ksi), a twelve foot double helix pipe pile (f_y=65 ksi), a twelve foot driven pipe pile (f_y=65 ksi), and a twelve foot hollow square section (HSS) tube single helix pile (f_y=65 ksi), all embedded in dense dry sand and under two different conditions: free head and free head with inertial vertical weights. The installation was conducted in the large scale laminar soil box on the shaking table located at the University of California-San Diego, where the piles were fully instrumented with strain gages to calculate bending moments and axial stresses. Accelerometers were installed on the pile heads, on the laminar box and throughout the sand bed to measure the accelerations during each shake and string potentiometers were utilized on the laminar box to measure deflections.

The analysis and conclusions of this research will help determine the seismic performance of helical piles in dense sand and quantify the contribution of the helix and shaft geometry to the overall seismic capacity of the piles. The report and findings of this research will allow engineers to incorporate design parameters or restrictions into the International Building Code (IBC) regarding the use of helical piles in seismic design categories D, E, and F, soil site classes D (stiff soil), and to ensure the correct use and implementation of this type of foundation in seismically active areas. Finally, this research will quantitatively evaluate helical piles for use within seismic prone areas which may provide solutions to lessen and mitigate earthquake damage.

1.1. OBJECTIVES AND SCOPE OF RESEARCH

The research goal is to advance the understanding of helical piles as capable foundation systems for retrofitting and supporting new construction within seismically active areas. The data generated through this project will provide quantitative information to guide future research in the calibration of finite element models for use in helical piles' seismic design.

The objectives of this research are to:

1. Quantify the influence of the number of helices on a helical piles' dynamic lateral resistance.

2 Characterize and compare different helical anchor geometries under seismic activities.

3. Report and document the general performance of single helical piles in dense sand subjected to two major earthquakes events (Takatori and Northridge).

4. Create a database that would allow future predictions of the behavior of helical piles with different helix configurations, shaft sizes and shapes geometries.

To meet the objectives of the study, the scope of the research encompasses:

2. Plan and perform large-scale shake table testing of ten helical piles at the University of California – San Diego's Englekirk Structural Research Lab - the largest outdoor shake table in the world.

3. Collect, organize and analyze the data from Testing Day 3 – Single Helical Piles with Inertial Weights. This includes writing a MatLab program to generate p-y curves using several curve-fitting methods for analysis.
4. Make quantitative observations about the seismic behavior of the single helical piles under inertial loads.

2. LITERATURE REVIEW

Piles are classified according to their material (concrete, steel, etc.) and installation method (boring, driving, jetting or screwed), and are generally designed to transmit surface loads from the structure to competent soil layers. The structures' pending movement observed during earthquakes is characterized by the propagation of dynamic waves from the crust to the foundation to the superstructure. During an earthquake, it has been found that seismic forces are mainly horizontal in nature (El Naggar et. al., 2007), and thus a pile must be designed to handle large transient lateral loads. Consequently, most of the research that has attempted to quantify the seismic behavior of driven steel piles focused on the lateral dynamic component. The performance of helical piles subjected to lateral dynamic loads has not been completely quantified, and the number of studies remains limited. Therefore, any conclusions regarding their slenderness, alleged high damping ratios, ductility, and seismic-resistant behavior remain largely anecdotal.

2.1. Pile installation: methods and associated effects

The available installation methods for piles range from boring to jacking or jetting to driving and drilling and can significantly affect pile behavior. Two main methods of pile installation were employed during the testing procedures, including driving and screwing and previous research utilizing the two methods will be described in this section. The pile driving method increases the density of the surrounding loose non-cohesive soil layers and this results in an increase of the end-bearing capacity and sometimes skin friction,

especially when installed in groups. However, in cohesive soils such as clays, the increase in pore water pressure causes a decrease in effective stress. As the pore pressure dissipates with time, the effective stress increases and therefore the bearing capacity of the pile would increase with time. Moreover, the final strength can exceed the initial undisturbed shear strength of the soil. On the other hand, the installation of screw piles disturbs the soil by the passage of the helices, which displaces the soil laterally and vertically, and the helices shear the surrounding soil layers. The shaft resistance and pile behavior is affected by the installation method and conditioned by the resulting soil-pile interaction as explained in the following sections.

2.1.1. Driven installation method

Driven piles are relatively long slender columns designed to provide support or to resist forces. Their installation could be conducted by impact hammering, vibrating or pushing into the earth. Installation conducted through impacts on the pile's head using a hammer can be executed using a drop hammer, a single or double acting hammer, a hydraulic hammer, air hammers, or a diesel hammer (Abdelghany Y. , 2008). The driven equipment should be selected according to the required number of hammer blows per inch at the ultimate pile capacity and the pile driving stresses. A helmet is often incorporated in a system that uses impact hammers to distribute each blow uniformly to the pile head. During installation, the pile is driven to the required ultimate pile capacity or a specified tip elevation. As the subsurface conditions may not be uniform, piles could either be cut-off or spliced to modify their lengths in accordance with the requirements of the terrain.

Furthermore, in cases where driving the pile will displace the upper soil enough to push adjoining piles or if the project requires limiting vibration in the upper layers, it may be necessary to use a continuous flight auger to predill or to use a wet rotary bit to remove soil.

Inspection of hollow-section driven piles could be conducted minutes after installation or through dynamic inspection when the pile is comprised of a solid-section. The main problems faced during installation are damage of the pile head (if the hammer cushion used is built of a non-durable material) and buckling. Generally, for steel piles, compressive driving stresses shall not exceed 90 percent of the yield point of the pile material. Additionally, it is known that driving a pile into the ground can potentially generate large stresses and deformations in the nearby soil, especially for cohesive clay soils, where excess pore water pressure is generated during installation. Nonetheless, pore water pressure eventually dissipates and a local consolidation is seen. Even more, the strength and stiffness of the soil increases after the installation (Holmquist & Matlock, 1976). In stiff clays, it has been reported that the propagation of stress waves during driving produces a vibration of the shaft that reduces the contact on the soil-pile interface, which leads to the formation of gaps, reducing any skin friction throughout the length of the gap. Therefore the factor of safety should account for this installation disturbance (Swan, 2016; O'Neill, 2001; Barnes, 2010). But in cohesionless soils, driving of high-displacement piles produces larger compressive stresses and generates large lateral effective stresses due to shearing and dilatation on very dense soils, which would partially be reduced over time due to the viscoelastic nature of the soils (Swan, 2016).

2.1.2. Screwing installation method

The installation of screw piles and anchors is conducted through the application of torque on the pile's head using a hydraulic torque motor attached to machinery such as an excavator, backhoe, fork lift, front-end loader, skid-steer loader, derrick truck or bobcat. The selection of the installation equipment should account for the torque requirements of any particular project, as overstressing a pile could result in its damage and underestimating the torque may result in a failure to complete the installation or can produce large soil disturbance. At the beginning of the pile installation, a small downward (crowd) force is generally applied to the pile head, to advance the lead helix into the ground. This crowd force may also be applied during installation to control the penetration rate at a pitch size per revolution (Perko H. , 2009). Nevertheless, the crowd force is not measured during installation, whereas the installation torque is always measured using either a mechanical gauge or an electronic torque transducer. The measured torque at the end of installation is correlated to the pile axial capacity through a proportional relationship (Hoyt and Clemence, 1989; Narasimha Rao et al., 1989; Ghaly & Hanna, 1991; Perko, 2000; 2009; Canadian Foundation Engineering Manual 2006; Tsuha & Aoki, 2010; Sakr, 2014). Different correlation methodologies have been proposed to predict the axial capacity of helical piles using installation torque readings. However, none of them account for the effects of the disturbances associated with the installation method such as predrilling and auguring effects. Some correlation methods do not consider soil profile characteristics or variations of soil properties throughout the length of embedment, (Sakr, 2014). Furthermore, the method proposed by Perko (2009)

requires a parameter, crowd force, that is not usually measured during installation. More research is needed to determine the influence of the installation method and soil disturbance effects on the correlation between installation torque and axial pile capacity in order to incorporate them into general construction practices.

The installation torque is a function of a wide range of parameters: soil properties (frictional resistance angle of the soil, interface pile-soil angle, relative density, effective unit weight of soil, characteristics of the soil particles), ground water level, loading path, helix configuration and geometry, shape and geometry of pile shaft, surface roughness of pile material, method used for helical pile manufacturing, method of installation and reliability of torque measurement (Sakr, 2014). For example, the presence of large-size gravel requires a higher installation torque, while the presence of boulders indicates that the installation of helical piles should be stopped in order to prevent pile or equipment damage. Full-scale and small-scale tests conducted on helical piles embedded in cohesionless soils reported that the installation torque increases as the pile diameter or helical plate diameter increases and it was also concluded that a single helix pile required a higher installation torque than a double helical pile to have the same capacity (Tsuha et al., 2013; Tsuha & Aoki, 2010; Komatsu, 2007; Ghaly and Hanna, 1991). Previous research assessed the effect of the water table level in the installation and performance of full-scale helical piles and concluded that the torque correlation design must consider the worst case long term ground water conditions in order to properly design piles subjected to dynamic loadings (Victor & Cerato, 2008).

The acceptance criteria to determine the ultimate static axial capacity of screw anchors is determined with the torque correlation factor (K_t) according to the AC-358 and is defined by the following equation:

$$Q = K_t * T$$

Equation 1. Torque correlation factor

Where:

K_t= torque correlation factor empirically developed, which ranges from 2 ft^{-1} to 13ft^{-1} typically

T= Final installation torque

Q= Ultimate axial capacity

While a helical plate is screwed into the ground, it produces a movement of the soil, or disturbance, from the lower edge to the upper edge of the plate (Kanai, 2007). Previous research conducted on small-scale helical piles focused on characterizing the installation effects of this type of foundation embedded in both sandy and clayey soils. It was concluded that the soil layers surrounding the pile shaft are displaced downwards due to the pile friction, while the soil above the pile's helix rises upwards and the soil beneath the helix is compressed (Komatsu, 2007).. Moreover, during the installation of small-scale helical piles in dry sand, the soil disturbance was recorded and it is mainly contained within the cylindrical installation zone as illustrated in Figure 1, where the shear resistance is changed, and therefore the load-displacement response and failure mechanism under uplift load are mainly controlled by the disturbed zone (Schiavon, 2016),. Nonetheless, the soil disturbance produced during installation is not uniform

along the cylindrical zone above the helix. Furthermore, it has been concluded that for multi-helical piles, the disturbance caused by the anchor installation is normally more pronounced in the soil above the upper plates than above the lower plates, as illustrated in Figure 2, because the upper soil layers are penetrated more times (Tsuha, 2012). Nevertheless, helical piles are manufactured so that trailing helices follow the same cutting path as their leading helix.

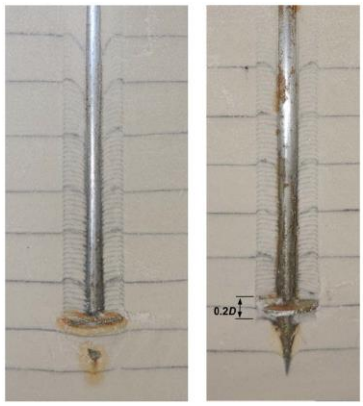

Figure 1. (a) Helical pile after model installation. (b) after uplift loading. from (Schiavon, 2016)

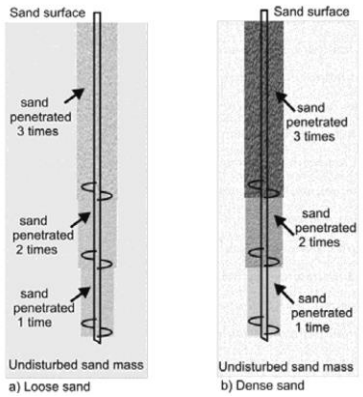

Figure 2. Hypothesis for sand disturbance after installation of three-helix anchor, from Tsuha et al., 2012a.

The characteristics and significance of the soil disturbance due to the pile installation depends on a wide range of parameters such as fluctuation of the ground-water table, embedment depth, shape of the pile shaft, pile geometry, soil-pile interaction and soil characteristics. It has been reported that the disturbance produced during installation is highly significant for cemented silt clay/clayey silt soils as the screwing process destroys the cementation between the soil particles (El Naggar et. al., 2011), which reduces the friction contact around the helices. Nevertheless, the disturbances in sands may vary depending on the high horizontal stresses generated and the lateral sand displacements; in deep anchors the installation densifies the sand, while in shallow anchors the installation mobilizes the sand upward (Clemence & Pepe, 1984; Clemence & Smithling, 1984), therefore a higher torque would be expected as the density of cohesionless soils increases. On the other hand, when a one-quarter scale helical pile was screwed into a dry sandy soil, the coefficient of lateral earth pressure at failure was observed to be 30% and 40% lower than the values determined for buried foundations, due to shear disturbances produced during installation (Clemence & Pepe, 1984),

The difference of the installation effects on sands has been characterized according with their densities: if a helical pile is embedded in loose sand, it tends to present lower uplift capacities than those embedded in dense sand under monotonic tensile loadings, which is mainly attributed to the local failure surface that loose sand presented. In dense sand, the failure was observed on a cone shape mainly at the helix interface. In addition, the differences in tensile capacities were reported ranging from 70% to 90% higher in dense sands than in loose sands (Nazir, et al., 2014). A monotonic uplift test conducted on

helical piles embedded in dry dense sand showed that the pile response improved after each test as a result of the soil compaction above the helices, which reduced the installation disturbances (Schiavon, 2016). In addition, the differences of installation effects are even greater under cyclic loadings. If the installation loosens the soil, the cyclic loads compact the soil and the static capacity of the anchor increases; nevertheless, if the pile installation densifies the soil, the cyclic load loosens the soil and reduce the static capacities of the pile (Clemence & Smithling, 1984). Schiavon (2016), however, found opposite results when he tested full-scale helical piles embedded in dry dense sand, where a negative skin friction was observed during the installation, and therefore residual loads were produced. However, when the piles were subjected to cyclic loadings, the negative friction decreased.

2.2. Behavior of helical piles under static loading; axial and lateral

Helical piles under static loading, in general, present a higher compressive axial capacity than an uplift capacity, because of disturbance effects. Their performance, however, varies depending on the installation process and their geometry. The main difference between screw piles' behavior under uplift and compressive loads relies on the behavior of their helices; the leading helix bears toward undisturbed soil under compression, meanwhile all the helices bear toward disturbed soil under tensile load. The quality of installation, therefore, is an important parameter of the pile's performance. Moreover, high strain dynamic testing conducted on helical piles demonstrated that most of the pile resistance (60%-75% under the higher energy impacts) was from end bearing on the

bottom helices when the piles were embedded in hard clay (White, B. et al., 2013). A complete compilation of existing static axial tests on helical piles are provided in (Lutenegger, 2015)

There are two main approaches to predict the ultimate compressive or tensile capacity for multi-helix screw plates. The first approach is the individual bearing method, which considers that the plates act separately and is typically used if the space between helical plates is at least 3 diameters apart. The second approach, namely the cylindrical shear method, considers a cylindrical failure surface that extends between the outer edges of the plates as the helices are closely separated (El Sharnouby& El Naggar, 2011; Perko, 2009). Furthermore, Rao & Prasad (1993) reported that for helical spacing ratios larger than 1.5, the failure surface is not cylindrical for helical piles in clay. On the other hand, it has been found that the p-y curve method can be used to estimate the lateral performance of helical piles (Sakr, 2009; Perko, 2009). Furthermore, according to the 2014 International Building Code (IBC), the lateral load capacity of a single pile or group of deep foundations should be determined "*using an approved method of analysis or by lateral load test to at least twice the proposed design working load*" (International Code Council, 2014).

Full-scale and model test experiments on helical piles under static lateral loading were conducted, and it was concluded that the resistance to lateral loads is mainly governed by the extension shaft diameter (Puri, et al. 1984). However, the static lateral behavior of helical piles is not only dependent on the shaft geometry, but also on embedment depth.

Prasad and Rao (1996) conducted model scale tests on two helical piles with two and four helices of 1.3 inch of diameter and a push pile, both with a shaft diameter of 0.5 inch. The testing matrix kept the distance from the top of the pile to the top helix constant at 14.3 inch and included installing a). a lead section embedded in clay with no extensions, and b). piles with different embedment ratios L/d (L=length of embedment and d= diameter of pile shaft) ranging from 12 to 18. They found that the lateral capacity of helical piles increases at higher embedment depths and the additional helices contributed to a higher lateral capacity, as the existence of helical plates increased the lateral capacity by 20% to 50% over that of the shaft alone (1996).

2.3. Deep foundations subjected to cyclic loading; axial and lateral

A cyclic loading is defined as a repetitive loading. A pile may be subjected to cyclic loading by mechanical actions, for example, when it is driven into the soil using vibratory equipment, which produces a cyclic shearing of the surrounding soil layers. In addition, different environmental conditions may generate cyclic loadings on any pile type throughout its lifetime; for instance, when wind loads are exerted on anchor guyed cables of transmission and wind towers, or wave movements impact offshore structures. To characterize a cyclic loading event, four parameters are generally defined; the number of cycles, the frequency of cycles, the mean load and the cyclic amplitude (Schiavon, 2016). Axial cyclic loadings were classified by (Clemence & Smithling, 1984) depending on their loading amplitudes as explained in Figure 3. A quasi-static cyclic loading is defined by (Wichtmann, 2005) as a repetitive loading with relatively low frequencies (< 5 Hz)

where inertial forces are neglected. Dynamic loads, on the other hand, are defined as high loading frequencies, where inertial forces are relevant. The earth plate's movement induces dynamic loadings to many foundations and superstructures through the propagating seismic waves produced during earthquakes. The limit between quasi-static cyclic and dynamic loadings is defined based on the cyclic loading amplitude and frequency. Often the amplitude dependence is disregarded and the frequency limit is established around 5 Hz (Wichtmann, 2005).

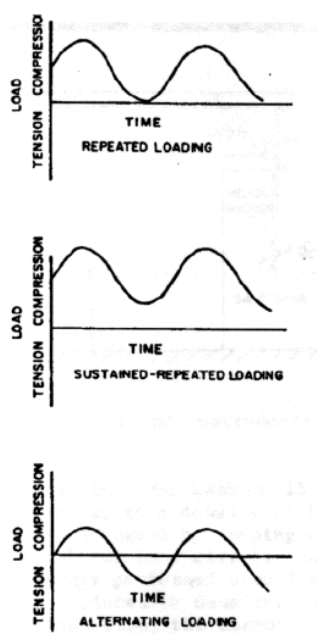

Figure 3. Cyclic axial loading classification, from (Clemence & Smithling, 1984)

After earthquakes, structural failure is frequently observed as a result of an excessive total or differential settlement of the piles (Read & Sritharan, 1993). Cyclic loads induce residual deformations on deep foundations because of the rearrangement of the soil particles, dynamic loading may even induce failure in certain pile types as a result of the

low resilience characteristics of the foundation. A pile is generally classified as flexible when the length over which the pile deflects due to a lateral cyclic load is less than the total length of the pile. The flexural behavior of a pile induces large strains, which produces an increased damping energy from the soil and some yielding, that may reduce the pile head acceleration up to 60% (Tabesh & Poulos, 1999). The dynamic response of a deep foundation depends on the dynamic impedances and the pile-soil interaction presented in every particular project, therefore, different models have been proposed to quantify these dynamic responses (i.e. Lumped mass models, Winkler models, finite element methods, cone models and the continuum approach). Yet, a limited amount of research is available to directly compare the cyclic or dynamic performance of different pile types with helical piles. Consequently, any contrast regarding their damping and resilience advantages under earthquakes events remains subjective and dependent to the particular soil characteristics tested. For instance, dynamic axial loadings were applied to full-scale double-helical piles and closed ended driven piles (that presented the same pile diameter and length) using an oscillator at the pile head that covered a frequency spectrum from 3 to 60 Hz. The oscillator comprised two counteracting shafts and each carried a set of eccentric masses to generate harmonic excitation. The test was conducted two weeks after the installation of the piles in a layered profile composed mainly of sandy and clayey soils. It was concluded that the response of driven and helical piles was close and therefore the performance was similar for the geometries tested (Elkasabgy & El Naggar, 2013). Conversely, high strain dynamic tests conducted on helical piles and driven piles (with the same shaft diameter and embedment depth) in a layered profile that consisted

mainly of silt and silty clay, concluded that helical piles provided about 230% to 290% higher capacities than driven piles (Sakr, 2013).

Since there does not seem to be a consistent conclusion when comparing the capacity of various pile types under lateral cyclic loads, it is recommended to conduct additional tests in order to understand the behavior of helical piles and driven piles under various lateral cyclic loading spans, as well as lateral dynamic loading. These tests should be conducted side-by-side in order to minimize variables and maximize similarities. Furthermore, it may be reasonable to consider other pile geometries before drawing any comparisons regarding their performance under earthquake events. To characterize the seismic performance of a foundation installed in a highly active seismic zone, it may be necessary to evaluate the long-term response of the pile by instrumentation and monitoring. While correlating separate studies conducted on helical piles to those conducted on driven piles, it is important to note that installation effects, soil conditions and properties, water table conditions, geometries and time of testing, among other parameters, are difficult to match and can only give some qualitative comparator data.

2.3.1. Screw piles subjected to axial cyclic loadings

Buhler & Cerato, (2010) recognized that the behavior of a helical pile subjected to axial cyclic loadings is further influenced by the cyclic span (difference between the minimum and maximum load) than by the maximum load applied. In addition, it was concluded that the uplift capacity of helical piers was reduced at large span cyclic loadings (greater

than 40% of the predicted static uplift capacity), which was corroborated by (Hanna et. al, 1978), who derived that large changes of loading accelerated helical pile's failure. Another factor that seems to decrease the uplift capacity of helical anchors is the number of cycles (Hoyland, 1993); it is well known that long-term cyclic loading in general affect the static uplift capacity of helical piles (Clemence & Smithling, 1982; Victor & Cerato, 2008) and degrade the strength of cohesive soils (Hanna et al., 1978; Clemence & Smithling, 1984; Trofimenkov & Mariupolskii, 1965; Dejong et al. 2003; Dejong et al. 2006). Moreover, from previous tests it may be concluded that one of the main factors that affect an anchor's life under dynamic loading is the displacement magnitude. Clemence & Smithling, (1984) observed that an increase in displacement results in a shorter helical anchor life. For instance, one-quarter scale anchors under a large displacement of 1/15" failed after 120 cycles, while the anchor with smaller displacement (1/37") failed after 1200 cycles, when they were subjected to dynamic loads up to 0.014 kips. In addition, Andreadis, (1981) reported that larger anchors deteriorate faster under cyclic loadings due to the greater elastic displacement per loading cycle. On the other hand, the proposed methodologies to increase helical piles' life include bringing the soil to equilibrium (Hanna et al., 1998) and pre-stressing the pile to values greater than the future cyclic loadings that the anchor would resist (Hanna & Mosawe, 1981).

The reduction in helical pile capacity under one-way cyclic loadings was studied by different researchers and the distribution of the helical pile's resistance under axial cyclic loadings and the location of the capacity lost were identified. The materials and methods of the available tests are summarized in Table 1. Nevertheless, the behavior of a helical

pile vary depending on the particular characteristics of each research program and the soil-pile interaction. In addition, a parameter that seems to greatly affect the performance of a helical pile is the soil disturbance generated during installation. Therefore, more research is suggested to propose any correlations. The results and conclusions of the available research are described below.

Table 1. Helical pile tests to quantify axial cyclic loading distribution and response.

Reference	**Pile dimensions**	**Soil**	**Testing**
(Schiavon, 2016)	Shaft diameter: 4” Helix diameter: 12” The helix was 49 feet from the ground surface	Clayey sand overlying a layer of pebbles and then clayey sand	Four series of uplift loads, each one involving a monotonic load followed by 50 tensile cyclic loads (See Table 2)
(Elkasabgy & El Naggar, 2011, 2013)	Diameter: 1’ ¾” Helix diameter: 24” Pile length: 29.5 feet	Sandy silt crust underlain by a layer of clay, underlain by silty sand and clay till, respectively	13 **dynamic**-quadratic testings (vertical harmonic motion) of different force intensities within a frequency range that covered the piles' resonant frequencies
(El Sharnouby & El Naggar, 2012 (b))	Diameter: 1’3/4” Helix diameter: 8”,10” and 12” Pile length: 24 feet	Stiff clayey silt till underlain dense sand	Axial monotonic load + 15 one-way compression loadings + static loading

Table 2. Field test description, adapted from (Schiavon, 2016)

Number of test	**Anchor: 1CHA**
First Test	1^{st} Monotonic loading
Second Test	1^{st} 50 tensile Cyclic loads
Third Test	2^{nd} Monotonic loading
Fourth Test	2^{nd} 50 tensile Cyclic loads
Fifth Test	3^{rd} Monotonic loading
Sixth Test	3^{rd} 50 tensile Cyclic loads
Seventh Test	4^{th} Monotonic loading
Eight Test	4^{th} 50 tensile Cyclic loads
Ninth Test	5^{th} Monotonic loading

The study conducted by Schiavon, (2016) observed that the reduction in the helical pile's uplift capacity was mainly located at the shaft. The initial shaft resistance measured at the monotonic uplift test corresponded to 3% to 30% of the anchor uplift capacity and after applying the four series of loading, a reduction in skin friction varied from 22% to 60% of the initial skin friction. Moreover, they observed that larger applied cyclic loads induced a greater reduction of the shaft resistance. On the other hand, at higher cyclic amplitudes (25% to 42% of the pile uplift capacity), 70% to 97% of the applied load during the first cycles was resisted by the helix. In the last cycles, the portion of the applied load resisted by the helix varied from 92% to 97% of the maximum load applied. Therefore, a helical pile's behavior under one-way cyclic loading was governed by the soil bearing on the helix or helices, with no loss of helix bearing capacity during the cyclic loading. Nevertheless, El Sharnouby & El Naggar, (2012 (b)) tested helical pulldown micropiles (reinforced with steel fiber) with a square shaft and found that the shaft contribution to the total resistance of the pile ranged between 72% to 80% at working levels (43% of ultimate capacity), and from 36% to 50% at higher loading levels (amplitude of 13% of ultimate capacity). Even with that high of a contribution, no

degradation of the stiffness was observed and the displacement during loading was 0.031 inch or 1.77% of the shaft diameter. In addition, Elkasabgy & El Naggar, (2013) conducted strain gauge readings along the length of a helical pile and concluded that the dynamic loads were transferred to the soil though the interface between pile shaft and soil. Moreover, 75% of the dynamic load applied to a helical pile was transferred to the soil through the first 19.7 feet of the pile's shaft and an insignificant influence of the helices was observed. Therefore, their behavior was close to the behavior of driven piles. Even more, each response curve was predicted more closely when they considered the soil-pile separation and soil disturbances (Elkasabgy & El Naggar, 2013). More attention should be focused to understand the influence of the installation effects on the capacity reduction or capacity influence of the pile.

The behavior of helical piles subjected to long-term cyclic loading seems to be independent of the frequency magnitude. Research conducted by Victor & Cerato, (2008) explained that the curves of load versus time of helical piles subjected to axial dynamic loads would be close either for 10 Hz or 50 Hz, therefore, the analysis of long term load-displacement could be conducted using 10 Hz. This statement was corroborated by (Elkasabgy, et al. 2011) when they noticed that the stiffness was not sensitive to frequency changes, especially at low frequencies where its value is close to the static stiffness. Furthermore, no variation in the stiffness and damping characteristics was observed during the dynamic testing due to frequency changes. Even so, the damping coefficient of the piles rapidly increased as the frequency approaches zero. In contrast, several researchers have observed that for other types of deep foundations the damping

coefficient is highly dependent on frequency changes (Dobry et al., 1982; El Marsafawi et al., 1992; Gazetas & Dobry, 1984; Michaelides et al., 1997; Mylonakis & Gazetas, 1999; Novak, 1991; Novak and El Sharnouby, 1983; Sun and Pires, 1993; Velez et al., 1983).

The use of helical piles for compression applications under dynamic loads has been constantly increasing. The results of the available cyclic load tests that assessed the compression performance of grouted helical piles are summarized in Table 3. The tests were conducted on SS 175 (Square Shaft 1-3/4") triple-helical piles with lengths of 24 feet (except El Naggar & Abdelghany, (2007) who used 9.8 ft, 11.8 ft, 14.8 ft, and 16.73 ft length) and helices with diameters of 8", 10" and 12", spaced 3 times the helix diameter, except for El Sharnouby & El Naggar, (2012 (b)) who used helices with diameters of 6", 8", and 10". All of the piles were grouted externally except when specified, with different types and amount of reinforcement to assess the effect on pile compressive capacity.

Table 3. Previous research to determine the effect of cyclic loading on reinforced and unreinforced grouted helical pile stiffness and compression capacity

Research	Type of pile	Cyclic loading applied	Span (kip)	Conclusion
(El Sharnouby & El Naggar, 2012(a))	Helical pulldown micropiles externally reinforced with fiber polymer and steel fiber	15-one-way cyclic compression loadings with a mean value of 43% of the ultimate pile capacity (maximum ultimate capacity of 900 KN)	20.2	Cyclic loading improved the pile's compression capacity by up to 15%

Research	Type of pile	Cyclic loading applied	Span (kip)	Conclusion
(El Sharnouby & El Naggar, Field investigation of axial monotonic and cyclic performance of reinforced helical pulldown micropiles, 2012 (b))	Helical pulldown micropiles reinforced with steel fiber	15-one-way cyclic compression loadings. Maximum cyclic load of 54% of the ultimate pile capacity (maximum ultimate capacity of 838 KN)	20.2	Cyclic loading Slightly improved the pile's compression capacity by up to 6%.
(Abdelghany & El Naggar, 2011)	RG-HSPs, P-HSPs, G-HSPs, and FRP-G-HSPs *	Initial compression loading followed by 15 cycles of axial load and a final compression loading.	13.5	P-HSPs: Average increase of 27% RG-HSPs: An averagen increase of 8% in their capacities, but one pile experienced a decrease of its capacity G-HSPs: Average increase of 14% of their capacities FRP-G-HSPs with internal grout: Average increase of 37% of their capacities FRP-G-HSPs with internal and external grout: An average decrease of 0.63%
(El Sharnouby & El Naggar, 2011)	Helical pulldown micropiles reinforced with steel fiber	15-one-way cyclic compression loadings. Maximum of 45% of the ultimate pile capacity	45	No effect on the stiffness and capacity.
(El Naggar & Abdelghany, 2007)	Ungrouted helical piles	15-one-way cyclic compression loadings. maximum value of 130 KN	13.5	The pile's compression capacity decreased by less than 5-10% after loading
	Externally-grouted helical piles			The pile's compression capacity varied ± 18% after the cyclic loading

* Where RG-HSPs are steel-Reinforced Grouted Helical Screw Piles, P-HSPs are ungrouted or Plain Helical Screw Piles, G-HSPs are Grouted Helical Screw Piles and FRP-G-HSPs are Fiber Reinforced Polymer Grouted Helical Screw Piles.

The first two tests and the fourth test described in were performed at the same site with similar soil conditions. The soil profile consisted of a layered soil composed of stiff clayey silt till on top of a dense sandy soil layer with the lead sections embedded in the sandy soil. Therefore, it was proposed that at high cyclic compression loads, the sand was densified around the helices and disturbance effects produced during installation were reduced (El Naggar & El Sharnouby, 2013; El Sharnouby, 2012; El Sharnouby & El Naggar, 2012 (a); El Sharnouby & El Naggar, 2012(b)). The first three projects detailed in Table 3 (grouted) showed that the static capacity and performance of helical piles subjected to cyclic loading improved after loading in the same soil conditions tested. However, the ungrouted results provided by (El Naggar & Abdelghany, 2007) suggest that the performance of a non-grouted helical pile is reduced after a cyclic loading when it is embedded in clayey silt soils. It is important to note that the embedment depth was shallower for the ungrouted helical piles, and the performance of a pile is directly dependent on the characteristics of the soil and the soil-pile interaction. Since the first two tests and the fourth test embedded their helices in a sandy soil, but the fifth test was embedded in a clayey silt, direct comparisons between the ungrouted test and the other grouted tests presented in Table 3 cannot be established. New research should be executed on both ungrouted and grouted helical piles with the same geometry and same embedment depth, to determine the influence of different dynamic spans and loading levels on the piles' compression capacity and to establish the limit of the dynamic span in which the helical pile's capacity is reduced. It should compare behavior in cohesive and non-cohesive soils using the same embedment depth.

In additional tests to study externally reinforced helical piles/micropiles, Abdelghany & El Naggar, (2011) and El Sharnouby & El Naggar, (2011) found that an externally reinforced helical pile/micropile provides a higher ultimate compression capacity and stiffness under axial cyclic loading than an ungrouted helical pile. The full-scale research conducted by Abdelghany & El Naggar, (2011) on helical piles embedded in cohesive soils consisted of an initial monotonic compression test followed by 15 cycles of loading and finally another static compression test was performed. Therefore, it was determined that after 15 cycles of loading, RG-HSPs presented higher compression performance than ungrouted helical piles (referred as Plain Helical Screw Piles (P-HSPs)), and G-HSPs and helical piles grouted externally and/or internally by a glass tube of Fiber Reinforced Polymer (FRP). Moreover, from the strain data analysis conducted to evaluate the load distribution, it was concluded that the average shaft resistance obtained on RG-HSPs was 55% of the total compression resistance of the pile, while on P-HSPs was only 14% of the total compression resistance of the pile. RG-HSPs displayed minimal degradation at the end of the test and showed the highest axial ultimate compression capacity and stiffness of all the piles tested. The results of the tests reported in Abdelghany Y. , (2008) are summarized in Table 4. In addition, El Naggar & Abdelghany, (2007) concluded that fifteen cyclic compression loads applied to ungrouted helical piles were transferred to the soil mainly through a cylindrical shear failure surface between adjacent helices and through the bearing capacity of the lead helix. Moreover, the percentage of the load transferred from depths above the helices increased from 10% for a ungrouted helical pile to 45% for a grouted helical pile.

Table 4. Tested ultimate capacity at 25 mm, adapted from Abdelghany Y. , (2008)

PHSP		RGHSP		FRP-G-HSP Internal and External grout		FRP-G-HSP Internal grout		G-HSP	
Before Cyclic loading (kip)	After Cyclic loading (kip)	Before Cyclic loading (kip)	After Cyclic loading (kip)	Before Cyclic loading (kip)	After Cyclic loading (kip)	Before Cyclic loading (kip)	After Cyclic loading (kip)	Before Cyclic loading (kip)	After Cyclic loading (kip)
	62.5	132	133	74	65	54.2	59.3	55.75	94.86
63.4		146	139	68	76	73.5	108.6	72.16	71.93
	62.4	118	137	103		69	97.2	76.43	62.94
54	70	97	124	73		52.8		76.65	90.37

Some research has been proposed to assess capacity estimation methods under cyclic loading. For uplift capacity estimations of a cyclically loaded helical pile, the torque correlation method could be used if the cyclic loading span is less than a load equal to 50% of the predicted static uplift capacity. Even so, the obtained estimation must be reduced by a factor of 3 to account for cyclic loadings effects (Buhler & Cerato, 2010). There are several uplift capacity prediction methods available, but it has been demonstrated that Helicap® predicts the dynamic-failure span magnitude of a dynamically loaded pile more closely than cylindrical shear methods, bearing plate methods, and torque correlation methods. Furthermore, Buhler & Cerato, (2010) concluded that the torque correlation method exhibited more consistent results than the soil mechanics approaches. However, Helicap® provided an inadequate factor of safety and the predictions are highly sensitive to the soil properties used. On the other hand, the analysis of (Abdelghany & El Naggar, 2011) detailed that the compression capacities of screw piles subjected to cyclic loadings are proportional to the installation torque, and the torque correlation factor, K_t, can be used to predict the compression capacity of ungrouted helical piles (but it cannot be used for grouted helical piles). However, the

observations presented by (Abdelghany & El Naggar, 2011) did not evaluate the effects of higher cyclic loading spans, or the effects of the change in the soil conditions from the moment of installation to the lifetime of the project on the compression capacity predictions. As specified by (Victor & Cerato, 2008) the torque correlation factor under-predicted the anchor uplift capacity and over-predicted the piles uplift capacity when the water table rose. As a conclusion, more research is needed to confirm the accuracy of the torque correlation methods to predict compression capacities on piles subjected to large span cyclic loading.

Load tests are frequently used to validate the installation process and design methodology of deep foundations. Load tests on helical piles are rarely performed because of the torque installation profile verification process, however, sometimes will be conducted if recommended by the engineer when large number of piles are being used, or when specified by municipalities or building codes, or when deflection is a critical concern (Perko H. , 2009). According to the 2014 International Building Code (IBC) at least one element should be subjected to a load test in each area of uniform subsoil conditions (following the guidelines of ASTM D1143 or ASTM D4945), when deep foundations are subjected to compressive loads that are greater to those determined using the allowable stresses of Equation 2, or when the design load is in doubt. In addition, past case studies conducted on full-scale helical piles suggested that high strain dynamic tests generate a better quantitative indication of the pile resistance than the installation torque (Cannon, 2000). Dynamic Loading Tests (DLTs) are conducted faster and at lower cost than Static Loading Tests (SLTs), and it has been proven that both methods provide an agreement in

their results when conducted on cohesive soils, although it is necessary to conduct one or more load tests to determine the best correlation factor for each particular site and pile geometry (Beim & Luna, 2012). Furthermore, full-scale static load tests are considered the most accurate method to estimate helical piles capacity under monotonic conditions (Sakr, 2009). Therefore, it is recommended to conduct research to compare the capacity predictions from High Strain Dynamic Tests and torque correlation factors on grouted helical piles subjected to dynamic loads installed in both cohesive and non-cohesive soils and to propose a failure criterion for High Strain Dynamic Tests.

Equation 2. Allowable stress for helical piles in compression, from (International Code Council, 2014)

$$0.6F_y \leq 0.5F_u \ (a)$$

(a) F_y is the specified minimum yield stress of steel and F_u is the specifies minimum tensile stress of structural steel.

Previous research conducted on full-scale helical piles subjected to axial dynamic loads suggested that the disturbance produced during installation significantly affected the dynamic response of the piles (Elkasabgy, et al., 2011; Elkasabgy & El Naggar, 2013). During the analysis, a linear approach to estimate the natural frequencies of the piles assumed that no disturbance effects due to installation were generated, but the values obtained were between 63% and 74% higher than the measured values. In addition, the vertical vibration amplitudes measured after installation on the pile head were different from the estimated ones. On the other hand, an estimation using a non-linear approach,

that included the pile-soil separation, was in agreement with the measured values. The disturbances observed during the test were mostly located around the pile due to the imperfect contact on the pile-soil interface, which was corroborated as the response of helical piles and driven piles with the same geometry was significantly close (Elkasabgy, et al., 2011; Elkasabgy & El Naggar, 2013). Even more, Elkasabgy & El Naggar, (2013) found that the stiffness and damping of the tested helical piles were increased as the time after installation increased, which was a result of the improvement in stiffness and strength of the disturbed soil; for instance, the maximum displacement amplitudes measured at the center of gravity of the static mass was 0.016 inch for a helical pile tested 2 weeks after installation and 0.012 inch for the same helical pier tested 9 months after installation.

The resilient behavior of helical piles under cyclic compression loadings has been characterized by Dilley & Hulse, (2007), Cerato & Victor, (2008, 2009), El Sharnouby & El Naggar, (2011) and El Naggar & El Sharnouby, (2012), who concluded that after high cyclic loadings were applied, the remaining displacements were minimal. In some cases, it was reported that the piles recovered almost 100% of their displacement (Cerato & Victor, 2008, 2009). Dilley & Hulse, (2007) observed that the helical pile reaction stabilized to zero displacement or creep within 24 hours following each loading cycle. Nevertheless, (Ghaly et al., 1993) specified that after one uplift cyclic loading, 100% of the displacement is recovered if (cyclic loading (P_c)/ the ultimate static (P_{ud}) capacity) ratio is under 25%, otherwise the percentage in creep recovery decreases as the number of cycles or P_c/P_{ud} increases. Furthermore, (Schiavon, J., 2016; El Sharnouby & El

Naggar, 2012(a)) reported that the cyclic performance of a helical pile is influenced by the preceding monotonic loads applied. For instance, (El Sharnouby & El Naggar, 2012(a)) observed that if the one-way cyclic loading range was below the maximum initial static load applied to the pile (around 400 KN), negligible permanent displacement was observed, although these conclusions are applicable for cyclic loading comprised by fifteen cycles. Even when the cyclic loading range was above the maximum initial static load applied, no degradation of the stiffness was detected.

The proposed theoretical linear approach introduced by (Novak and Aboul-Ella 1978 (a), 1978 (b)) was used by (Elkasabgy & El Naggar, 2011, 2013) to derive impedance functions of piles embedded in layered soils and determine their damping and stiffness characteristics. A parallel approach, the nonlinear approach proposed by (Novak & Sheta, 1980), was employed to account for installation disturbances effects, nonlinearity of the soil at the zone of high strain, lack of bond at the pile-soil interface and separation. The results demonstrated that the helical piles' response manifested a reduction in the resonant frequency with an increase in the excitation intensity, due to the moderate nonlinearity response curves measured for the pile. Moreover, the linear approach overestimated both the stiffness and damping of the pile due to the assumed perfect bonding between pile and soil, while, the nonlinear approach provided a reasonable estimation for the pile response curves and impedance parameters. The nonlinear approach predicted an average increase of 42% in stiffness and of about 90% in damping for the helical pile after nine months due to the stiffening of the soil. On the other hand, (Elkasabgy et al., 2010) characterized the behavior of 29.5 feet tall, double 24-inch helix-diameter piles,

embedded in clay, and he found that as the excitation intensity increases from 0.091 kg.m to 0.21 kg.m, the resonant frequency varied slightly from 7.5 to 6.85 Hz, and the damping ratios decreased slightly from 7.5 to 6.85 %.

2.3.2. Driven piles subjected to axial cyclic loadings

Unlike screw anchors, when a driven pile is subjected to a cyclic loading, the degradation in the shaft resistance is not compensated by the bearing of the helices on the lead section. McCabe, (2002) reported that the level of degradation of the shaft capacity under one-way cyclic loadings depends on the magnitude of the load applied. He observed that if the loading applied was lower than 50% of the static ultimate tension capacity of the concrete driven pile, there is an insignificant reduction in the shaft capacity, but if the load applied is between 50% to 70% of the ultimate tension capacity, reductions up to 25% in the shaft capacity can be seen. In addition, Van Weele, A. F., (1979) conducted full-scale and small-scale tests on steel driven piles embedded in sand and concluded that at a cyclic loading range of 20%-30% of the ultimate static capacity, failure was observed after 3000 cycles, while at a loading range of 0-25% of the driven pile's ultimate static capacity, failure was obtained after 10000 cycles.

The amount of shaft degradation due to cyclic loadings is also highly dependent on the pile-soil interaction (Puech & Jezequel, 1980; Steenfelt, et al., 1981; Poulos, 1982;). For example, a small-scale test conducted by Chan & Hanna, (1980) reported that the maximum load before failure that a model 0.75 inch diameter driven pile embedded in

medium dense sand could sustain under one-way cyclic loading was around 30% of the ultimate static value. In addition, a one-way cyclic test conducted on model driven piles embedded in sand showed that at 30% of the ultimate static capacity, failure occurred close to 40 cycles due to accumulation of the deformation, but incremental collapse was observed at cyclic loading levels as low as 10% of the ultimate static capacity on small-scale driven piles in sand (Gudehus & Hettler, 1981). Furthermore, for driven piles embedded in sand, the increase in permanent displacement with an increase in the number of cycles had been attributed to the continuous rearrangement of the soil particles (Van Weele, 1979). A contrasting scenario was tested (maximum loading level of 1.06 lbs) on an aluminum model pile embedded in clay where failure was reported at 29 one-way cycles, because it was measured that the stress level at the pile surface was equal to the peak vane shear strength of the soil (Holmquist & Matlock, 1976). Furthermore, Grosch & Reese, (1980) tested model piles in soft clay and observed that a decrease in the overall pore pressure during cyclic loading was accompanied by a reduction in the skin friction capacity. On the other hand, several tests in clays, concluded that the rate of application of a cyclic loading had a great significance on the driven pile's capacity and stiffness; at faster rates larger pile capacity and stiffness are obtained (Bea et al., 1980; Bjerrum, 1973; Gallagher & St. John, 1980; Kraft, et al., 1981; Poulos, 1981a). Although (Poulos, 1982) specified that from static triaxial test, the rate of application of a cyclic loading on driven piles embedded in sand does not affect the shear strength of the pile.

Nonlinear methodologies had been developed to determine the effect of vertical harmonic dynamic loadings on piles embedded in clay, and it was concluded that as the load

amplitude increases, the magnitude of the material damping increases, therefore, the magnitude of the propagation of seismic waves away from the pile is reduced (Michaelides et al., 1997). On the other hand, tests conducted on driven piles embedded in clay observed that initially the pile-soil interface was overconsolidated due to the pile installation. During cyclic loadings, however, the interface became reconsolidated and the soil dilated due to the rearrangement of the clay particles (Grosch & Reese, 1980). The rearrangement of the soil particles parallel to the direction of shear strain and the destruction of the interparticle bonds were identified as the primary mechanisms of cyclic load-transfer reduction Grosch& Reese, (1980).

McCabe, (2002) stated that the rate of accumulated permanent displacement increases as the one-way cyclic loads approach the dynamic pile capacity. Furthermore, it has been determined that the sum of static and one-way cyclic axial load should be kept below 80% of the pile's ultimate capacity to avoid large cumulative settlements (Bea et al.,1980). For instance, (Mcanoy et al., 1982) conducted a full-scale test on steel driven piles embedded in sandy silty clay till and reported that after loading levels of 80% of the pullout capacity, the piles failed at 564 cycles and presented a drastic change in behavior with cumulative displacements of 0.65 inch. At loading levels, up to 60% of the ultimate pullout capacity, the piles failed at 11000 cycles and presented permanent displacements of only 0.005 inch. On the other hand, (Jaime et al., 1990) concluded that for loading levels lower than the ultimate pile capacity, P_u, the permanent displacement observed on concrete driven piles after 30 cycles of loading was less than 0.2 inch, but this permanent displacement increases for loading levels greater than P_u. Moreover, for loading levels

greater than $1.5P_u$, the pile capacity is reduced to $0.8P_u$ and the permanent displacements were recorded up to a magnitude of 1.77 inch.

Mcanoy et al., (1982) concluded that at one-way cyclic loading levels greater than 80% of the driven pile's ultimate static capacity, there is a change in the behavior of the pile that may lead to a failure at a lower number of cycles. In addition, several studies concluded that when a large number of cycles are applied, the pile's cumulative displacement does not stabilize. Chan & Hanna, (1980) found that the permanent settlement of a driven pile increased even after a larger number of cycles (up to 31000 cycles with a loading level of 10% of the ultimate tensile pile capacity was applied). Puech & Jezequel, (1980) found that the pile top displacement was not stabilized even after 1500 cycles. Moreover, Van Weele, (1979) suggested that the permanent deformation of a driven pile will increase with an increase in cycles without reaching a constant and final value. Poulos, (1982) defined failure as a continued accumulation of permanent displacement that reached values up to one pile diameter, while Chan & Hanna, (1980) defined failure up to a displacement of three pile diameters. Nevertheless Holmquist & Matlock, (1976) reported that when a pile was subjected to one-way cyclic loading up to failure, the observed accumulated displacement after 60 additional cycles (where yielding of the pile was presented) was 0.3 inch, but even with the increased deformation, the resistance of the pile was not significantly reduced. Furthermore, Holmquist & Matlock, (1976) reported that under eight one-way loading cycles, no progressive deformation was observed. However, at the ninth cyclic loading, a progressive deformation was observed. Nevertheless, this deformation stabilized at the

30^{th} cycle. In conclusion, it would be interesting to test the reaction of helical piles under a large number of axial one-way cycles (greater than 11000 cycles).

Holmquist & Matlock, (1976) conducted several two-way cyclic loadings tests (with reversals) on different aluminum driven piles, using a frequency that ranged in the quasi-static cyclic spectrum and they found that the maximum resistance of a pile is reduced around one-third of the initial measured static resistance. In addition, it has been reported that loading conditions that comprise full plastic shear reversals cause a reduction in the capacity of a driven pile up to 31% of the initial measured static capacity. Nevertheless, the amount of reduction depends on the soil type (Doherty, 2009). On the other hand, several researchers reported that under one-way cyclic loadings the capacity and stiffness of driven piles are less affected than under two-way loading conditions (Broms, 1972; Holmquis & Matlock, 1976; Poulos, 1982; Steenfelt et al., 1981). A full-scale one-way cyclic loading conducted on steel driven piles embedded in sandy silty clay till concluded that the cyclic stiffness of the tested piles did not vary with the number of cycles even during failure (Mcanoy et al., 1982). In addition, full-scale test showed that one-way uplift cyclic loadings up to 80% of the steel driven pile static capacity did not affect the ultimate capacity of the pile (Kraft et al., 1981).

All this being said, there is no agreement on the influence of the number of cycles in the reduction of the shaft capacity. Previous tests proved that the degradation on the shaft capacity for a driven pile under cyclic loadings not only depends on the magnitude of loading, but it also depends on the number of cycles (Poulos, 1982). Moreover, Grosch

& Reese, (1980) and Poulos, (1982) reported that most of the shaft capacity reduction was observed during the first 10 to 20 cycles. Nevertheless, the application of a large number of small non-alternating two-way cycles to a small-scale steel-driven pile embedded in silica dense sand resulted in a densification of the pile-soil interface that actually increased the pullout resistance of the pile (Silva, et al., 2013).

It has been shown that the method of installation affect the rate of degradation of a pile's performance during cyclic loadings (Holmquist & Matlock, 1976). They conducted two-way cyclic loadings on model piles embedded in clay and found that the minimum resistance of the tested driven piles was reached at 30 cycles of loading, while a bored pile required 90 cycles of loading under the same test conditions. Nevertheless, it has been concluded that increasing the confining pressure of the clayey soil or its time of consolidation reduces the rate of degradation of the driven piles' performance under cyclic loadings but not the amount of degradation (1976). On the other hand, even though tests comparing the rate of performance degradation for helical piles with those of driven piles under two-way cyclic loadings have not been conducted yet, previous research (Schiavon, 2016) concluded that one-way cyclic loadings reduce the disturbances produced during the installation of helical piles, which actually increases their performance.

Group effects have been shown to increase displacements and pile degradation when they are subjected to cyclic loadings (Poulos, 1982). For example, a test conducted on a group of steel pipe piles concluded that the ultimate tensile capacity of a pile is reduced by 19%

when a load of just 48% of the pullout capacity of the pile was applied (Mcanoy et al., 1982). Even more, a theory proposed by (Poulos, 1982) specified that as the number of piles in a group increases, the maximum cyclic load that could be applied to each pile decreases. A summary of the principal characteristics of the driven piles under vertical cyclic loading that were found during the literature review of is summarized in Table 5.

Table 5. Summary of research considering cyclic loading effects on steel driven piles

Reference	**Soil**	**Diameter (inch)**	**Length (feet)**	**Full scale/Small scale**
(Seed & Reese, 1955)	Soft clay	6.00	15	Full scale
(Broms, 1972)	Silty clay	11.18	1	Small scale
(Broms, 1972)	Silty clay	14.88	52	Full scale
		6.77	58	
(Broms, 1972)	Clay underlying sand	11.22	47	Full scale
		11.22	75	
(Holmquist & Matlock, 1976)	marine clay	1.00	3.60	Small Scale
(Puech & Jezequel, 1980)	Layered profile	10.79	42.7	Full scale
(Puech & Jezequel, 1980)	Layered profile composed by silts, loose sands and silty clays	10.79	55.8	Full scale
(Gallagher & St. John, 1980)	Cowden series	18.00	30	Full scale
(Kraft, Cox, & Verner, 1981)	layered profile- empire series	14.00	53	Full scale
(Mcanoy, Chasman, & Purvis, 1982)	Sandy silty clay till	7.56	32.5	Full scale
(Bergdahl & Hult, 1981)	Glacial varved clay	4.06	49	Full scale
(Doyle & Pelletier, 1985)	Layered profile	30.00	190	Full scale
		30.00	265	
(Bogard & Matlock, In-Situ	Layered profile	3.00	16	Full scale

Reference	Soil	Diameter (inch)	Length (feet)	Full scale/Small scale
Pile Segment Model Experiments at Empire, Louisiana, 1990a)				
(Bogard & Matlock, 1990b)	Layered profile	3.00	16	Full scale
(Jaime, Romo, & Resendiz, 1990)	Layered profile that consisted of silt overlying a layer of clay with interbedded layers of sand	13.4	33	Full scale
(Bogard & Matlock, 1991)	Layered profile	3.00	16	Full scale
(Cox, Cameron, & Clarke, 1993)	Silty clay	30.00	98.5	Full scale
(Cox, Cameron, & Clarke, 1993)	glacial till	30.00	98.5	Full scale
(Bogard & Matlock, 1998)	Layered profile	30.00	220	Full scale
(Huybrechts & Legrand, 1998)	Sand	10.7, 16.54 with an enlarged base of 18.5 and 11.42 by 11.42 for the square shaft	34.5, 36 and 39.5	Full-scale
(McCabe, 2002)	Soft clay	11.10	20	Full scale
(Rollins, Hales, Ashford, & Camp, 2006)	Alluvial sands underlying a clay layer and then underlying a stiff layer of Cooper Marl	101.97	154	Full-scale
(Hussein, Tobita, & Susumu, 2010)	Dry silica sand	0.39	1	Small-scale
(Silva, et al., 2013)	Silica Sand	1.42	3	Small-scale
(Unsever, Kawamori,	Dry sand	0.39 by 0.59	1	Small-scale

Reference	Soil	Diameter (inch)	Length (feet)	Full scale/Small scale
Matsumoto, & Shimono, 2013)				
(Silva, et al., 2013)	Sand	1.42	3	Small-scale

2.3.3. Screw piles subjected to lateral cyclic loadings

Under cyclic lateral loadings, it has been observed that the lateral deflection of helical piles is caused primarily due to the plastic deformation of the soil, which is the reason why other deep foundation elements deflect as well. Nevertheless, helical piles recovered most of the deflection during unloading, indicating minimal structural damage (El Sharnouby & El Naggar, 2011). The failure of a pile due to lateral loading may arise in two ways depending on the pile depth; for shorter piles, failure in the soil mass may occur due to the rotation of the pile as a rigid body, but longer piles collapse when a plastic hinge is formed at some depth along the pile shaft and a differential displacement is produced between the upper and bottom sections of the pile.

The amount of research conducted to quantify the performance of helical piles under cyclic lateral loadings is limited. In clayey soils, helical piles experience a great reduction in their lateral and pullout capacities (Prasad and Rao 1993; Basack and Purkayastha 2007), which is mainly attributed to the soil contraction in the shear zone with results in the reduction in the mobilized shear strength and normal stresses (Dejong et al., 2006). In addition, there is just one test on helical piles that quantified the resonant frequencies, resonant ratios and damping ratios presented on this type of piles. Elkasabgy, et al. (2010)

tested helical piles under lateral dynamic loadings and he found that as the excitation intensity increases from 0.091 kg-m to 0.21 kg-m, the resonant frequency increases slightly from 3.43 to 3.67 Hz, and the damping ratios increases from 2.72 to 2.91 %. He also observed that at higher frequencies the horizontal response amplitudes started to increase due to the vibration.

Helical piles were found to perform better after high cyclic lateral loads than regular pipe piles, as they exhibited higher pullout capacities than pipe piles when both types of deep foundations were subjected to a sequence of loads that consisted on an initial lateral static load tests, followed by a lateral cyclic load test, and a final vertical pullout test (Prasad & Rao, 1994). Even more, no reduction in the pullout capacity was observed on helical piles that presented lateral deflections up to 10% of the pile diameter, as the gaps are mainly formed around the shaft and the bearing interaction, and therefore capacity of the helices is not affected. The tested specimens consisted of ½ - ¾ inch diameter model helical piles and driven piles. The lead section was a quadruple 1.3-inch diameter helix with the top helix at 14.3 inch from the top of the pile. The test was conducted on different embedment ratios, L/d (L is the length of embedment and d is the pile diameter), of 11, 15, 17, and 20 for the 1/2-inch pile diameter and L/d of 15 for the ¾ inch pile diameter, all embedded in marine clay. In addition, previous research specified that at embedment ratios, L/d = 0 and L/d = 2.5, the formation of a gap and the reduction in soil strength are present only in the soil immediately surrounding the pile and therefore the pullout capacity is not affected. Although, at L/d=4 a relatively negligible reduction in uplift capacity was found (Prasad and Rao, 1993). Nevertheless, more research on other types of soils is needed to identify the influence of the soil-pile

interaction, different cyclic amplitudes and loading levels on the helical pile's behavior under lateral cyclic loadings.

Higher lateral capacities and pile performance were observed in helical piles using different types of pile reinforcements or external grout columns. Previous research concluded that RG-HSPs had higher ultimate capacities and better cyclic performance than ungrouted helical piles. However, at higher loading levels, the displacement increased as the number of cycles increased (El Sharnouby & El Naggar, 2011). In addition, steel-fiber reinforced grouted helical piles presented higher capacities than FRP-G-HSPs with internal and external grout, which presented higher performances than grouted helical piles and FRP-G-HSPs with internal grout. It has been established that RG-HSPs presented lateral capacities up to three times the capacity of un-grouted helical piles (Abdelghany & El Naggar, 2011). It was observed that the pile performance might be affected by the grout characteristics within the top pile portion and the failure mechanism was mainly due to the separation of the grout column and the grout-soil gap. Furthermore, El Sharnouby, (2012 & 2013) specified that the performance of the pile is determined by the opening and closing of the gap on both sides of the pile. He also observed that the performance of 5-foot-long triple-helical piles (8, 10, 12 inch diameter) embedded in clay under two-way cyclic loadings were degraded because of the gap formation. In addition, they exhibited a preferential direction due to the resistance of the pile.

2.3.4. Driven piles subjected to lateral cyclic loadings

According to Perko, (2009), under dynamic lateral loadings, the damping response of a pile increases as the flexural characteristics (i.e. embedment depth, diameter) of the pile increases; therefore, a lower pile head displacement is obtained. Driven piles under lateral dynamic loadings demonstrate a highly dependent relationship between the frequency of loading and the damping response of the piles (Dobry, et al., 1982). In addition, Perko stated that a lower slenderness ratio (ratio of pile length=L to its diameter=d) results in a lower lateral flexural response. Moreover, lateral cyclic loadings produce a degradation of the ultimate lateral capacity of driven piles embedded in cohesive soils, but the amount of degradation of a pile-soil system mainly depends on the number of cycles, the frequency and the cyclic load amplitude (ratio of cyclic load amplitude to the lateral static ultimate pile capacity), (Matlock, 1970; Reese, 1977; Poulos, 1982; Long & Vanneste, 1994; Basack, 1999; Basack, 2008; Basack, 2011). Nevertheless, it has been reported that dynamic soil-pile-structure interaction under earthquakes is modeled considering soil and structural yielding, pile-soil gap formation, radiation damping and cyclic degradation of soil stiffness and strength (Allotey & El Naggar, 2008). Cyclic loads rearrange the soil particles of any soil mass, and in clayey soils, cyclic loads develop excess pore-water pressure that produces plastic deformations around the pile and some gaps that frequently extend from the ground surface down to 10-15% of the embedded pile length. In addition, heaves and cracks may generate normal to the direction of loading at large amplitudes. On the other hand, (Cuellar et al., 2009, 2012) conducted model tests on piles subjected to long-term cyclic loadings and observed a densification of the sand. Even more, it has

been observed that long term cyclic loading may stiffen the soil which would lead to an improvement in the pile capacity (Basack & Bhattacharya, 2009). However, they reported an elliptical depression that formed around the pile group at the ground surface, more over, the diameter of this depression increases with the frequency and amplitude of the cyclic loading.

Therefore, there are two main recognizable effects of lateral cyclic loading on the performance of driven piles in cohesive soils; degradation of soil strength and stiffness on the pile-soil interface and the 'shakedown' effect caused by the accumulation of permanent plastic deformations (Basack & Dey, 2011). In addition, Guo, (2006) stated that the response of a laterally loaded pile is mainly dominated by the Limiting Force Profiles (LFP) and the depth of mobilization, which change with the magnitude and number of cycles (Guo & Zhu, 2005). Furthermore, it has been demonstrated that the ultimate pile capacity decreases with the number of cycles and increases with the frequency; however, the capacity decreases with an increase in the amplitude (Basack & Bhattacharya, 2009). On the other hand, (Prasad & Rao, 1994) observed that for driven piles in dry sand at low loading levels of 30% (lateral cyclic load/static lateral capacity), the deflection was stabilized at 250 cycles and its magnitude was less than 3% of the pile diameter, but at a loading level of 50% the deflection was stabilized at 500 cycles, which shows that as the percentage of applied load increases, it takes longer for the deflection to stabilize. Furthermore, for a loading level within 50%-70% (lateral cyclic load/static lateral capacity), the driven pile deflection increased from 3% up to 10% of the pile diameter, and from a loading level of 55%, there is a reduction in the capacity as the

number of cycles increase. In addition, for helical piles subjected to lateral cyclic loading levels of 70%, failure occurred at only 400 cycles, while a pipe pile failed at 150 cycles, when they were tested under the same conditions. Therefore, as the loading increases, the driven pile deflection increases and the capacity decreases as a result of the formation of a gap around the pile, which additionally affects the skin friction (Matlock, 1970).

Furthermore, it has been demonstrated that the pullout capacity of a driven pile after lateral cyclic loadings is also dependent on the slenderness ratio, L/d, as well as on the cyclic load amplitude and lateral deflection. For instance, Rao & Prasad, (1993) conducted lateral cyclic loadings on model piles embedded in dry sand and having L/d values of 20. They observed that up to a lateral deflection of 0.05 diameters, there is no reduction in the pullout capacity, but beyond this value, there seems to be a reduction in the helical pile's pullout capacity with an increase in lateral deflection. However, the degradation factors had lower values for piles having L/d of 15. They concluded that if the ratio of lateral cyclic load to static lateral capacity is kept below a value of 0.3 - 0.4, the lateral deflection of the pile will be less than 2.5% to 3% pile diameters and there will be no reduction in pullout capacity. Qin & Dong Guo, (2016) tested model piles driven in sand and concluded that the lateral cyclic load level has a greater impact on the modulus of subgrade reaction (1.5 to 2.8 times) and the ultimate pullout capacity of the piles (10% reduction) than the number of cycles. Nevertheless, (Basack & Bhattacharya, 2009) reported that the ultimate capacity increases as the number of cycles, frequency and/or amplitude increases. Therefore, a relationship between these parameters can not be established without further research. On the other hand, (Qin & Dong Guo, 2016)

established a linear relationship between maximum bending moment and the lateral load, without regard to the number of cycles.

Another parameter that seems to have a great influence in a pile behavior when embedded in sandy soils is the sand density. Raongjant & Meng, (2011) reported that the peak lateral strength that a model aluminum pipe-pile could sustain under lateral cyclic loadings when it was embedded in dense dry river sand was about double that of the pile in loose sand. However, when the gap around the pile was formed, the lateral strength of the pile embedded in dense sand was reduced 30% to 40% of its peak strength. Due to the decrease in the passive resistance of the soil bed. The influence of long-term lateral cyclic loadings on driven piles behavior in sand has been studied widely. It has been reported that cohesionless soils subjected to long-term cyclic loadings increase their deformations indefinitely over time, (Long &Vanneste, 1994; Peng et al., 2006; LeBlanc et al., 2010; Peralta and Achmus, 2010) which depends on the installation methods, soil density and load ratio, but in all cases, produces a decrease in pile capacity associated with increased pile-soil stiffness (Basack & Dey, 2011). Roesen et al., (2011) concluded that after one-way cyclic loadings on a pile embedded in saturated sand with relative densities of 78% to 87%, the accumulated rotation of the pile stabilized after 15000 cycles. Conversely, most of the design guidelines of several countries as Denmark are established based on full-scale testing that used just a low number of cycles (less than 500 cycles) (L. Rasmussen, et al., 2013).

The behavior of piles in other types of soils (with different densities) subjected to lateral loadings had been widely studied as well. For example, (Chen et al., 2015) evaluated the influence of long-term cyclic loadings on monopoles embedded in river silt, and concluded that the accumulated displacement has a direct relationship with the cyclic load ratio but no relation to the relative density of the soil. However, the unloading stiffness is dependent of the relative density of the soil but is independent of the cyclic ratio. Moreover, they calculated that the peak and residual accumulated displacements increased linearly with the logarithm of the number of cycles. On the other hand, different approaches have been developed to approach the soil-pile-structure interaction under dynamic loadings to account for these variations in pile's behavior depending on the characteristics of the soil. For example, finite element models, semi-analytical and boundary element models, the extended Tajami formulation have been used, but the most frequently used is the beam on a nonlinear Winkler foundation (BNWF) method and therefore several improvements had been proposed (Allotey & El Naggar, 2008; Allotey, 2006; Finn, 2005; Gerolymos & Gazetas, 2005; Brown et al., 2001; El Naggar & Bentley, 2000; Boulanger, et al., 1999). BNWF are widely used to model liquefaction events during earthquakes as it will be explained in section 2.1.

Most of the tests that assessed the influence of lateral cyclic loads on the behavior of driven piles has been conducted on pile groups (Brown et al., 1988; Morrison and Reese, 1988; Ruesta and Townsend, 1997; Hussein, et al. 2010). For instance, a test conducted on a group of model steel pipe-piles in sand that were attached by a pile cap, which supported a superstructure on top, consisted in inducing dynamic loadings with different

amplitudes and frequencies, it was observed that at low frequencies, the pile response is controlled by its bending rigidity rather than by its kinematic or inertial effects, nevertheless, the amplification of the pile cap displacement started at low frequencies due to inertial effects, which was sustained up to the fundamental frequency, where the pile mass and the superstructure acceleration are in phase. After the fundamental frequency, the superstructure mass decreased the pile cap displacement (Hussein, et al., 2010).

2.4. Influence of the helical pile geometry on its cyclic behavior

2.4.1. Single helix vs. Multi-helical pile

Several studies specify that helical piles' performance after compression or tension monotonic loading is improved as the number of helices is increased and even more as the diameter of the helices increases. For instance, Sakr, (2009) tested full-scale 19-foot-long piles with single or double 16-inch diameter helices (spaced 3 times the helix diameter in the double helix configuration), subjected to compression static loadings on oil sand, and he found that double helical piles were 40% more resistant than single helical piers. However, it has been demonstrated that the quality of installation and the disturbances associated affect the performance of a helical pile (Tshua, et al., 2013). A tensile loading test conducted on small-scale 0.4", 0.6" and 0.8" single, double and triple-helical piles embedded in dry sand with the same helix diameter concluded that the efficiency of the second helix depends on the amount of disturbance produced during installation (which was correlated to the initial relative density of the sand and the diameter of the helix). Therefore, as the second helix diameter increased, its efficiency

decreased. Even so, the ratio of the measured displacement at failure to the helix diameter was not affected by the number of helices (Tshua, et al., 2013).

The advantages provided by the extra helix of a triple-helical pile compared to the performance of a double-helical pile under dynamic loading has been reported for guyed cables applications, where triple-helical piles (8, 10 and 12 inch of helix-diameter) sustained greater dynamic spans than a double helical pile (8 and 10-inch diameter) when embedded at 10 ft in a layered profile composed of clayey soils (Buhler & Cerato, 2010). Even more, it was suggested that when comparing single- to double-helix piles, a lower number of helices increased the possibility of a failure due to local bearing capacity. In addition, according to (El Sharnouby & El Naggar, 2012 (b)) it is favorable to use multi-helix lead sections instead of single helix under cyclic compression loading conditions, as the shaft resistance decrease is compensated by the lead section. They proposed that the helices dissipated the excess load transferred to the lead section. However, a cyclic test conducted on double, triple and quadruple-helical piles (installed in the same soil conditions presented in (Buhler & Cerato, 2010)) suggested that a triple-helical pile (8, 10, 12 inch) is more efficient on guyed cable applications than the quadruple helical piles, as the fourth helix (14 inch) did not increase the strength of the pile with a proportional increasing torque (Cerato & Victor, 2008, 2009). As the test described were conducted under the same soil conditions, it is concluded that the characteristics of the installation and the associated disturbances influence the behavior of the pile more than the number of helices under cyclic loadings.

According to El Sharnouby M. , (2012), the top helix contributes more to the cyclic compression resistance of a pile than the other helices, based on his testing of a triple-helical pile (8", 10" and 12" helix- diameter) subjected to one-way cyclic loading. Moreover, it has been proven that three helices increase the resistance of a pile to the fluctuation in water table levels when the helices are embedded below the average water table and are subjected to vertical dynamic loadings. To minimize creep during dynamic loadings, triple- and quadruple-helix piles should be installed to the design torque and below the lowest known water table. Moreover, Cerato & Victor, (2008, 2009) found that a triple-helix pile (8, 10 and 12 inch) performed well in minimizing creep subjected to long-term cyclic loading when the top helix was embedded 11 feet below the water table. A double-helix pile (8 and 10 inch), however, with the top helix embedded about 15 feet below the water table experienced a high rate and magnitude of displacement which could be due to spanning a weaker soil layer or having a smaller bearing area that did not allow the anchor to "set" during tensile loads.

2.4.2. Shaft section shape (geometry)

Commercially, circular pipe shafts present larger cross-sectional areas than square shafts and therefore they provide a greater structural capacity under certain loading arrangements. For example, they may provide more resistance to buckling and bending as a result of their geometry. Nevertheless, the installation of square shafts produces

fewer disturbances than pipe section shafts (Abdelghany, 2008), and as explained in previous sections, the capacity and behavior of helical piles under cyclic loadings is greatly influenced by the quality of installation and by the disturbances of the soil. Therefore, it could be expected that the axial compression and tension performance of helical piles with square shafts would be higher than the performance of pipe cross-section piles, as the soil bearing is stronger. Furthermore, the installation process is expected to be more efficient with square shafts as the extensions are easily installed (i.e., bolts are not needed). According to (Abdelghany, 2008) the resistance of a helical pile with square shaft is due to the bearing associated with the helices, while the circular-shaft helical piles works with bearing from the helices and skin friction. Furthermore, under one-way cyclic compression loadings, the contribution of the shaft depends on the level of loading.

2.1. Liquefaction and cyclic loading of sands

Saturated cohesionless soils under undrained conditions are susceptible to liquefaction under monotonic, transient, or cyclic loadings (in loose soils), as a result of the increase in pore-water pressure and consequently the loss in shear strength. The tendency of loose soils to decrease in volume when they are sheared is appreciated at a micro-scale as the soil skeleton structure tend to rearrange the soil particles into a denser structure, the volume of voids is reduced and the water in the void spaces is forced out. When drainage is restricted, however, the pore water pressure increases as the effective stress decreases, therefore the shear resistance of the soil is reduced. When the shear resistance of the soil

is lower than the static driving shear stress, the soil can experience large deformations (Martin, et al. 1975; Seed & Idriss, 1982). The liquefaction phenomenon can be divided in two categories: flow liquefaction and cyclic mobility. The first type generates the greatest damages as is characterized by large deformations produced by static shear stresses (the shear stress required for static equilibrium of the soil), when they are greater than the shear strength of the soil in its liquefied state. Although cyclic mobility can also produce large deformations, it occurs when the static shear stress is less than the shear strength of the liquefied soil, and the deformations are developed incrementally due to both static and cyclic shear stresses (lateral spreading). Nevertheless, for dense sands subjected to cyclic loadings an initial state of deformation may be presented. As the shear strain increases, dilation is observed and the excess pore water pressure decreases, leading to an increase in shear strength.

Deep foundations frequently fail under seismic loadings due to liquefaction and the reduction in bearing capacity (Kishida, 1996). Nonetheless, liquefaction affect foundations especially on the surficial soil layers (upper 30 to 50 feet) of a loose sand deposit (Martin & Lam, 1995). Moreover, Ashford et al., (2006) characterized the moment distribution in a liquefiable layer when a steel pipe-pile of 12.5 inch of diameter by 37.7 feet was embedded in a layered profile (composed by silty sand overlying a 11.5 feet layer of fat clay, overlying a 3.2 feet layer of loose liquefiable sand and followed by gravel bedrock). He found that the maximum bending moment was observed at the top of the dense gravel bedrock, and in the liquefiable sand layer the moment distribution of the piles was linear. Nonetheless, as will be discussed later, the maximum bending

moment under earthquake-induced liquefaction, generally is encountered in the boundaries between liquefiable and non-liquefiable layers.

The behavior of piles embedded in liquefiable soils when they are subjected to earthquake loadings has been studied widely. For instance, Mizuno et al., (2000) concluded that each pile of a 2 steel-pile group embedded in Kasumigaura sand at the beginning of a liquefaction event was greatly affected by the inertial forces, but as liquefaction progresses, the behavior of a pile was governed by the soil movement. Even more, at a high excess pore water pressure ratio (excess pore water pressure by effective overburden pressure) a large damping ratio and a low resonant frequency was observed, while exactly the opposite was observed at low excess pore water pressure ratios (Mizuno et al., 2000b). Another test (Haeri et al., 2012) conducted on small-scale aluminum pipe piles in a layered profile (silica sand a liquefiable layer overlying a non-liquefiable layer) concluded that under 1-g accelerations, the piles reached the maximum displacements (1.42 inch) and maximum bending moments just minutes after lateral spreading, but the displacement was reduced to a residual value of 0.24 inch during the rest of the shaking, and the bending moment also was reduced continuously during the rest of the shaking. This could be explained by the fact that maximum moments are observed in the transition prior to liquefaction and at the beginning of liquefaction or induced lateral spreading. Then, at the stage of 'slow flow', a rebound in the maximum displacements and moments are observed (Tang, et al., 2015). In addition, the stiffness of the soil and the horizontal subgrade reaction are recovered with the dissipation of the excess pore water pressure (Mizuno et al., 2000b). Furthermore, it has been concluded that maximum lateral

displacements of the pile head increase when the peak acceleration increases and/or when the predominant frequency decreases. It has been concluded that the pile settlement increases as the predominant frequency decreases (Naeini et al., 2013).

A factor that has a significant influence on a pile response when it is subjected to ground motions is the water table level as it influences the liquefaction susceptibility of the soil. Liquefaction is frequently observed in areas with a ground water table within a few meters of the ground surface. A previous research showed that at a low water table level (4.6 ft below the ground surface) the pile's internal bending moments are lower than when water table levels are at the ground surface (Mizuno et al., 2000). Therefore, several p-y curves and relationships had been developed to characterize the behavior of deep foundations in liquefiable soils with different water table levels. Although some of the p-y curves obtained have some limitations (i.e. allowable depth of liquefiable zone, relative density and/or maximum soil resistance) (Gerber, 2003), all of the p-y curves show that for liquefiable sands an increase in soil resistance is observed as the lateral deflection increases. Furthermore, it has been shown that the behavior under lateral spread pressures is greatly influenced by the pile material. Cubrinovski et al., (2006) tested a single steel pipe-pile and a single pre-stressed high-strength concrete pile with the same dimensions (16 foot long and 1 foot diameter) and concluded that the steel pile presented a larger lateral resistance and reached just 60% of the yield moment at a constant displacement of 2 inch. The pre-stressed high-strength concrete pile reached the yield moment at 3.54 inch of displacement at the same loading level and failed at a lateral displacement of 6.7 inch.

Consequently, a FEM model should include the pile-soil separation to predict accurately bending moments and deflections as (Hussien, et al., 2010) corroborated.

A study conducted on model piles concluded that the maximum bending moments are observed at the interfaces between liquefied soil and non-liquefied strata (Abdoun & Dobry, 2002). In addition, several research and case studies that exhumed reinforced concrete piles (Hamada, 2000; Hamada, M., 1992a.; Hamada et al., 1988; Kawamura et al., 1985; Yoshida, N. & Hamada, M., 1990) up to 20 years after the 1964 Niigata earthquake (7.6 Mw), observed that the piles of several structures (i.e., Niigata Family franglible Court House concrete piles, S-Building reinforced-concrete friction piles and east bridge over railway concrete piles) were broken exactly at the elevations where were the boundaries between the non-liquefied soil and the liquefiable soils. Even more, a posterior analysis determined that during the first 7 seconds of shaking, inertial forces governed the piles behavior. Lateral spreading of the ground started at 83 seconds, however, (Bhattacharya et al., 2014) and therefore, most of the failures were caused by the ground movement. A photo of one of the exhumed reinforced concrete piles is shown in Figure 4. The NHK building in Niiagata used reinforced concrete piles (13.8 inch diameter and 39.4 feet) and after the earthquake the foundations were severely damaged, but the building continued to be used after superficial repairs to the floor were made. The piles were exhumed 20 years after the earthquake and a picture is shown in Figure 5.

Figure 4. Broken reinforced concrete pile of S-building, from (Yoshida & Hamada, 1990)

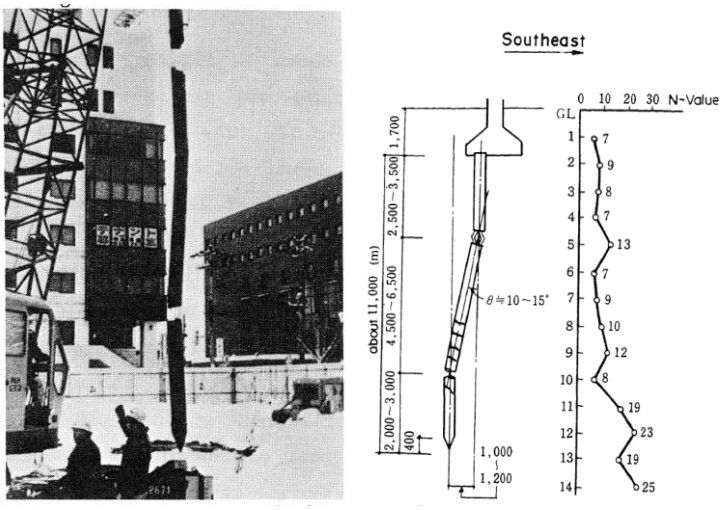

Figure 5. Damaged pile of the NHK-Building, from (Kawamura et al., 1992)

Figure 6 shows the deformation obtained on a broken reinforced concrete pile (11.8 inch diameter and 32.8 feet long) from the collapsed bridge Yachiyo in the neighborhood of Niigata Railroad Station. The soil profile was composed of sandy silt, overlying a layer

of medium sand, over fine sand, and the N-values are reported in Figure 6. From the analysis conducted to the piles, a theory proposed that more of the cracks were concentrated at the points where the greater bending moments were generated and the failure was produced by ground displacements that exceeded the shearing resistance of the piles as they were restricted at the top by the girders. Furthermore, a steel pipe-pile of 2 feet of diameter and 82 feet long was exhumed from the Showa Bridge after the Niigata earthquake. The bridge was composed of a simple steel girder with pile foundations. Even though the construction of this bridge was completed just five months before the earthquake in a medium sand overlying layers of fine sand, the piles presented a deformation and bent toward the right as observed in Figure 7. Nevertheless, two contradictory theories has been proposed to explain the failure. Hamada, (1992a.) based his theory on eye-witnesses testimonies. He proposed that the collapse of the bridge was caused by permanent ground movements that deformed the piles and caused the girders to fail. Nevertheless, a theory based on a numerical model (non-linear Beam on Nonlinear Winkler Foundation) analyzed by a finite-element-based structural analysis program, concluded that the failure of the bridge was caused by the difference in natural periods between the ground motion and the bridge. At 70 seconds from the beginning of the earthquake a jolt was produced (Bhattacharya et al., 2014), generating large displacements and unseating the deck, which triggered the collapse of the bridge. Even more, it was reported that the bridge did not collapsed during full liquefaction. The Japan Society of Civil Engineers, (1966) reported that the difference in natural periods caused relative displacements that exceeded the allowable displacement of the piles and produced the bridge failure. In conclusion, according to the exhumations conducted 20

years after the 1964 Niigata earthquake, the reinforced concrete piles exhumed from the Yachiyo Bridge (peak residual deformation at pile head 41.34 inch) presented a lower peak residual deformation after the the Niigata earthquake than the steel pipe-piles extracted from the Showa Bridge (peak residual deformation at pile head 78.74 inch), even though, the slenderness ratio of the steel pipe-pile was 1.23 times the slenderness ratio of the reinforced concrete pile. Nevertheless, the N-values recorded on the Yachiyo Bridge area were slightly higher.

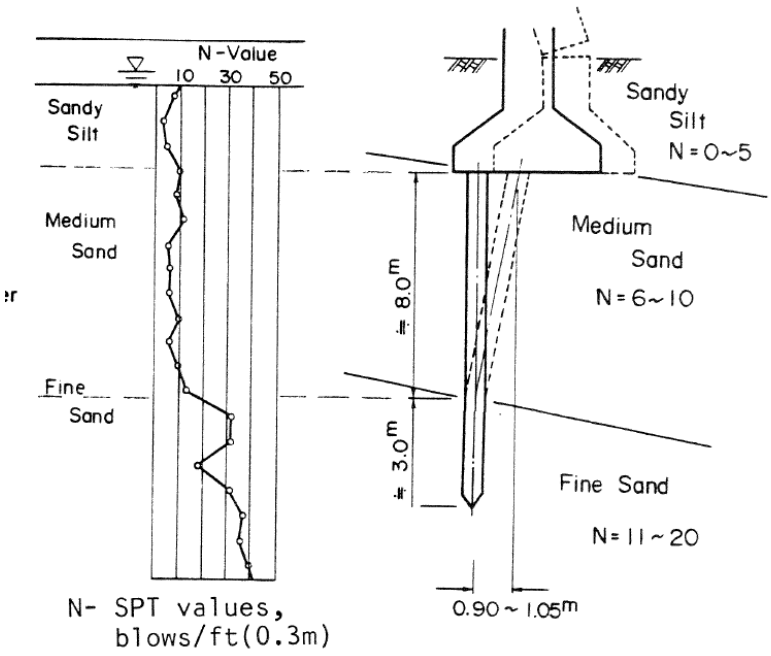

Figure 6. Deformation of broken pile of the Yachiyo Bridge (units in meters), from (Kawamura et al., 1985)

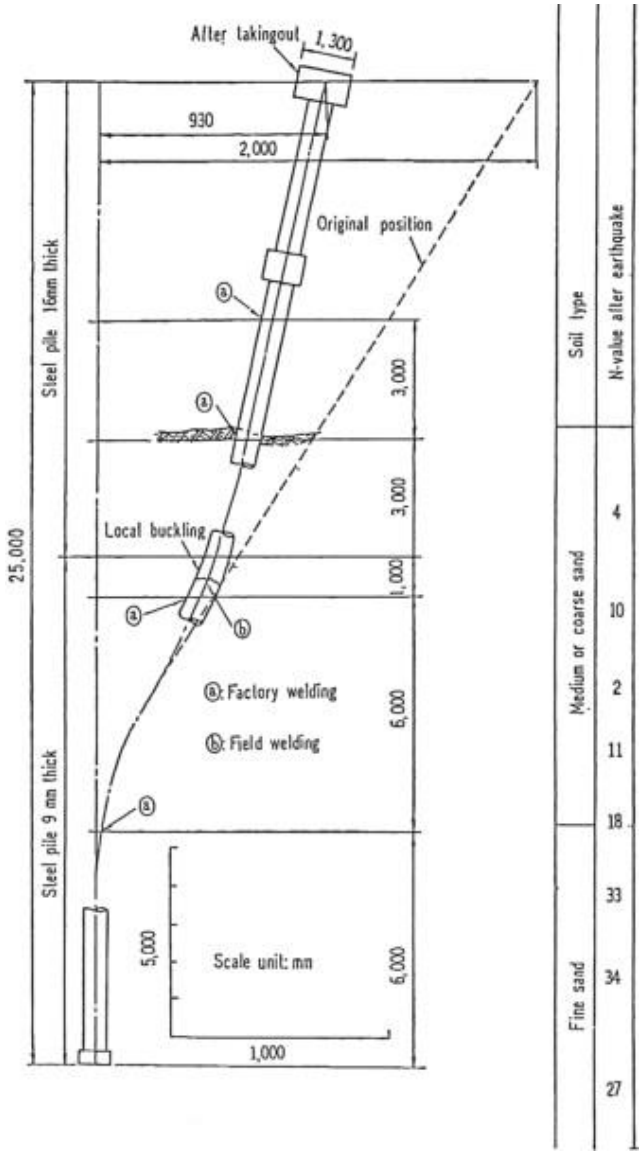

Figure 7. Deformation of a steel-pipe pile of the Showa Bridge after the Niiagata earthquake (units in milimiters), from (Hamada, M., 1992a.)

Tests on model piles embedded in similar soil conditions as the Niigata case-studies were conducted to quantify the behavior of the piles under liquefaction and the results demonstrate a clear deformation between the boundary of the non-liquefiable soil and the liquefiable layer (Hamada, 2000). Even more, after the assessment of several structures damaged by major earthquakes such as the 1923 Great Kanto earthquake (7.9 Mw), the

1948 Fukui earthquake (6.8 Mw), the 1983 Nihonkai-Chubu Earthquake (7.9 Mw) and the 1990 Luzon earthquake (7.8 Mw) it was concluded that the governing factors that cause damages to structures are permanent ground displacement caused by lateral spreading and liquefaction (Hamada, M., et al., 1988; Wakamatsu, K., et al., 1992; Hamada et al., 1992a; Hamada et al., 1992b; Hamada, 1992b.). Nonetheless, Bhattacharya, et al., (2012) points out the deficiencies of the proposed pile failures theories and thinks that the piles behave as an unsupported long slender column that buckles due to the axial forces produced by the super structure; lateral loads (slope movement, inertia or any eccentricities) on the other hand, increase deflection.

Liquefaction is a major concern for the geotechnical engineering community, therefore, different alleviation measures had been tested to reduce the damages induced during earthquakes in structures constructed in liquefiable soils, and the more relevant are presented in this chapter. Ashford et al., (2000) tested a full-scale steel fiber reinforced grouted pile and a group of two by two steel pipe piles embedded in loose sand overlying layers of fat clay and silty sand. He found that ground improvement through the installation of stone columns around the piles in a 4 by 6 grid increased the performance of the piles, as they increase the density of the soil and the stiffness of the foundation by more than 2.5 to 3.5 times. Nevertheless, increasing the diameter of the piles by 50% or doubling the number of piles did not affect the performance of the foundation. This conclusion is supported on a case study conducted on the Hokuriku-Building located in Japan, where no damage was presented on the superstructure, nor cracks or inclination was observed after the Niiagata earthquake, due to the implementation of several

reinforced concrete piles that induced densification of the soil and prevented lateral ground displacements. The addition of various materials has been shown to reduce liquefaction potential, including soft clay layers and sand-type clays. For instance, soft clay layers were found to reduce the bending moments produced at the pile head of small-scale piles embedded in liquefiable sand, more over, it reduced the maximum pile head displacement by a factor of 2 (Abdoun & Dobry, 2002). Another study showed that vertical drains are not effective to reduce excess of pore water pressure during earthquakes, but they reduce the time of dissipation by a factor of 4 after the earthquake (Mizuno et al., 2000).

Even more, sand-tyre mixtures were texted under a wide range of amplitudes, it was concluded that at gravimetric contents of tyre chips greater than 20%, the liquefaction potential is reduced for all the amplitudes tested, more over, at gravimetric contents of tyre chips of 30%, the damping ratios and the number of cycles required for liquefaction increases (Mashiri et al., 2015).

2.2. Construction codes and regulations: Seismic Resistance

Deep foundations are required to resist earthquake loads depending on their seismic design category. According to Perko H. , (2009) helical piles can be designed using the same procedures specified in the Interational Building Code (IBC) for deep foundations. Nevertheless, special attention should be provided to structures constructed in liquefiable soils, as the 2014 International Building Code specifies that deep foundation elements

standing unbraced in water or fluid soils must be classified and designed as columns from the top down to the point where adequate lateral support is provided. For piles embedded in stiff soil this is the first five feet and for piles embedded in soft soil this is the first ten feet (to prevent buckling) (International Code Council, 2014). Nevertheless, for a cast-in place foundation with a ratio of unsupported height to least horizontal dimension of less than three, the element should be designed as a pedestal according to the ACI 318. In addition, all deep foundations that are not defined as a laterally braced pile must be designed in accordance to the minimum unbraced length. Conversely, the Acceptance Criteria for helical foundations, the AC358, was adopted in June 2007 by the IBC and is frequently used by building officials in non-seismic areas as an evaluation guideline (Perko H. , 2007).

2.2.1. Site classifications

According to chapter 7 of (American Society of Civil Engineers (ASCE), 2005), soil classification should be conducted based on the information obtained for the upper 100 feet and the soil properties could be estimated from geologic conditions. Nonetheless, when the information is not available and the authorities or the geotechnical data do not provide any recommendations that specify that either site E or F are present, site class D should be used. Site classification is summarized in Table 6.

Table 6. Site classification , adapted from (American Society of Civil Engineers (ASCE), 2005)

Site Class	Soil Profile Name	Soil Shear Wave Velocity, vs (ft/s)	Standard Penetration Resistance, N	Strength,Su (psf)
A	Hard Rock	> 5000	NA	NA
B	Rock	2500 to 5000	NA	NA
C	Very dense soil and soft rock	1200 to 2500	>50	>2000 psf
D	Stiff soil	600 to 1200	15 to 50	1000 to 2000 psf
E	Soft clay soil	< 600	<15	< 1000 psf
		Any profile with more than 10 ft of soil having the following characteristics: - Plasticity index PI >20, - Moisture content w ≥ 40% and Undrained shear strength Su < 500 psf		
F	Soils requiring site response analysis in accordance with section 21.1	1. Soils vulnerable to potential failure or collapse under seismic loadings; liquefiable soils, quick and highly sensitive clays, collapsible weakly cemented soils. (except for structures having fundamental periods of vibration ≤ 0.5s, site-response analysis is not required to determine spectral accelerations for liquefiable) 2. Peats and/or highly organic clays with thickness > 10 feet. 3. Very high plasticity clays with thickness > 25 feet and PI > 75. 4. Very thick soft/medium stiff clays with thickness >120 ft and su <1000 psf		

2.2.2. Seismic design categories

Seismic design categories are assigned considering the risk category and the severity of the design earthquake ground motion at the site (International Code Council, 2014). Risk categories I and II are assigned for agricultural buildings, temporary facilities, minor storage facilities and other low-occupancy structures, category III is assigned to high-occupancy structures and category IV represents essential facilities. To determine the seismic design category of a project, first it is necessary to obtain the mapped spectral

accelerations for short periods, S_S, and/or the mapped spectral accelerations for a 1-second period, S_1, which are available in figure 1613.3.1.(1) through 1613.3.1(8) of the IBC 2014. An example of the conterminous United States of 0.2-second (short period) spectral response acceleration is shown in Figure 8. Secondly, it is necessary to calculate the maximum considered earthquake spectral response acceleration for short periods, S_{MS}, and/or at 1-second period, S_{M1}, adjusted for site class, according to Equation 3 and Equation 4,where F_a and F_v are site coefficients that are determined according to Table 7 and Table 8. Finally, the design spectral response acceleration parameters are determined with Equation 5 and Equation 6, to then obtain the seismic design category using either Table 9 or Table 10.

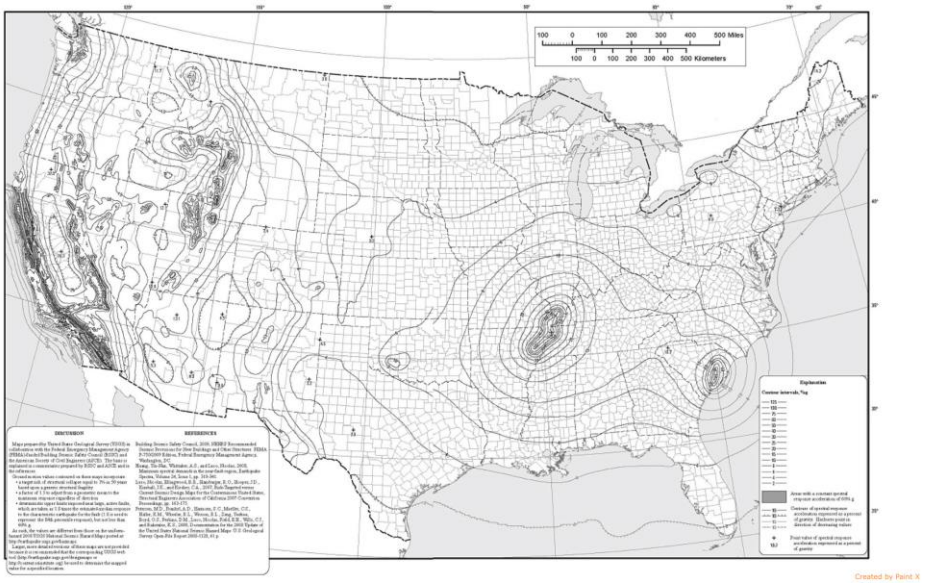

Figure 8. Conterminous United States of 0.2-second spectral response acceleration, adapted from (International Code Council, 2014)

Equation 3. Maximum considered earthquake earthquake spectral response acceleration for short periods

$$S_{MS} = F_a * S_S$$

Equation 4. maximum considered earthquake spectral response acceleration at 1-second period

$$S_{M1} = F_v * S_1$$

Table 7. Values of site coefficient, Fa, adapted from (International Code Council, 2014)

Site Class	**Ss ≤ 0.25**	**Ss=0.5**	**Ss=0.75**	**Ss=1**	**Ss≥1.25**
A	0.8	0.8	0.8	0.8	0.8
B	1	1	1	1	1
C	1.2	1.2	1.1	1	1
D	1.6	1.4	1.2	1.1	1
E	2.5	1.7	1.2	0.9	0.9
F	Necesary to conduct a site response analysis (include base ground motions, site condition modelling and site response analysis, consult				

Table 8.Values of site coefficient , Fv, adapted from (International Code Council, 2014)

Site Class	**S1 ≤ 0.1**	**S1=0.2**	**S1=0.3**	**S1=0.4**	**S1≥0.5**
A	0.8	0.8	0.8	0.8	0.8
B	1	1	1	1	1
C	1.7	1.6	1.5	1.4	1.3
D	2.4	2	1.8	1.6	1.5
E	3.5	3.2	2.8	2.4	2.4
F	Necesary to conduct a site response analysis (include base ground motions, site condition modelling and site response analysis, consult				

Equation 5. Five-Percent damped design spectral response acceleration at short periods, S_{DS}, from (International Code Council, 2014)

$$S_{DS} = \frac{2}{3} * S_{MS}$$

Equation 6. Five-Percent damped design spectral response acceleration at 1-second periods, S_{D1}, from (International Code Council, 2014)

$$S_{D1} = \frac{2}{3} * S_{M1}$$

Table 9. Seismic design category based on short period (0.2 second) response acceleration

Values of SDS	**RISK CATEGORY**		
	I or II	**III**	**IV**
SDS < 0.167g	A	A	A
0.167g ≤ SDS < 0.33g	B	B	C
0.33g ≤ SDS < 0.5g	C	C	D
0.5g ≤ SDS	D	D	D

Table 10. Seismic design category based on 1-second period response acceleration

Values of SDS	**RISK CATEGORY**		
	I or II	**III**	**IV**
SD1 < 0.067g	A	A	A
0.067g ≤ SD1 < 0.133g	B	B	C
0.133g ≤ SD1 < 0.2g	C	C	D
0.2g ≤ SD1	D	D	D

According to the IBC, structures classified as risk category I, II or III with a value of S_1 greater than or equal to 0.75 correspond to the seismic design category E. On the other hand, structures classified as risk category of IV with S_1 greater than or equal to 0.75 correspond to the seismic design category F. Furthermore, for structures assigned to seismic design categories D, E or F, the International Building Code require not just a geotechnical investigation analyzing the liquefaction potential, slope instability, total and

differential settlements, and lateral spreading or flow, but it also requires providing a more detailed dynamic analysis and mitigation measures. For seismic design categories D, E or F, the section 18.13 of the ACI 318 must be used during the design of deep foundations under seismic loadings (with the exception of detached one- and two-family dwellings of light frame construction and two stories or less above grade plane). Nevertheless, the conditions of the international building code from sections 1808 to 1810 prevail over the specifications of ACI 318. According to (American Society of Civil Engineers (ASCE), 2005) for site class E or F foundations, they should be "*designed and constructed to withstand maximum imposed curvatures from earthquakes ground motions and structure response*". Therefore, the free field soil strains should be modified for soil-foundation-structure interaction. More over, the analysis should contemplate the deformation of foundation elements. In addition, the ACI 318 specifies the reinforcement required for concrete columns and structures to resist seismic loadings. Finally, the design of structures on seismic design categories A and B should be conducted considering seismic load combinations. Further instruction on how to design pile caps and the connection between piles and the pile cap are provided in (International Code Council, 2014). Even more, Perko (2009) stated that "*helical pile couplings need to develop the full tensile strength of the pile or be designed to resist seismic load combinations.*"

3. MATERIALS AND PROCEDURES

3.1. General

The tests were conducted on a laminar shaking box located at the University of California - San Diego. This test used an existing sand bed that had been shaken several times with a buried tunnel. The tunnel was removed and the sand bed was built up to a 15 foot depth in 1 foot intervals. The sand was compacted to 100% relative density to maintain the base sand. The sand bed was instrumented every foot on the east, center and west sides. To correlate the seismic performance of helical piles with their specific geometric and shape characteristics, as well as to compare their behavior with other types of deep foundations, a full-scale testing plan was determined and implemented. The plan included testing a total of seven pipe helical piles with two diameters (3.5” and 5.5”), using a single helix configuration and a 3.5” helical pipe pile with a double helix configuration, even more, one of the 3.5” single helical pipe piles had a longer length. A 3.5” driven pipe pile and a 3” square shaft helical pile (with similar cross sectional areas as the 3.5” helical pipe piles), were selected in the hopes of comparing installation methods as well as geometry. Five days of testing were conducted in the research plan: Day 1 tested the dry dense sand bed only, to understand the shear wave velocity and shear wave propagation; Test Day 2 consisted of shaking the box with the embedded piles to understand the increase in stiffness in the system and to understand the kinematic behavior of the soil-pile system. Test Day 3 included inertial concrete weights on top of each pile head. Test Day 4 tied four of the 5.5” helical piles together in a group and four of the 3.5” helical piles together

in a group and used a fixed connection, nevertheless on Test Day 5 a pinned connection was used. This thesis focuses on Test Day 3.

To accurately simulate an earthquake condition, the instrumented helical piles were installed on the largest outdoor shake table in the country where seismic inputs were applied on each Test Day to simulate the Great Hanshin and Northridge earthquakes at 50%, 75%, and 100% of their respective amplitudes. The unscaled time histories of the Northrige and Takatori earthquakes are presented in Figure 9. The frequency content of the unscaled Northridge and Takatori earthquakes are presented in Figure 10. According with the fast fourier spectra performed, the energy content of the Takatori earthquake was concentrated within the range of 0.5 Hz to 1.5 Hz, while the energy content of the Northridge earthquake was spread over a wide range, and within higher frequencies (2 Hz to 5 Hz). The maximum acceleration applied to the shaking table was estimated at 0.67g and in a one-dimensional direction (east-west). The installation of the ten instrumented piles was conducted by a professional contractor, who also supervised the installation of the inertial weights. A description of the instrumentation, testing setup, equipment and a description of the testing procedures are provided on the following sections.

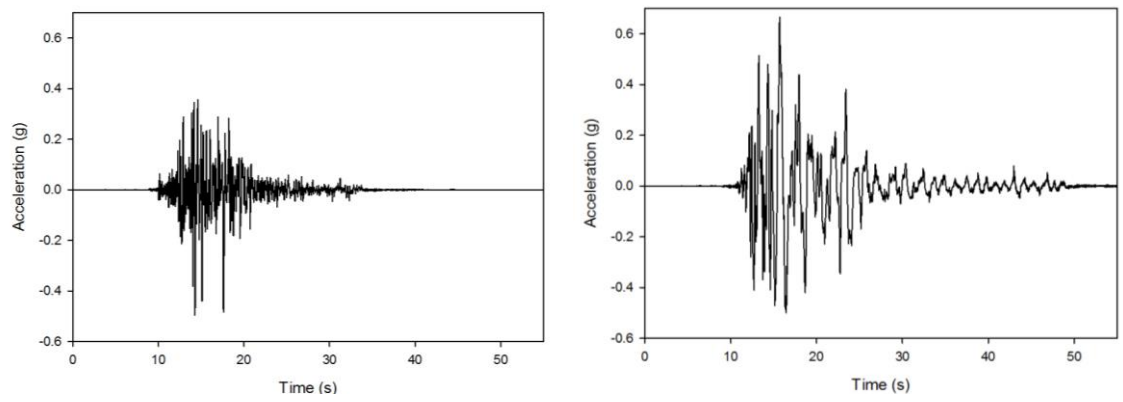

Figure 9. (a) Northridge Unscaled time history, (b) Takatori Unscaled time history

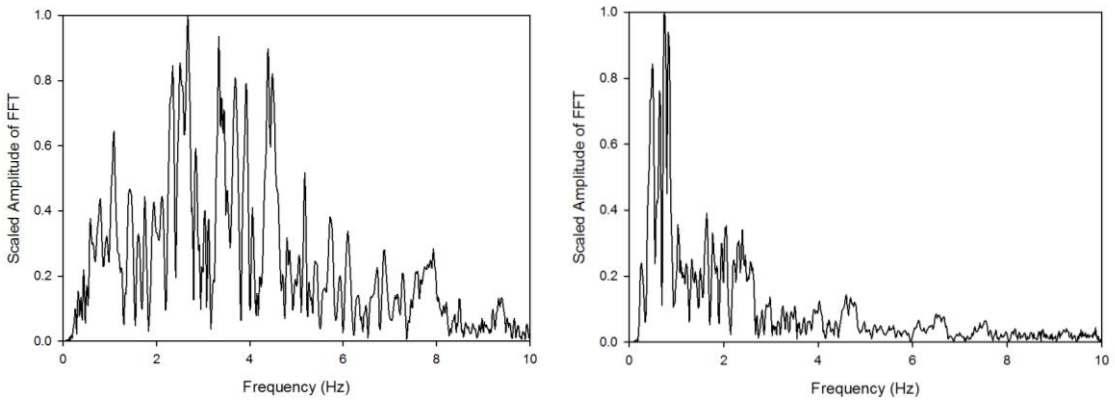

Figure 10. Frequency content of Unscaled (a) Northridge earthquake, (b) Takatori earthquake

3.2. Pile description and Instrumentation

The characteristics of the piles used in the test are summarized in Table 11. The shaft of nine helical piles and one driven pile were marked with chalk along the East, West, North and South axes. Then the grid location of strain gauges were marked at 6-8 levels, as the shake table is bidirectional on the East-West plane. Vertical strain gauges were marked to register bending moment on the East and west axes and holes were drilled to introduce

the strain gage wires internally and then were covered with silicone. The surface of each strain gage location was prepared with a 60-grit sanding wheel, then a 120-grit, a 220-grit and finally a 320-grit sand paper was used to ensure a smooth surface. A layer of laquer thinner and acetone was then wiped on the steel to completely clean the surface. During the gauge sticking procedure, an anti-static tape was used to fix the gauge to the steel shaft as illustrated in Figure 11, and the gage was stuck with a special glue and held in place with a static-free tape for 1 minute to assure proper bonding. Then an epoxy layer was applied to protect the gauges and the wires, a silicone layer was used to protect the wire holes, then fiberglass tape and resin covered each strain gage level to add an additional layer of protection during installation. A total of 152 strain gauges were installed and connected as quarter bridges to the data acquisition system. The shafts were also instrumented with accelerometers at the pile heads to record accelerations; all the accelerometers were installed on the east sides of the piles to facilitate their connection to the measuring system.

Table 11. Pile properties

Pile	Type	Outside Diameter (in)	Wall Thickness (in)	Yield Strength, Fy (ksi)	Length of Pile (ft)	Pile Head Above Ground (ft)
P1	3.5" Single Helix Single bolt	3.47	0.25	65	13	1
P2	3.5" Single Helix Double bolt	3.47	0.25	65	12	1
P3	3.5" Single Helix Double bolt	3.47	0.25	65	12	1
P4	3.5" Double Helix; Double bolt	3.47	0.25	65	12	1
P5	Driven Pile	3.47	0.25	65	12	1
P6	Square Single Helix		0.25	60	12	1

Pile	Type	Outside Diameter (in)	Wall Thickness (in)	Yield Strength, Fy (ksi)	Length of Pile (ft)	Pile Head Above Ground (ft)
P7	5.5" Single Helix Double Bolt	5.5	0.425	80	14	2.83
P8	5.5" Single Helix Double-Bolt	5.5	0.425	80	14	2.83
P9	5.5" Single Helix Double-Bolt	5.5	0.425	80	14	2.83
P10	5.5" Single Helix Double-Bolt	5.5	0.425	80	14	2.83

Figure 11. Strain gauge installation procedure

As noted in Table 11, for 3.5” piles, pile 1 had a total length of 13 ft (Figure 12) and the rest of the piles had a total length of 12 ft, which were instrumented around each foot from the pile head as illustrated in Figure 13 and Figure 14. On the other hand for the 5.5” piles; piles 7, 8, 9, and 10 had a total length of 14 ft, and were instrumented as illustrated in Figure 15. The push pile was instrumented as illustrated in Figure 16 and the square shaft helical pile was instrumented as illustrated in Figure 17. The strain gauges in gray demonstrate the instrumentation lost during installation. The accelerometer arrangement is illustrated in Figure 18.

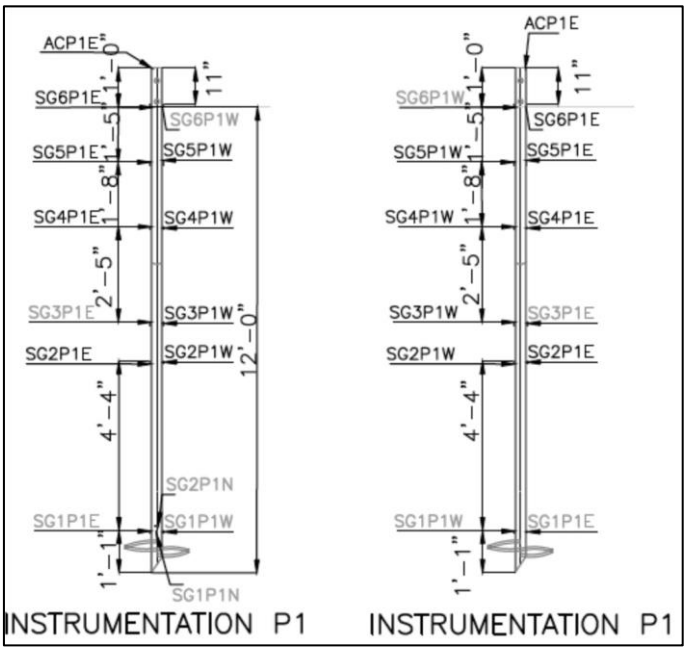

Figure 12. Instrumentation from North and South view for the larger single 3.5" helical pipe pile.

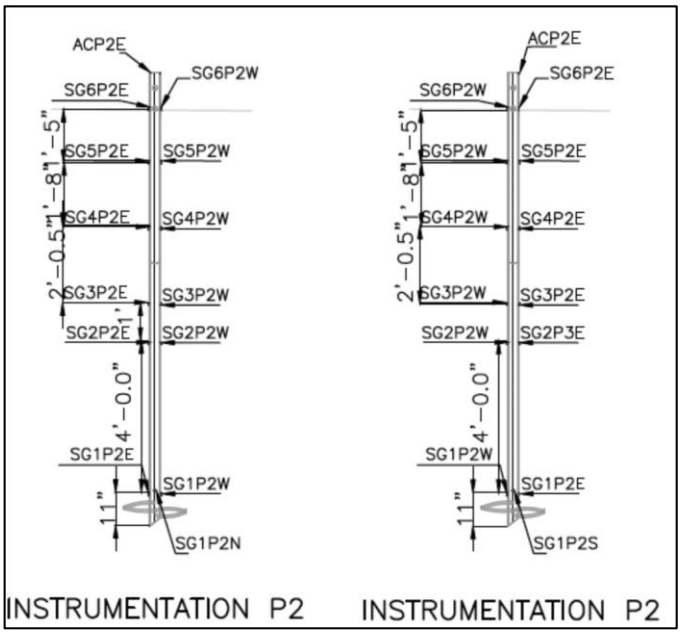

Figure 13. Instrumentation from North and South view for the single 3.5" helical pipe piles

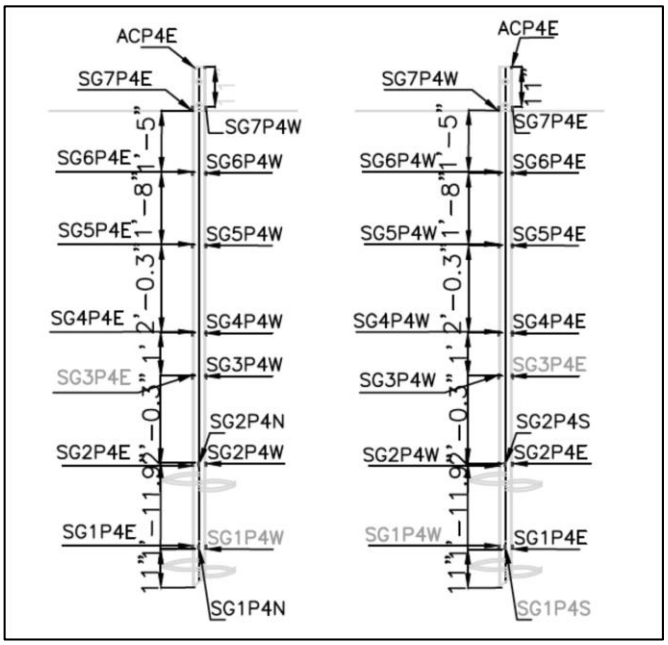

Figure 14. Instrumentation from North and South view for the double helical pile.

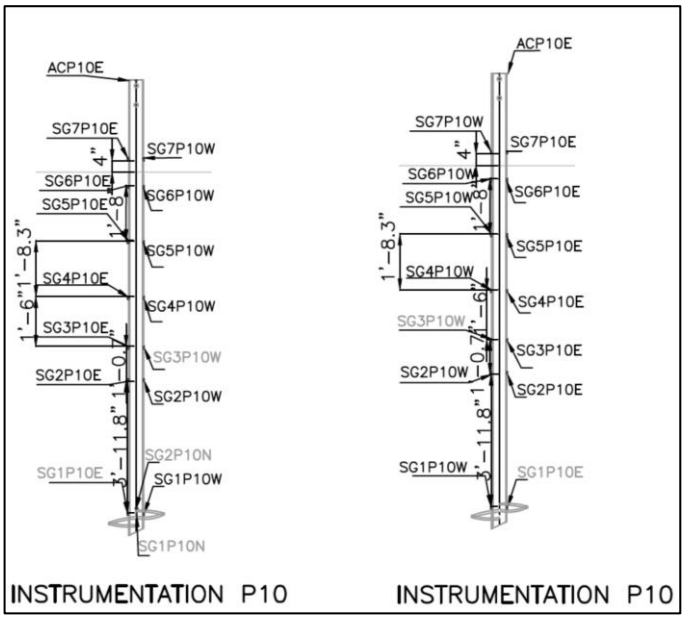

Figure 15. Instrumentation layout North and South views and for all 5.5" O.D Piles., The gray accelerometers did not work during the test.

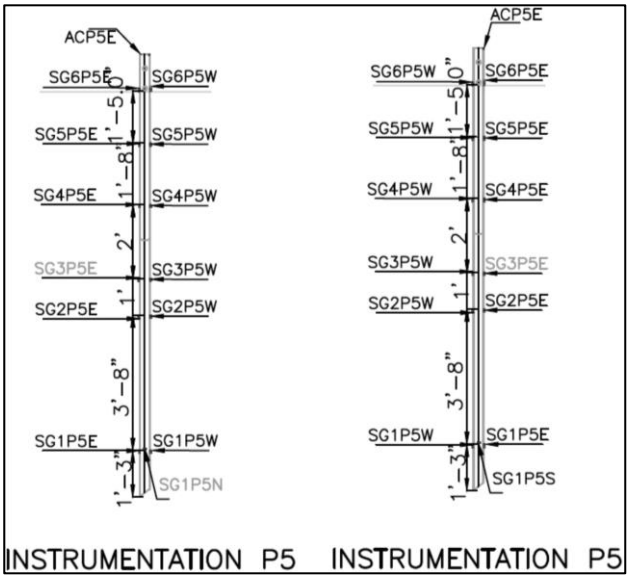

Figure 16. Instrumentation layout for North and South views for the 3.5" O.D push piles

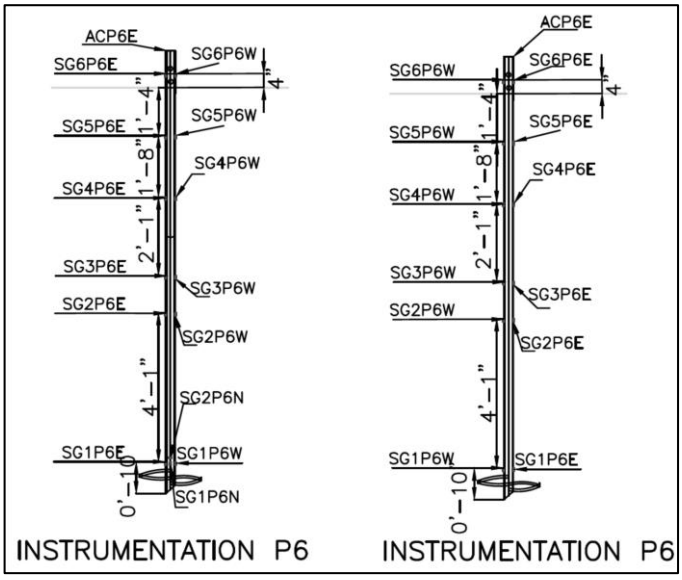

Figure 17. Instrumentation layout for North and South views for the 3" O.D square shaft pile

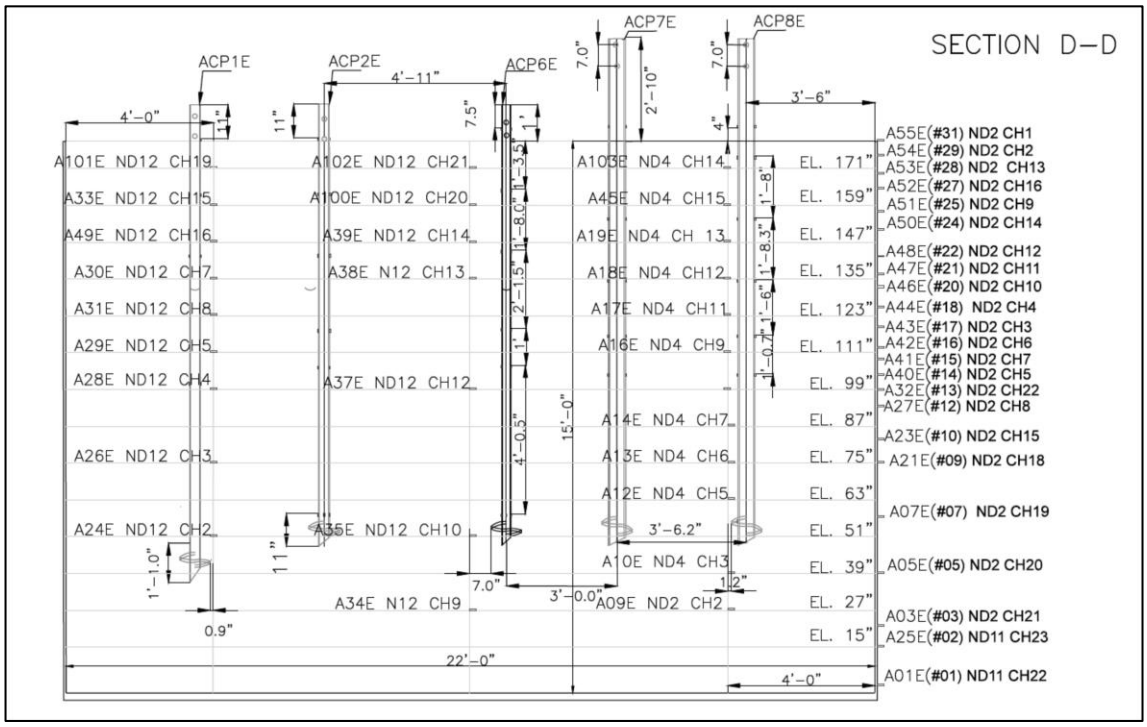

Figure 18. Accelerometer arrangement,

3.3. Shake Table description

The large outdoors shake table of the University of California, San Diego has a plane area of 24.93 ft by 40 ft and a vertical payload capacity of 4.4 million pounds. A picture of the facility is illustrated in Figure 19. The maximum horizontal peak ground of the table alone is over 1g, and the combined force capacity of the actuators is 6.8 MN. The maximum overturning moment is 50 MN-m. In addition, the maximum peak velocity is 1.8 m/s and the maximum stroke is 2.5 ft.

Figure 19. Outdoor shaking table at University of California San Diego, from: http://nheri.ucsd.edu/facilities/shake-table.shtml

3.4. Large Soil Confinement Box

The design and construction of the shaking box was executed by (Sander, et al., 2013). After an extensive analysis, the weight of the original box design had to be reduced to achieve a minimum acceleration of 0.7g. Even more, the flexibility of the structure should be reduced by the incorporation of stronger connections in order to resist the maximum dynamic force from the wall. In addition, the cantilever floor required a higher stiffness to avoid contact with the pad surrounding the table, therefore, the interior width and height of the box were reduced to 15.1 ft and 22.97 ft, respectively, which resulted in a lower overturning moment demand. Numerical simulations, using the finite difference code FLAC, were tested using an elastic material approach to determine the viability of the rear fluid boundary condition, which consisted of a water-filled geomembrane bladder that allowed for 10% of shear strain of the backfill soil (22.97 ft height and friction angle of 30º). The hydrostatic pressure from the bladder approximated the static lateral soil pressure from the soil column. Even more, side boundaries were incorporated, which initially was conceived to be composed of a thin layer of bentonite slurry between two geomembranes to maintain a low friction and plain strain condition. During the

numerical simulations, two cycles of sinusoidal motion were applied to the base with a frequency of 1 Hz and a peak acceleration of 0.5g. It was concluded that the fluid boundary condition was not suitable, and a semi-flexible, energy-absorbent geofoam boundary would be used instead, which allows for two-way shearing and some dissipation of wave energy.

The final design of the large soil confinement box consisted of an exterior steel frame with interior precast reinforced concrete panels (height 10 ft to 25 ft) that were assembled and post-tensioned to the large shaking table. The final box dimensions were; 24.93 ft height (composed by 18 horizontal panels), 19 ft width, and 33.14 ft of length. The minimum fundamental frequency is 30 Hz in the longitudinal direction and maximum out-of-plane deflections of 6 mm along the side walls were predicted. Even more, tests conducted on the empty box indicate first resonance at 22-23 Hz. Thicker panels (1 foot) were used along the traverse walls and 0.833 ft thick panels were used along the side walls to comply with the shear demand at the corners. Furthermore, the Mechanically Stabilized Earth (MSE) wall tested was 16.4 ft to 22.97 ft high and the foundation is composed of soil layer, the rear boundary condition is composed of geofoam, the side boundary condition was constructed with multiple layers of plastic sheets and grease instead of bentonite slurry, because it present lower desiccation issues. A layout of the conceived design of the shaking box is illustrated in Figure 20, nevertheless the box offers flexibility in order to accommodate the dimensions to the desired height, and it could be fixed into two configurations; a narrow (15 ft wide) and a wide configuration (19 ft) (Fox, et. al, 2015) .

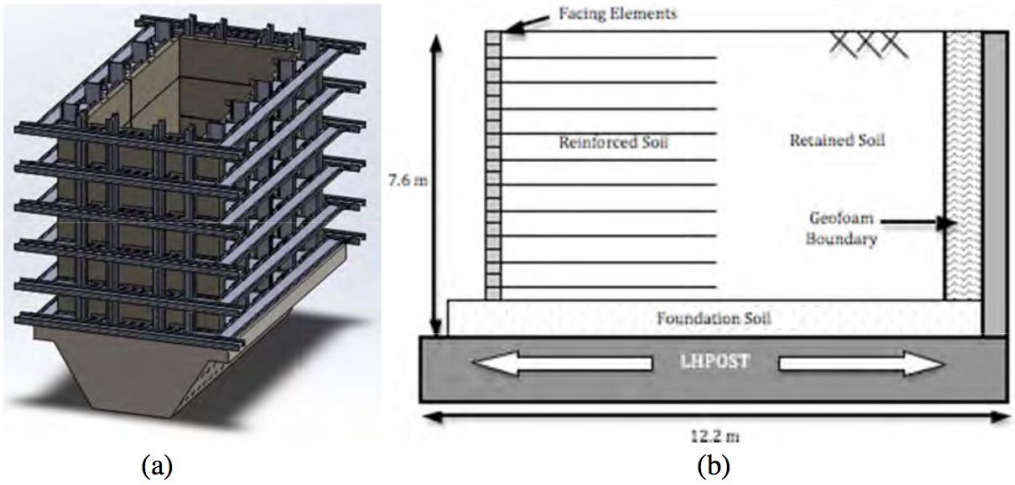

Figure 20. (a) Final Design of Large Soil Containment Box. (b) MSE wall specimen. From: (Sander, et. al, 2013)

The dimensions of the box that was used for the current testing were accommodated for the project and the final design used a box of 22 ft long by 9ft 6 inch wide and 15 feet deep.

3.5. Pile Installation

The length established for the center to center distance of the piles was determined after considering the anticipated maximum deflections of each pile modeled with the available software (PYLAT), as well as the location of the existing sand bed accelerometer wires. The piles had to be installed at a minimum spacing of three-foot center to center, but the two center piles had to be adjusted to accommodate the central accelerometer wires laid for the original tunnel testing. The pile masses were determined after a dynamic FEM program (PYLAT) was performed. The intention was to push the piles to a maximum bending moment corresponding to 100% of the plastic bending moment. The idea was to

capture the full capacity of the pile without yielding, so as to use the piles again under group capacity. The results of the preliminary modeling are shown in Table 12

Table 12. Modeling of helical piles maximum deflection

D, in	Eq.	Mass, lb.	y_{max}, mm	M_{max}, kN-m	h @ M_{max}, m	Inelastic Region, m	Pile behavior
3.47	Nor.	818	9	2.789	0.440	---------	Elastic
3.47	Nor.	1587	35	6.970	0.587	---------	Elastic
3.47	Nor.	2723	53	7.811	0.543	---------	Elastic
3.47	Jap.	818	10	3.142	0.543	---------	Elastic
3.47	Jap.	1587	48	8.568	0.677	---------	Elastic
3.47	Jap.	2723	191	16.193	0.948	0.135-1.219	Elasto-Plastic
5.5	Nor.	2861	28	23.07	0.853	---------	Elastic
5.5	Jap.	2861	29	22.75	0.853	---------	Elastic

After all the installed sand-accelerometers were connected to the data acquisition system and the locations of the piles were marked, each helical pile was installed with a torque-motor connected to a 328 D Excavator by the contractor TorcSill. 125 strain gauges (27 were lost during the installation procedures) and 10 accelerometers were connected to the data acquisition system. The torque installation profiles for each pile are shown in Figure 22 and Figure 23.

Figure 21. Installation of piles into the sand shaking box

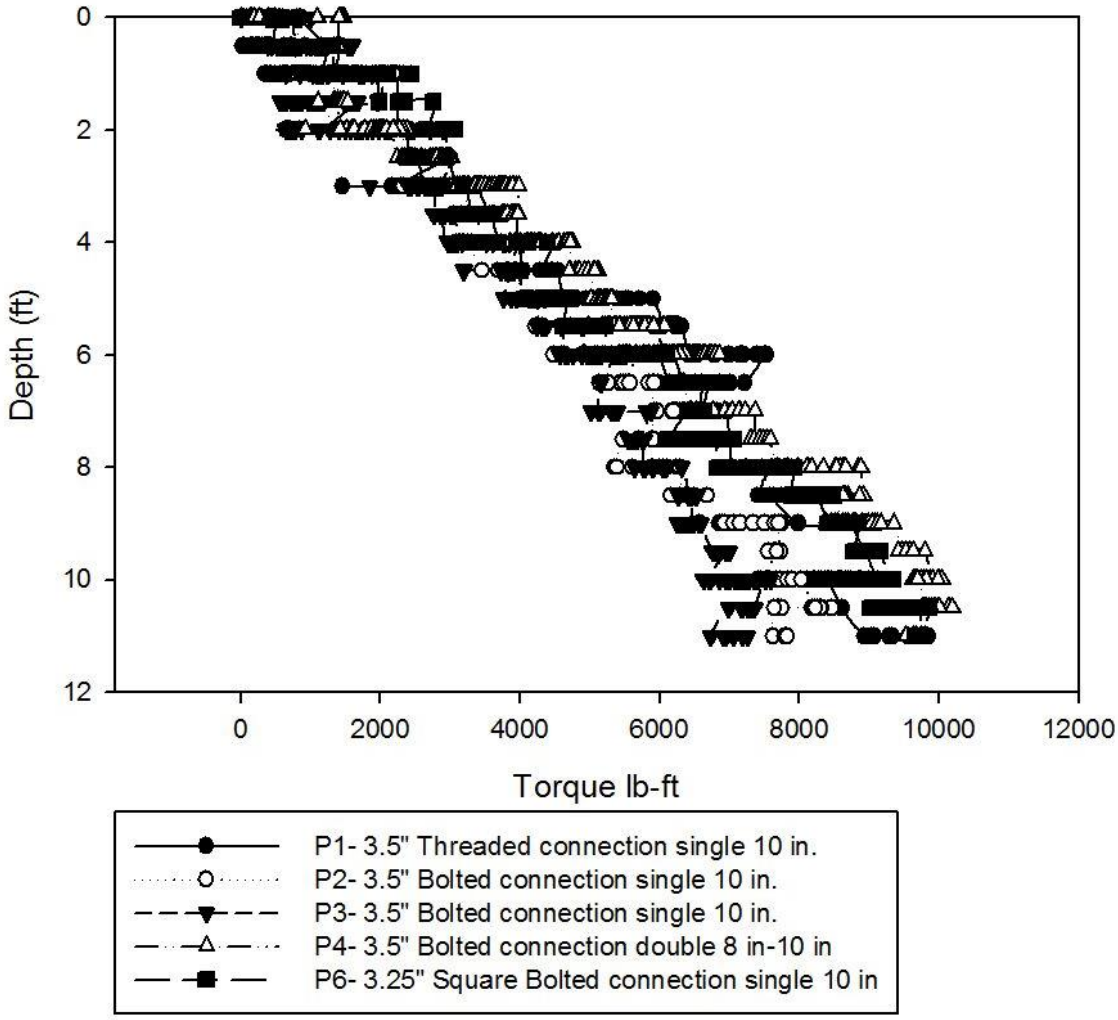

Figure 22. Installation torque 3.5 inch helical piles

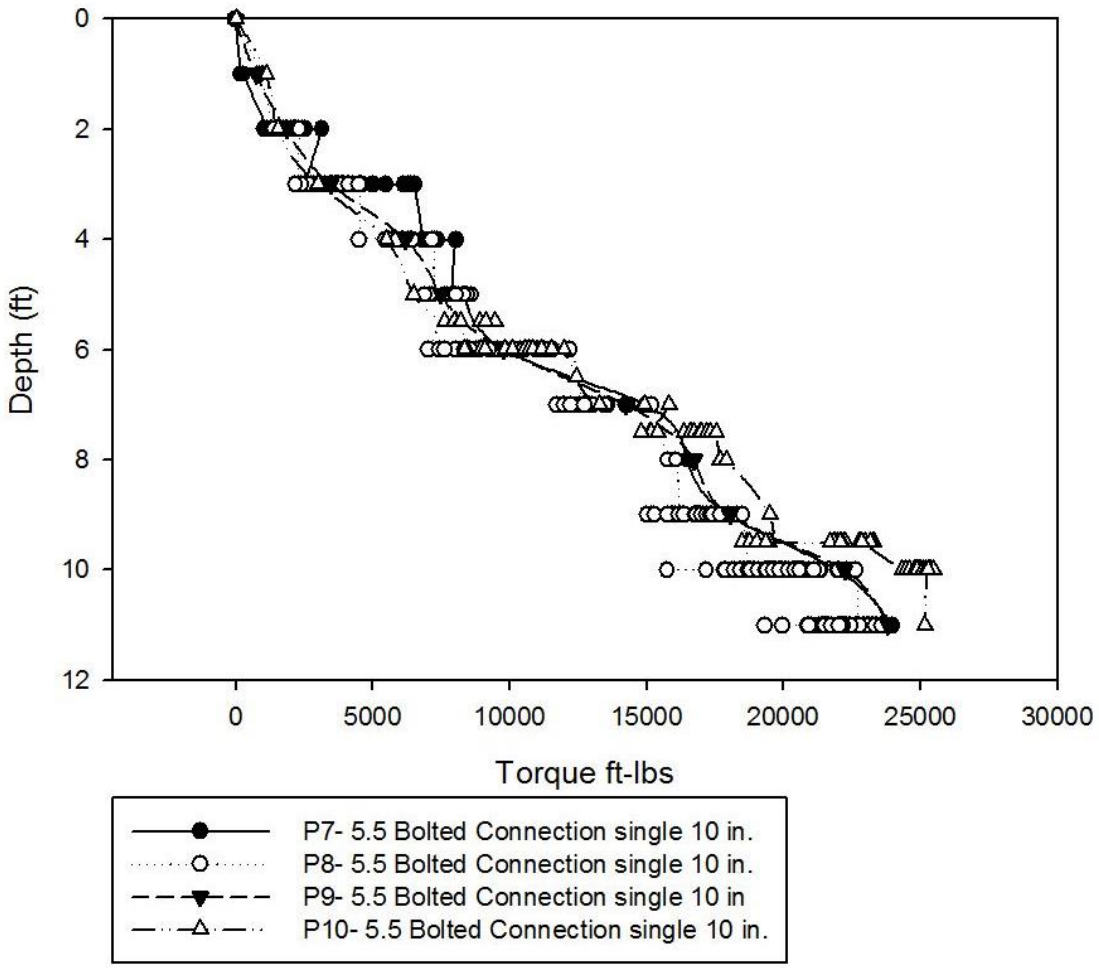

Figure 23. Installation torque 5.5 inch' helical piles

It should be noted from the torque installation profiles that the piles had axial capacities that far exceeded the masses placed on them. However, it was the lateral capacity that governed. In the case of the 5.5 inch piles, due to space and safety concerns, we only placed weights to bring the bending moments to 60% of capacity. These masses are presented in Table 14.

3.6. Testing set up

As mentioned, the shaking box at the University of California-San Diego facility is 22 ft long by 9.5 feet wide and 15 feet deep, and it is filled with dense dry sand up to an elevation of 14 ft. The sand was compacted at 100% relative density, and all sand parameters are shown in Table 13. Figure 24, present the sand grain size distribution. DCP test results are shown in Figure 25. Sand average wave velocities are shown in Figure 26, which were calculated from the accelerometer readings that were installed in the sand box. The shake sequences were conducted over three days. In the first day a shaking sequence was commenced on just the sand bed to understand the shear wave velocity. The second shake day included all the shaking sequences on the ten piles, which simulated a kinematic free head condition. During the third day a Inertial free head condition was evaluated, and each one of them is explained in the following sections.

Table 13. Sand parameters

Parameter	**Value**	**Units**
Average natural water content, ωn	5.5	%
Friction angle Direct Shear, Øds	47.6	degrees
Friction angle triaxial test, Øt	53.2	degrees
Average grain size, D50	0.0335	inch
Fines content (Fc)	4.5	%
Unit weight, γ	124.22	(lb/ft^3)
Relative density, Dr	100	%

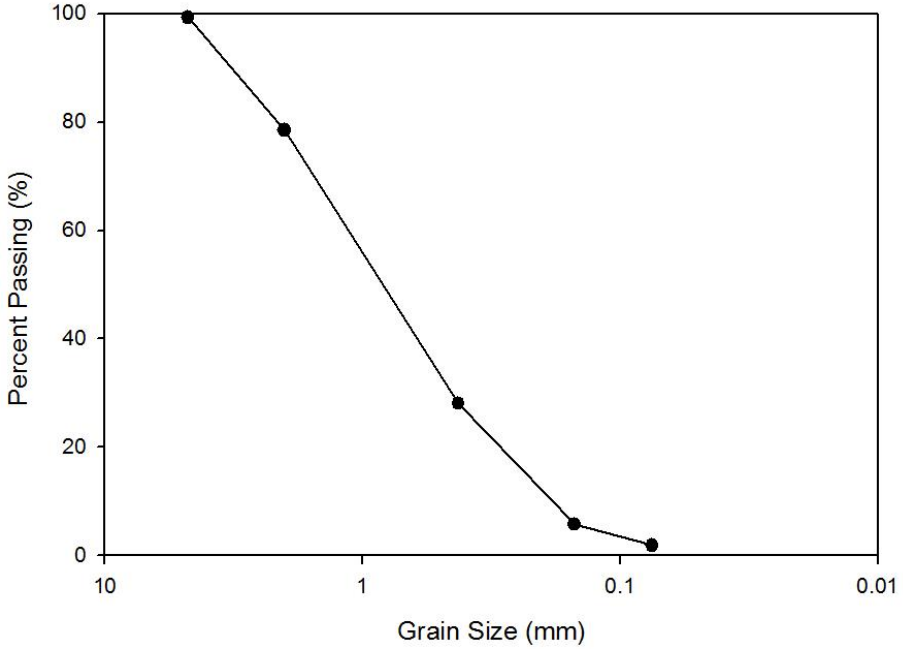

Figure 24. Sand grain size distribution

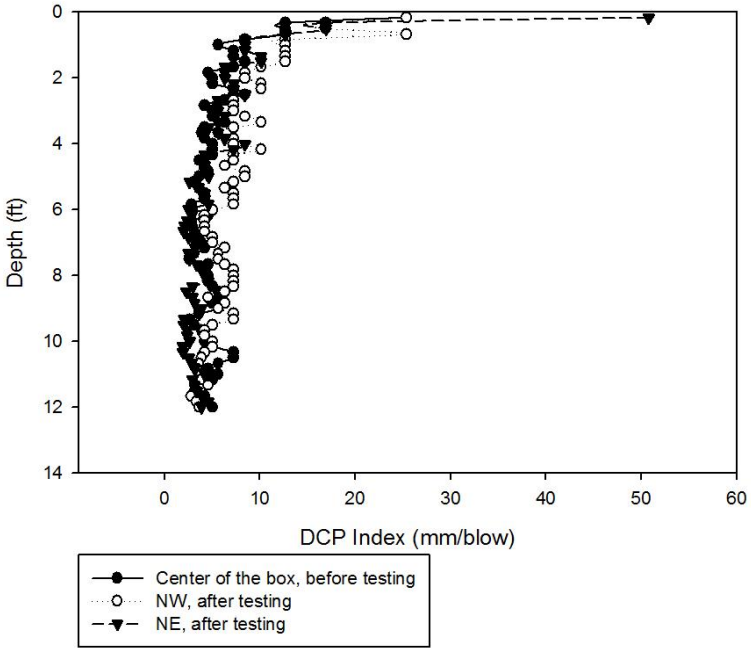

Figure 25. DCP Test results

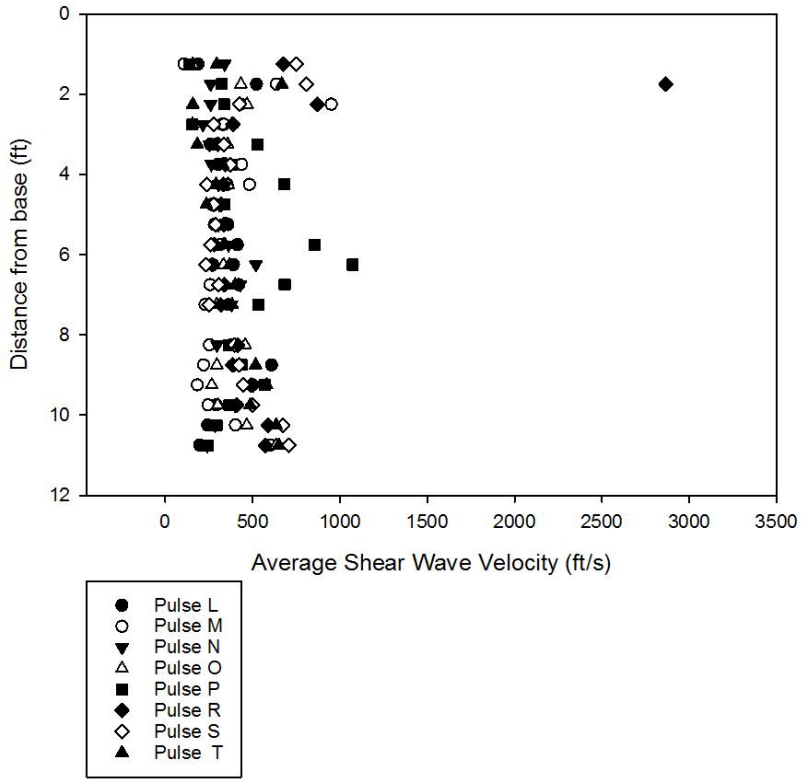

Figure 26. Sand average shear wave velocity

Day 1: Sand Bed Shaking

During the first day of testing, the sand bed was shaken with just the sand and instrumentation, as illustrated in Figure 18. The shakes consisted of a pulse, white noise and pulse.

Day 2: Kinematic Free head condition

The test set up consisted of ten piles subjected to dynamic loadings that replicated the Northridge and Great Hanshin eartquakes at different amplitures (50%, 75% and 100%) as mentioned in section 3.1. The piles' layout is illustrated in Figures 27 and 28.

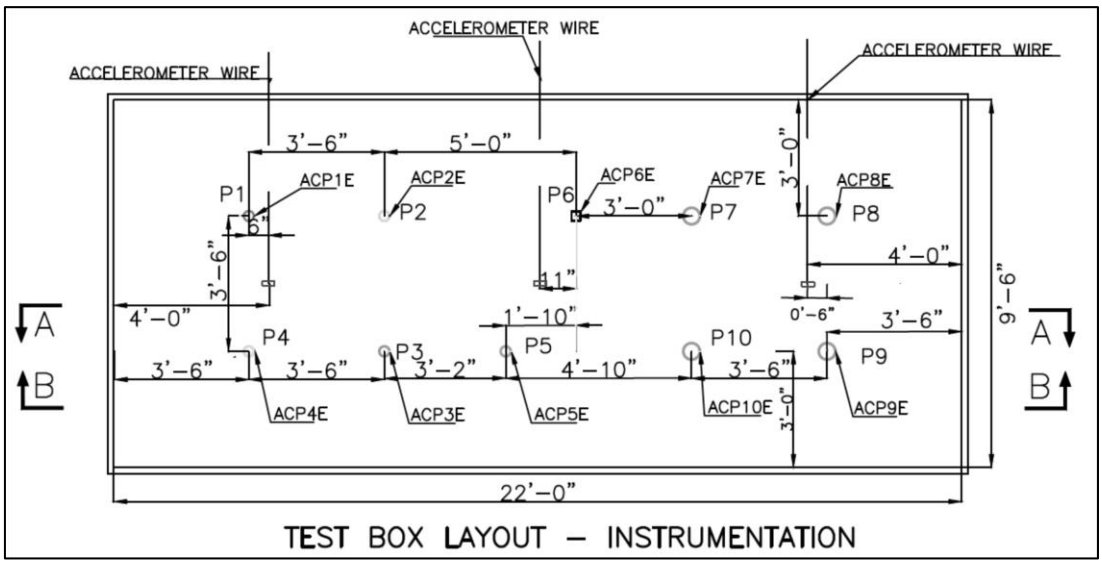

Figure 27. Plan View of Phase I Shaking box layout.

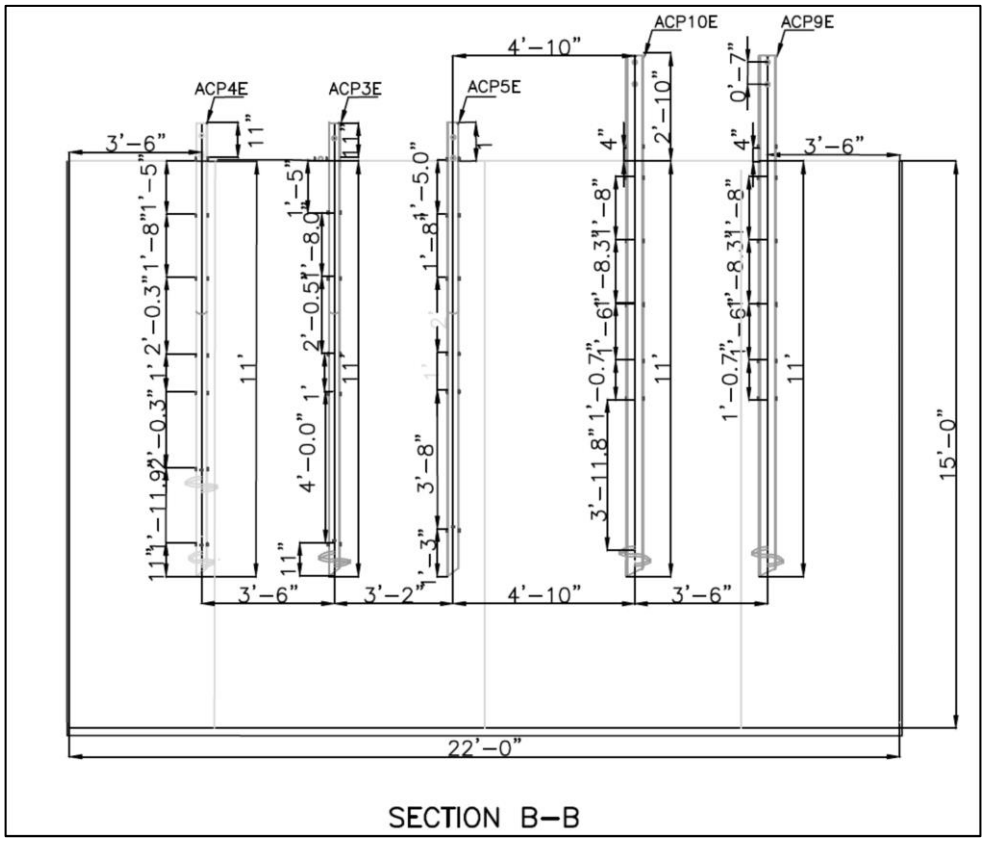

Figure 28. Profile view of Phase I shaking box.

Day 3: Inertial Free head condition

The layout and profile of the proposed installation are illustrated in Figure 29, 30 and 31. The proposed setup implemented 20 inertial weights on top of the piles and the distribution of the weights are explained in Table 14. Twenty-two concrete weights were fabricated by RamJack and AMSquared Construction, and the height dimension of each concrete weight varied as illustrated in Figures 30 and 31.

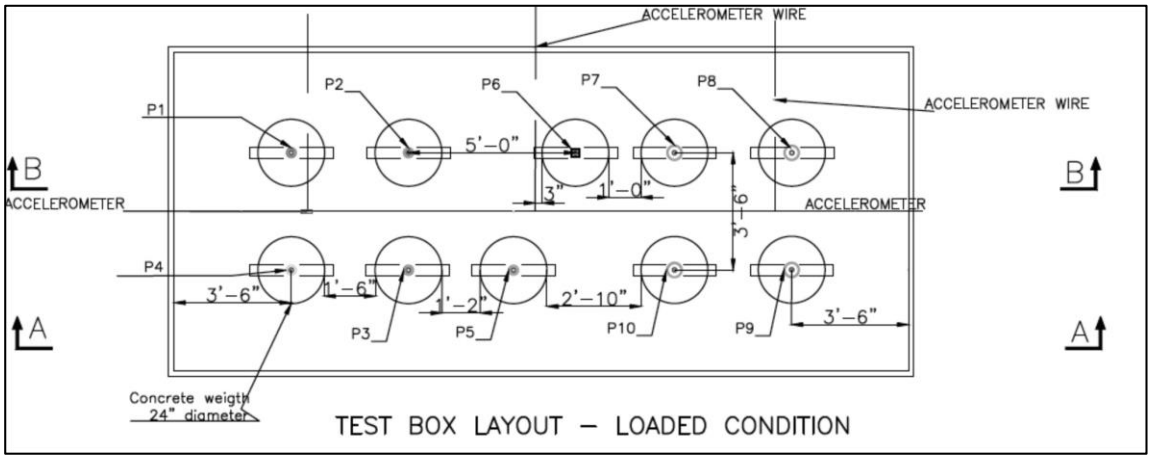

Figure 29. Phase II: Test box layout kinematic inertial condition

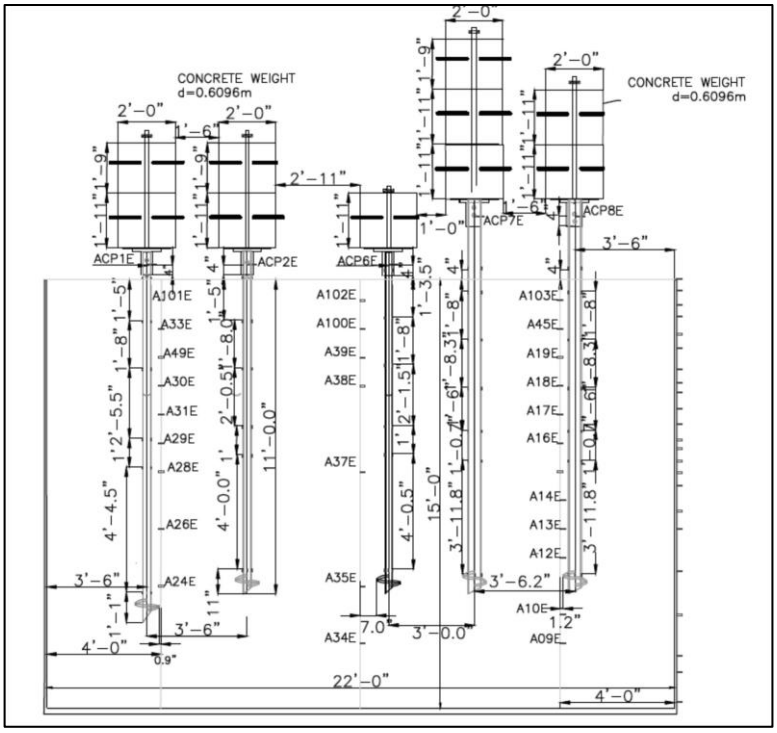

Figure 30. Phase II: Profile of inertial condition P1, P2, P4, P7 and P8

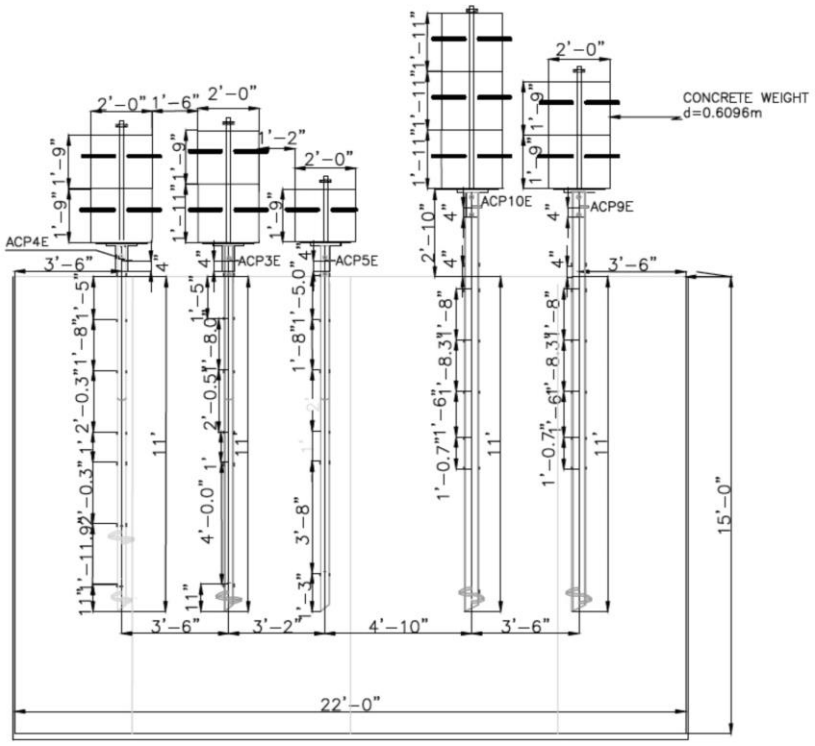

Figure 31. Phase II: Profile of inertial condition P4, P3, P5, P10 and P9

Table 14. Inertial weight distribution of helical piles

PILE	No. weights	Total weight per pile (lb)
P1	2	1693
P2	2	1652
P3	2	1714
P4	2	1648
P5	1	818
P6	1	955
P7	3	2724
P8	2	1731
P9	2	1545
P10	3	2742

3.7. Testing

After splicing, dropping and bundling 125 strain gauge cables, the strain gauge cables and accelerometer cables were connected to the data acquisition system. Day 1 of testing started with the calibration of all the instrumentation and then the test consisted in the application of a series of three shakes to characterize the sand bed; pulse, white noise and pulse. Day 2 shakes started with the application of a white noise pulse, then the shake table induced accelerations to replicate the 1994 Northridge California earthquake to an amplitude of 50%, 75%, 100% T0 and 100% T1, where T0 refers to the application at the base of the shaking table and T1 was a scaled shake and will not be discussed in this thesis. In addition, a series of accelerations were applied to replicate the Great Hanshin earthquake at 50%, 75% and 100% T0 and T1 of its amplitude. It is important to note that previous to each shake, the table controller applied a pulse to the table that could be

registered by the instrumentation to assess sand bed densification. The test set up used was the same on Day 3 as the kinematic free head condition described in Section 3.6 and the acceleration on the pile top, across the sand bed and on the box were recorded with the described accelerometers. In addition, the strain along the length of the piles were recorded throughout for each shake using the installed strain gages in order to determine bending moments on future calculations.

On day 3, the contractor on site installed the corresponding concrete masses on top of each pile and readjusted the accelerometer locations at the pile head. The same series of shakings as employed on day 2 were applied following exactly the same order to compare future results. In addition, the same pulses were induced previous to each one of the shakes.

3.8. Data Analysis

3.8.1. Data filtering

Two data filtering procedures were employed; first, a manual identification of the strain gauges was conducted using the software BIM VIEWER to see if they were reading correctly. Once viable strain gages were identified, the data was filtered in MatLab using a fourth degree Butterworth with a frequency range from 0.25 Hz to 8 Hz. This frequency range covered the frequency range of the shakes. The Butterworth filter reduced the noise obtained at high frequencies from the strain gauge readings. The maximum moments calculated for each level were determined following a filtered and a non-filtered

procedure, as shown in Figure 32 to Figure 35. The data were fit using a quintic spline interpolation and three extra points were included to assist with the fitting. Two points were included at the pile tip with a bending moment of zero, then an extra point was added at the center of the mass of the concrete weights and a bending moment of zero was added.

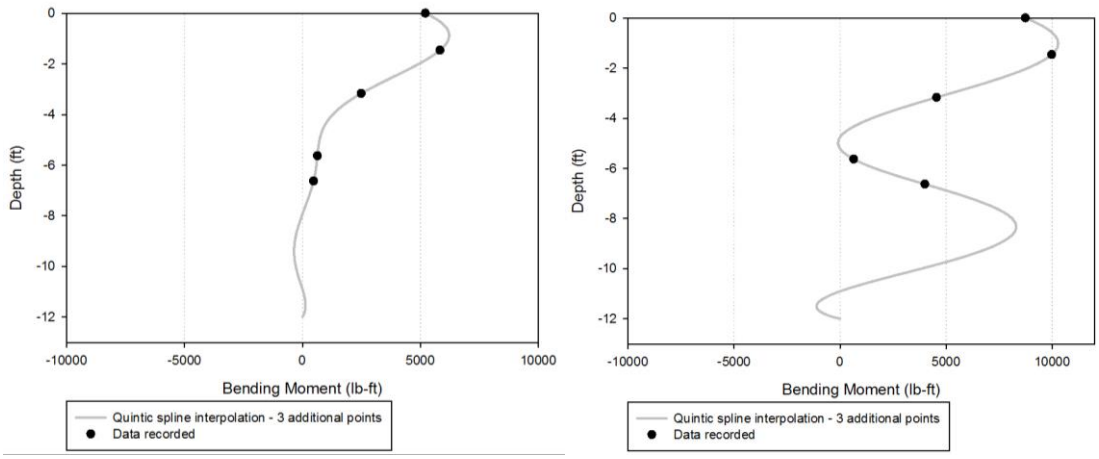

Figure 32. P1: Maximum bending moments without filter for (a) Northridge 100% (b) Takatori 75%.

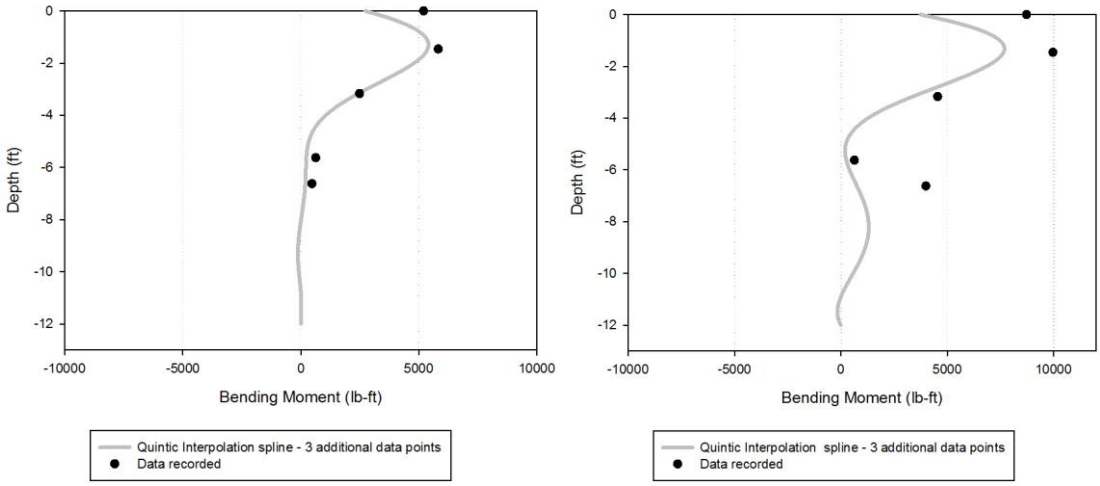

Figure 33. P1: Maximum bending moments with filter for (a) Northridge 100% (b) Takatori 75%.

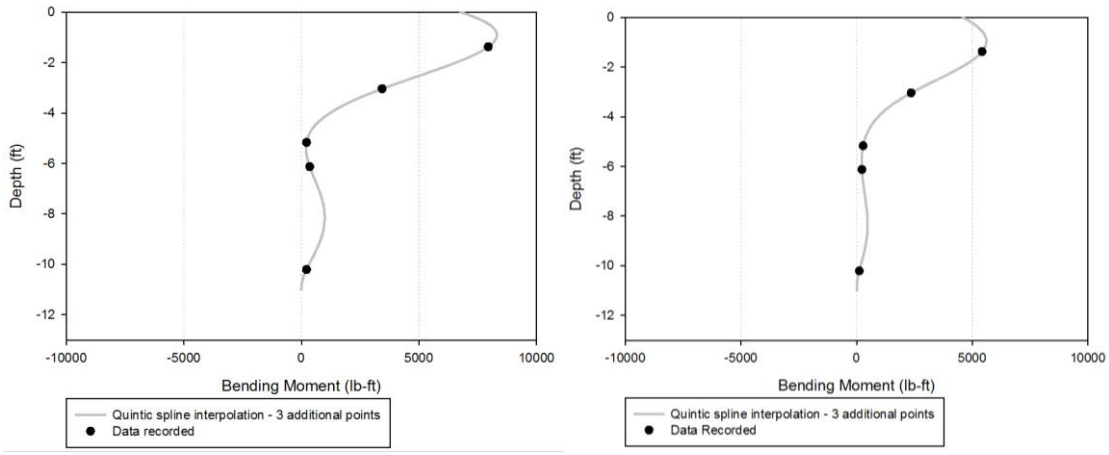

Figure 34. P6 (square pile) : Maximum bending moments without filter for (a) Northridge 100% (b) Takatori 75%.

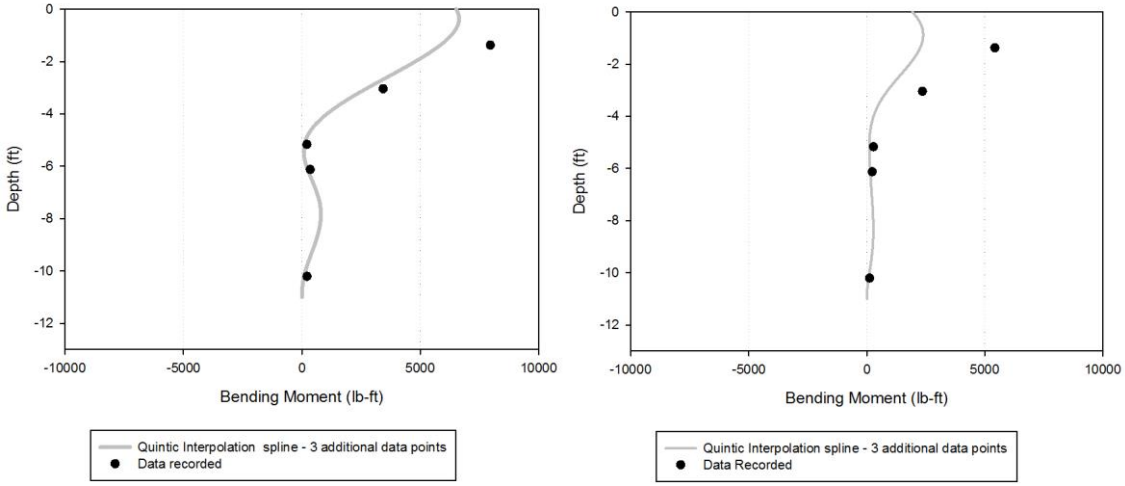

Figure 35. P6 (square pile) : Maximum bending moments without filter for (a) Northridge 100% (b) Takatori 75%.

3.8.2. Computations

The software used to conduct the data analysis was MATLAB; the bending moment at each strain gage location was calculated using Equation 7 and then these bending moments were fit with a curve after several curve-fitting methods were explored. These resulting curves were used to determine the soil reaction, p, and the pile deflection, y, using Equation 8 and Equation 9, respectively. While the bending moments are directly measured, the soil reaction is calculated by double differentiating the bending moment values and the deflection is calculated by double integrating the bending moments. The soil reaction (p) and pile deflection (y) were calculated for each time step. The dynamic pressure due to the inertial component of the pile was ignored during the computation of the soil reaction, in accordance with (Ting, 1987). The far-field soil movement relative to the base was included to consider dynamic p-y conditions. In addition, the shear force was calculated with Equation 10, which constitutes differentiating (single) the measured bending moments. The total deflection was calculated according to Equation 11. A visual of what these equations look like for one of the tested piles is presented in Figure 36.

Equation 7. Bending Moment

$$M(z)=\frac{E_p I_p(\varepsilon_1-\varepsilon_2)}{d}$$

$\varepsilon_1, \varepsilon_2$: Strain gauge readings

E_p, I_p : The elastic modulus of pile material and its cross-sectional moment of inertia

d : Outer pile diameter.

Equation 8. Soil reaction

$$p(z) = \frac{d^2 M(z)}{dz^2}$$

Equation 9. Pile lateral deflection

$$y_{pile}(z) = \iint \frac{M(z)}{E_p I_p} dz$$

Equation 10. Shear force

$$V(z) = \frac{dM(z)}{dz}$$

Equation 11. Deflection

$$y = y_{pile} - y_{soil}$$

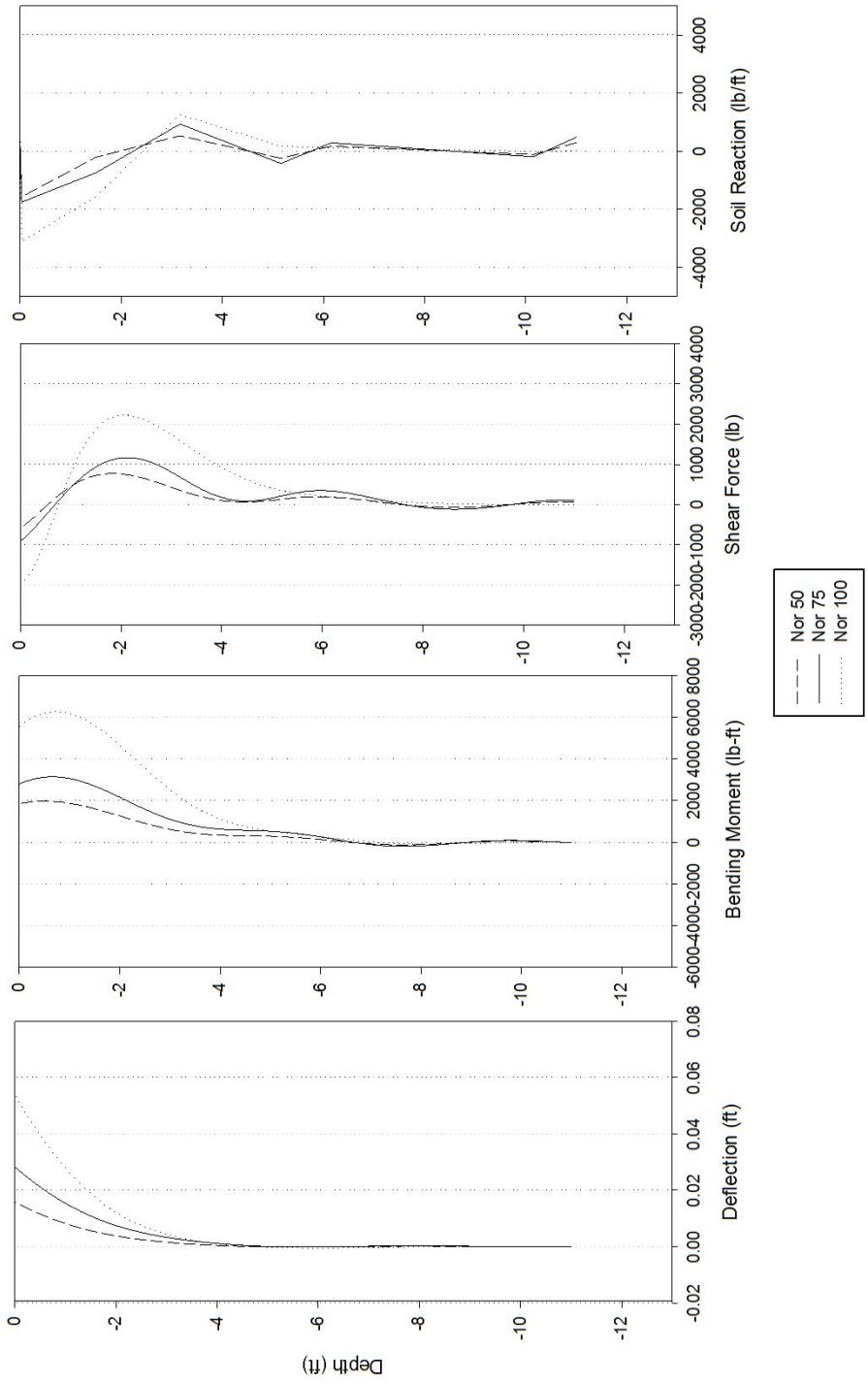

Figure 36. P2 (3.5" O.D. double-bolt couple, single helix) (a) Maximum Pile deflection (b) Maximum Bending Moments (c) Maximum Shear Force and (d)Maximum Soil Reaction for the Northridge shakes

Several curve fitting methods were attempted with the measured bending moment data and it was found that splines worked the best because they were continuous throughout their first and second derivatives. Five artificial points were included; two points at the pile tip with a bending moment of zero, a point at the center of mass of the concrete weights with an assigned bending moment of zero. Two points near the sand surface (at 0 ft and 0.0328 ft) were included with a bending moment calculated from the back calculated shear force in order to preserve the bending moment slope obtained at the top strain gauges. Two spline fitting methods were settled on to determine the p-y loops: the first method was a quintic spline interpolation, which was employed to determine the pile deflection, y. A spline interpolation curve passes through all the data points, and the procedure implemented was conducted following the methodology described by Haiderali & Madabhushi (2016) in which an algorithm available in MATLAB is used to determine the knot sequence.

The soil reaction, p, however, was determined using three curve fitting methodologies for the bending moment curves, and the results were compared. The first methodology was conducted using a quartic approximation spline. In an approximation spline, the curve does not necessarily pass through all the data points, therefore, a weight of 1000 was assigned to all the artificial points. The second method implemented was the one described by (Hajialilue-bonab, et al., 2007), which used a quintic smoothing spline for the measured points and a cubic spline was used at the boundaries of the smoothing interval. Therefore, an optimization code was developed in MATLAB to calculate the appropriate tolerance. The third method used a cubic spline interpolation. The method

that produced better results for P2 was a cubic spline interpolation, for P4, and P5 was the one described by Hajialilue-banab et al. (2007). Nevertheless, the method that produced better results for P1 and P6 was the quartic approximation spline. This procedure was followed for both the maximum bending moments and for each time step. Section 3.9 shows the fitted curves of the maximum bending moments and for two time steps.

3.9. Fitting methods

The different fitting methods that were tested to identify the trendeline of the bending moment curves are shown from Figure 37 to Figure 42. It was observed that the quintic interpolation splines produced a $R^2 = 0.99$ for each shake and in general the interpolation that produced improved results was the one that used three additional points with bending moment set to zero (two at the tip of the pile and one at the center of the mass of the inertial weights on top of the pile). It was observed that the incorporation of three additional points into the quintic spline interpolation produced superior results than when the curves were interpolated with five additional points (the three points described above plus two points at the sand surface 0ft and at 0.0328 ft). Therefore, the fitting method that would be used to calculate deflection would be the interpolation spline using three additional points. This conclusion was especially supported when P6 (square helical pile) was analyzed.

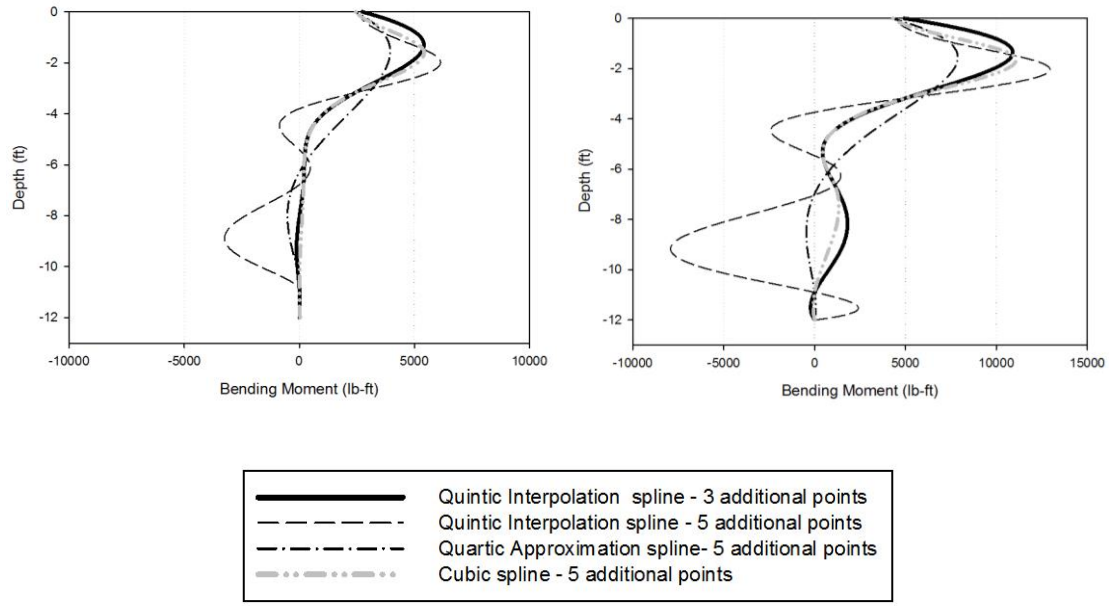

Figure 37. P1: Maximum bending moment by fitting method (a) Northridge 100%, filtered (b) Takatori 100%, filtered

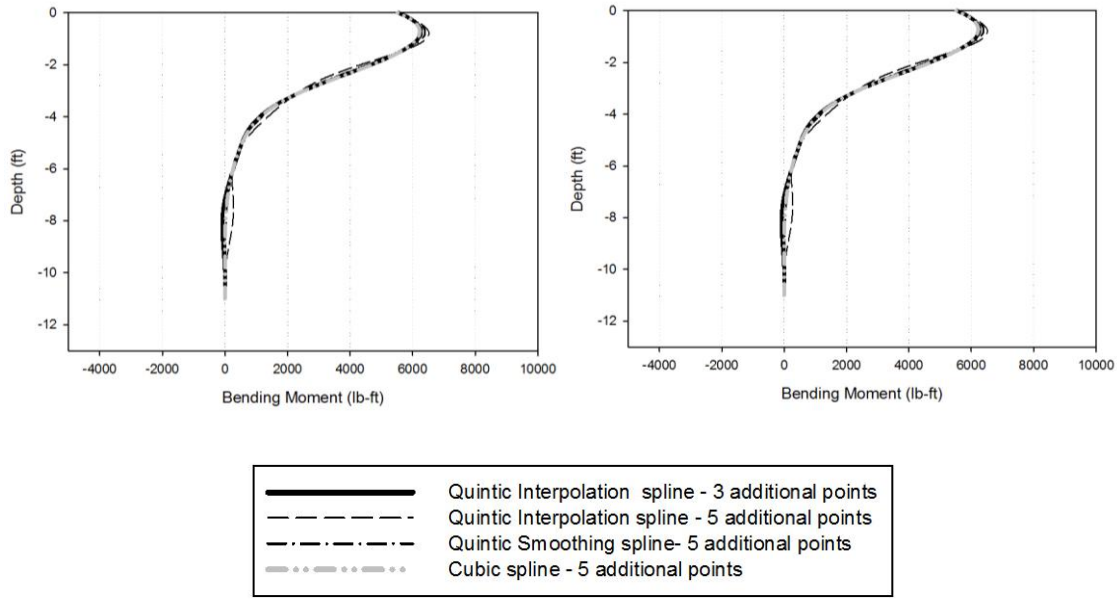

Figure 38. P2: Maximum bending moment by fitting method (a) Northridge 100%, filtered, (b) Takatori 100%, filtered

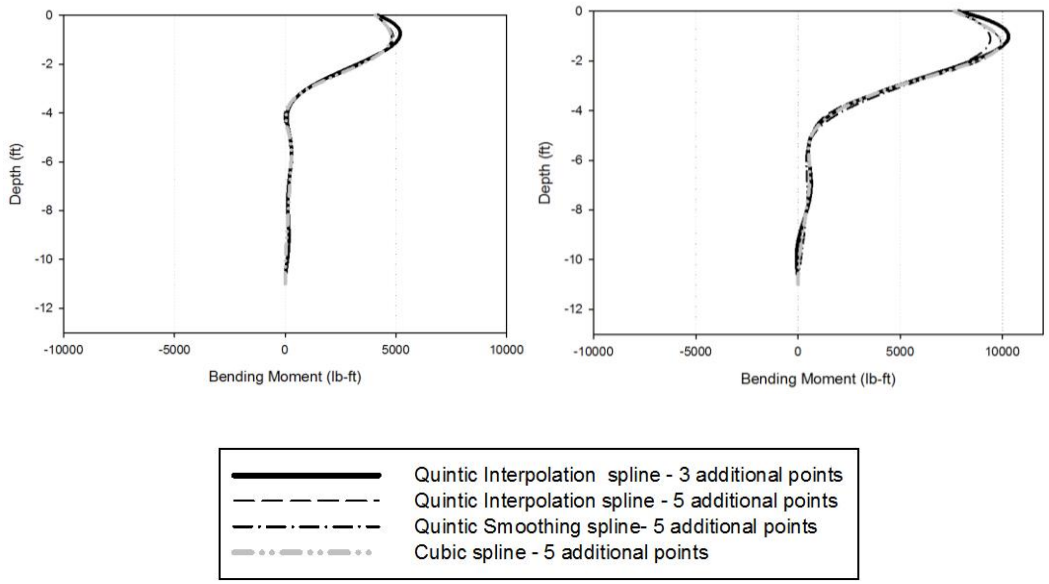

Figure 39. P4: Maximum bending moment by fitting method Northridge 100%, filtered, (b) Takatori 100%, filtered

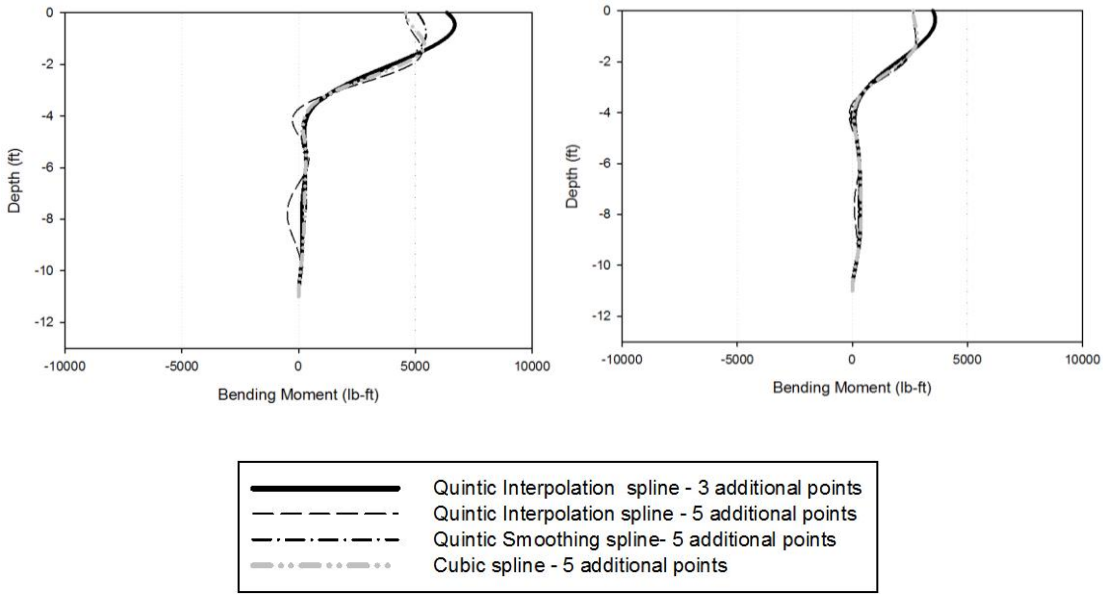

Figure 40. P5 (driven pile): Maximum bending moment by fitting method (a) Northridge 100%, filtered, (b) Takatori 100%, filtered

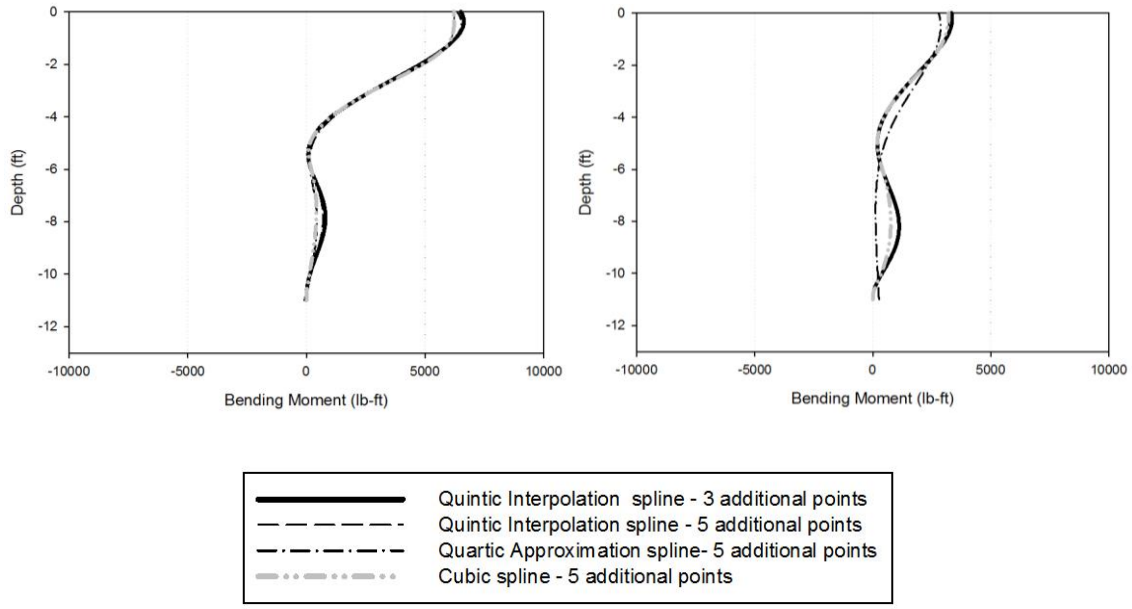

Figure 41. P6 (square helical pile): Maximum bending moment by fitting methods (a) Northridge 100%, filtered, (b) Takatori 100%, filtered

The top two strain gauges of P6 were installed four inches above the sand surface, while the rest of the piles had top strain gauges that were installed at one inch from the sand surface. The resulted bending moment profiles that were calculated for P6 under the Takatori and Northridge 75% shakes were overfitted, as illustrated in Figure 42. Therefore, the points that were calculated at the sand surface were eliminated to obtain smoother predictions. The deflection of all the piles would be calculated using a quintic interpolation using just three additional points, as it was the most accurate method. Figure 43, shows that the selected fitting method works at any timestep, which would be used to create the p-y loops.

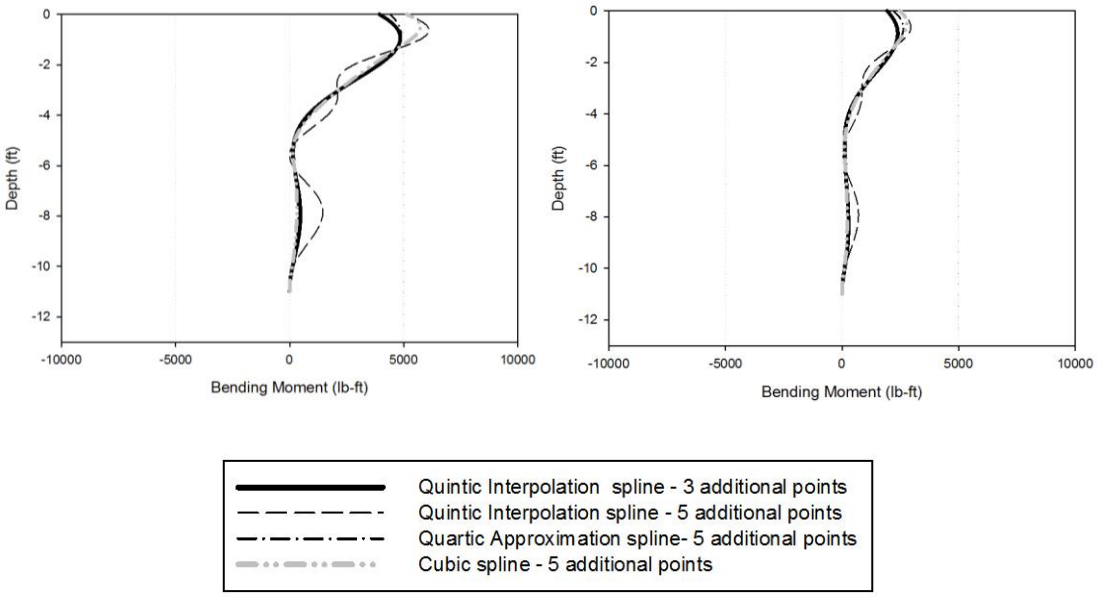

Figure 42. P6 (square helical pile): Maximum bending moment by fitting methods (a) Northridge 75%, filtered, (b) Takatori 75%, filtered

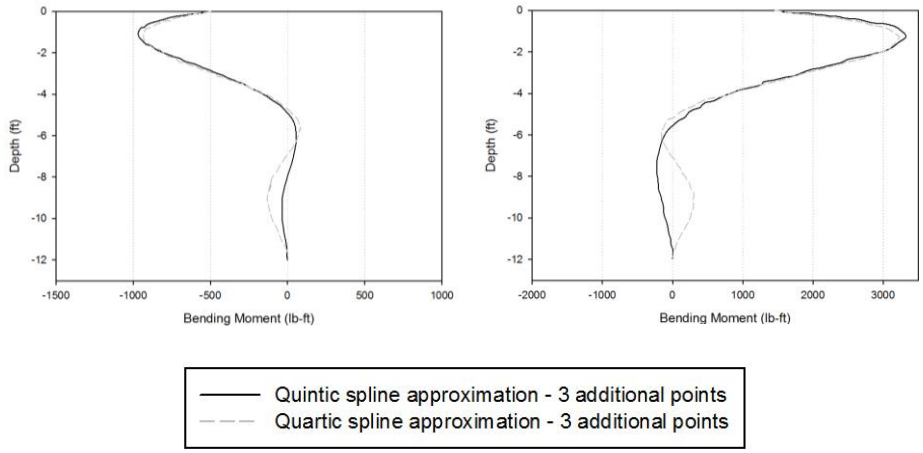

Figure 43. P1: Bending moment at time step (a) 12.5042 and (b) 14.5875 sec for Takatori 75% with fitting methods, filtered

3.10. LPILE comparison

Several tests were conducted in LPILE to compare the different fitting methods. The sand properties used were the ones described in Table 13 and the bending moments and shear forces were back calculated from the bending moments obtained at the top strain gauges. The configuration tested was the one that employed six strain gauges. It was observed that the bending moment and deflection curves, were more closely approximated by the quintic spline interpolation using 3 additional points, than by the other methods. In addition, the soil reaction and shear force for P5 was more closely approximated by the method described by Hajialilue-banab et al. (2007). As shown in Figure 44, there are some difference between the calculated curves for P5 and the LPILE responses, which may be attributed to the high density of the sand that was used during the testing procedures.

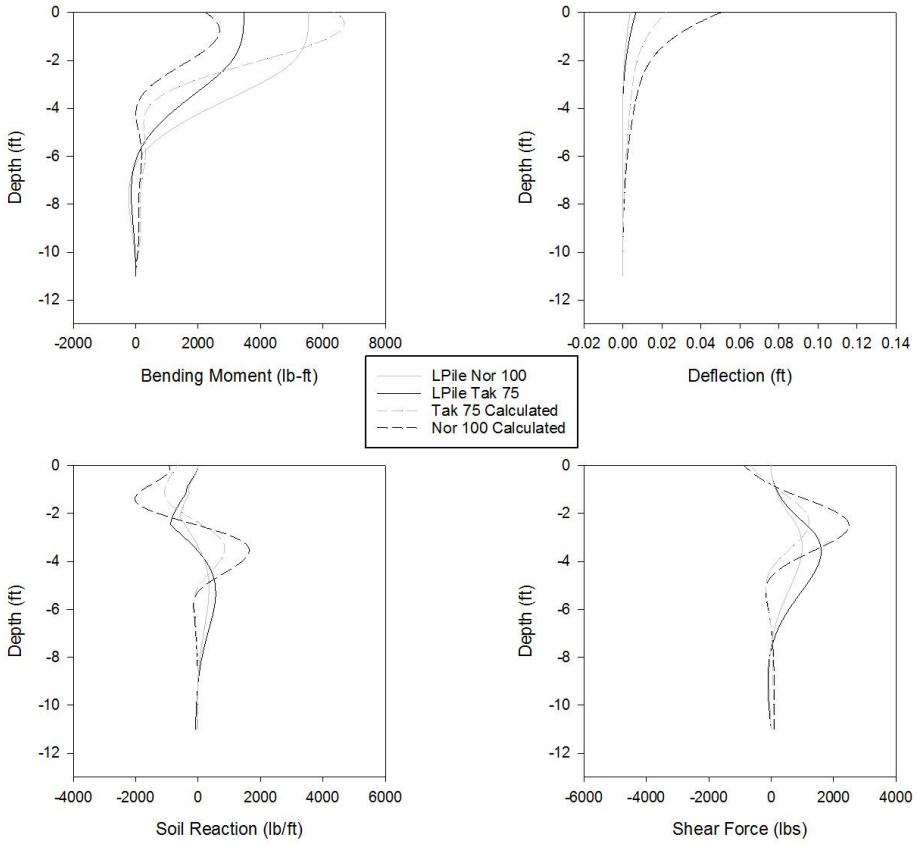

Figure 44. LPILE results compared to the quintic spline interpolation with 3 additional points for P5 – Configuration with 6 strain gauges.

4. RESULTS AND DISCUSSIONS

4.1. Natural frequency content of piles

For day three of the testing procedures, concrete weights were installed on top of the piles to include inertial conditions as discussed in section 3.5. The weights were placed on top of a cap and the accelerometers were installed around the caps. The caps had some movement, independent of the pile, due to a loose fit, and therefore showed an out-of -phase rocking, which was recorded by the accelerometers, as observed in Figure 45. Therefore, the natural frequency of the piles was calculated using the filtered strain gauge readings, instead of the pile head accelerometers. If this loose fit had been noticed prior to the shaking sequence, the cap would have been shimmed to prevent any additional movement or the accelerometes would have been moved off the cap sleeve and onto the pile. The fourier transform of the response of piles 2, 4 (Double helix), 5 (Push pile) and 6 (Square helical pile) under white noise using the strain gauge measurements are presented in Figure 46, Figure 47, Figure 48 and Figure 49 respectively. Table 15 summarizes the peak natural frequencies of the piles, which can be directly correlated to the inertial weight of the piles. On the other hand, it is important to highlight that the objectives of the present research was to evaluate the influence of the helix in the general seismic resistance of the pile, the influence of the geometry of the pile-shaft and the influence of the installation method in the seismic behavior of the piles. Therefore P3 was not evaluated, as it presented the same characteristics as P2 and would not provide additional comparisons.

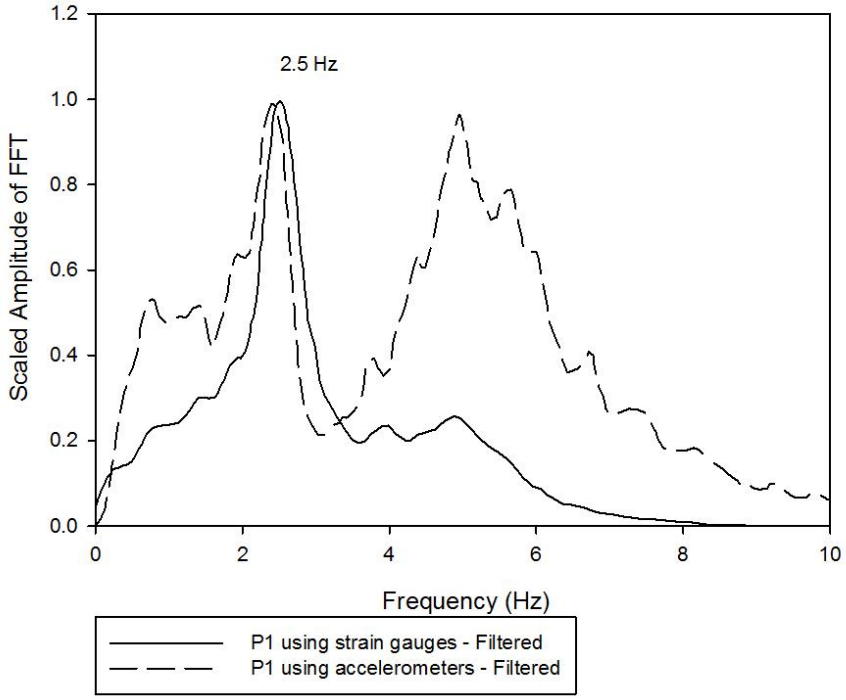

Figure 45. Natural Frequency of P1

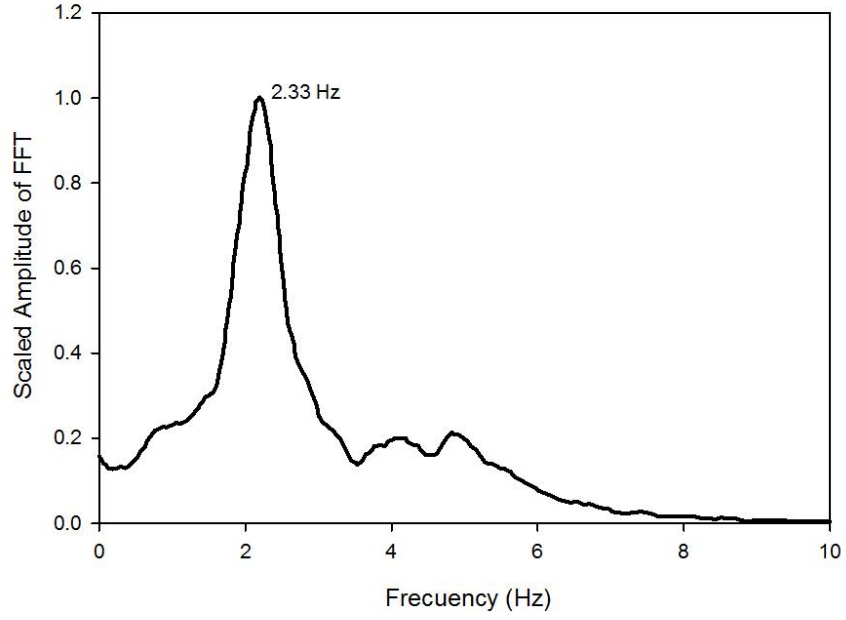

Figure 46. Natural Frequency of P2

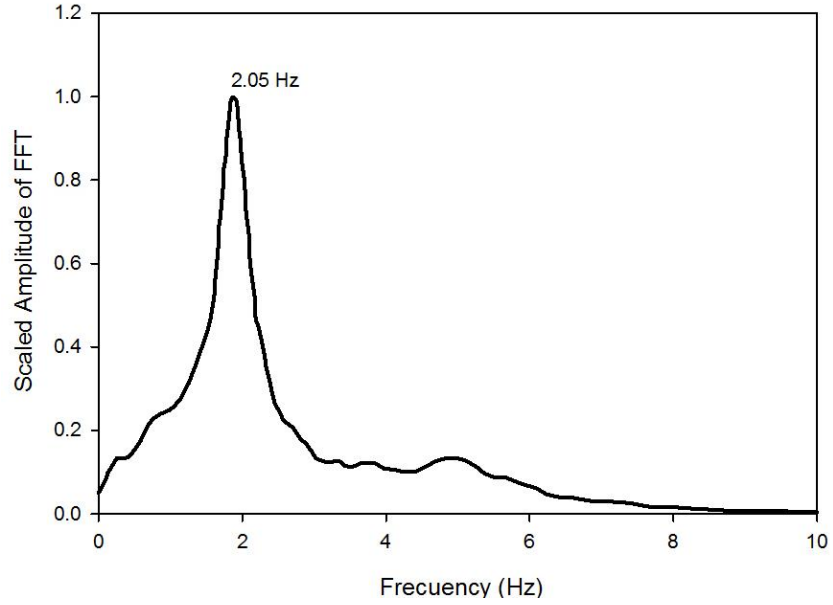

Figure 47. Natural Frequency of P4 (double helical pile)

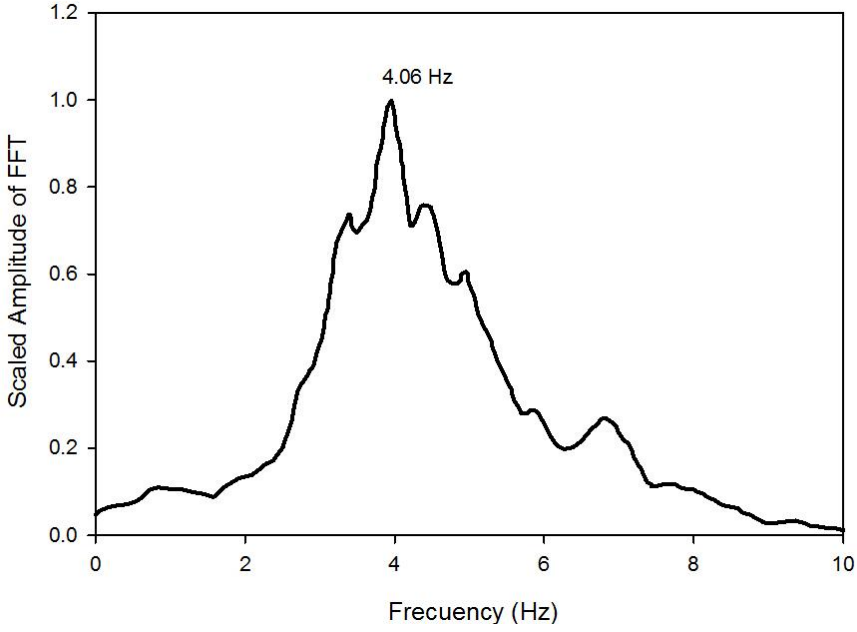

Figure 48. Natural Frequency of P5 (Push pile)

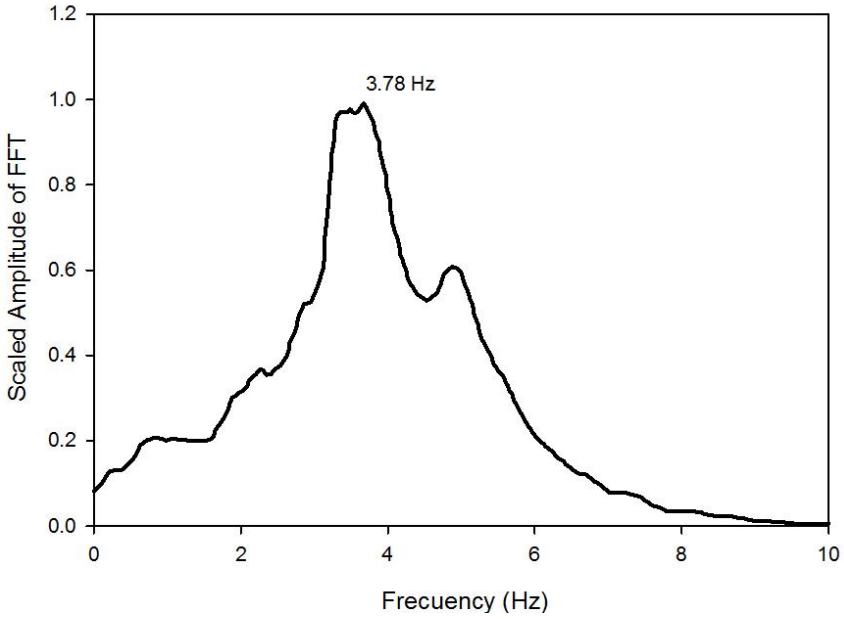

Figure 49. Natural Frequency of P6 (square helical pile)

Table 15. Natural Frequency of tested piles

Pile	Inertial Weight (lbs)	Natural Frequency (Hz)
P1	1693	2.5
P2	1652	2.33
P4 (double helical pile)	1648	2.05
P5 (push pile)	818	4.06
P6 (square helical pile)	955	3.78

4.2. Soil Reaction profile comparison by fitting method

The soil reaction obtained from a cubic spline interpolation and from quartic spline approximation or quintic smooting spline are presented from Figure 50 to Figure 77. It was concluded that for P1 and P6 (for both Takatori and Northridge earthquakes), the double derivation of the bending moments fitted by a cubic spline interpolation generated greater soil reaction (p) values than the results obtained from the double derivation of the bending moment fitted by the modified method that comprised a quartic spline approximation and a cubic spline interpolation for the two points of the boundaries.

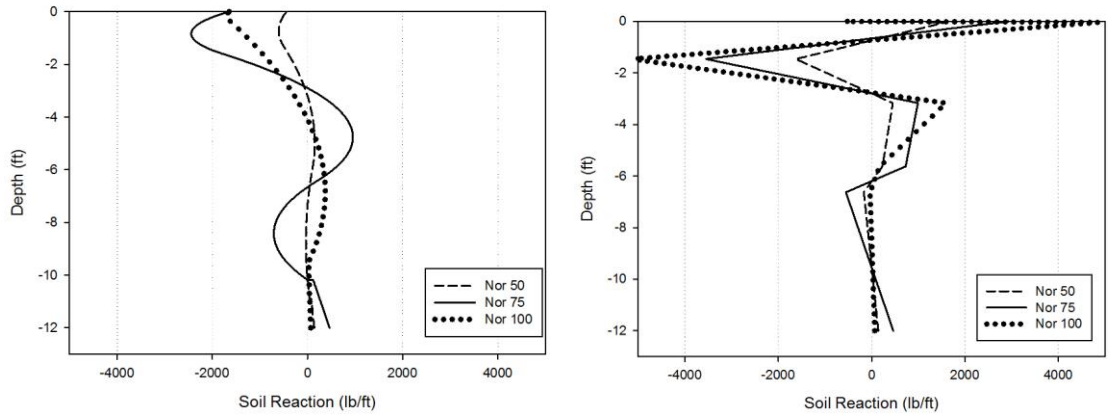

Figure 50. Comparison of soil reaction for P1 Northridge (a) From quartic spline approximation and cubic spline interpolation of boundary points (b) from cubic spline interpolation

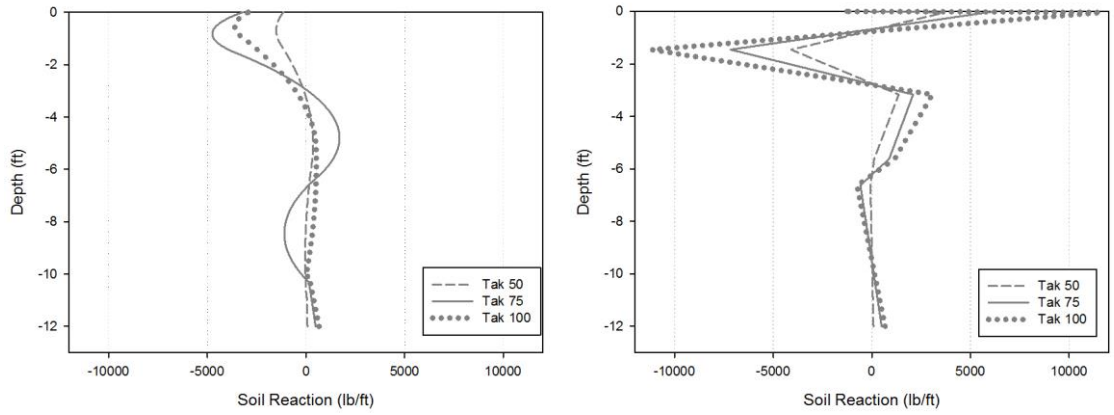

Figure 51. Comparison of soil reaction for P1 Takatori (a) From quartic spline approximation and cubic spline interpolation of boundary points (b) from cubic spline interpolation

On the other hand, the double derivation of the bending moment profile to find soil reaction (p) that was fitted by a cubic spline interpolation presented roughly the same values obtained for the bending moments fitted by a quintic smoothing spline (Figure 52 to Figure 54) for P2 and P4 (just Northridge earthquake). In general, it was concluded that the cubic spline interpolation was not suitable for all the conditions and therefore the

methods described in section 3.8.2 were used, except for P2, in which a cubic spline interpolation was used.

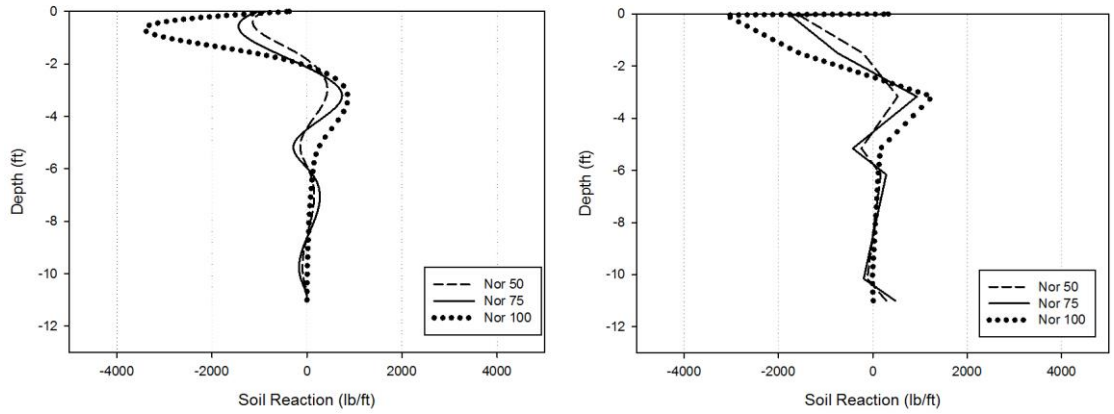

Figure 52. Comparison of soil reaction for P2 Northridge (a) From quartic spline approximation and cubic spline interpolation of boundary points (b) from cubic spline interpolation

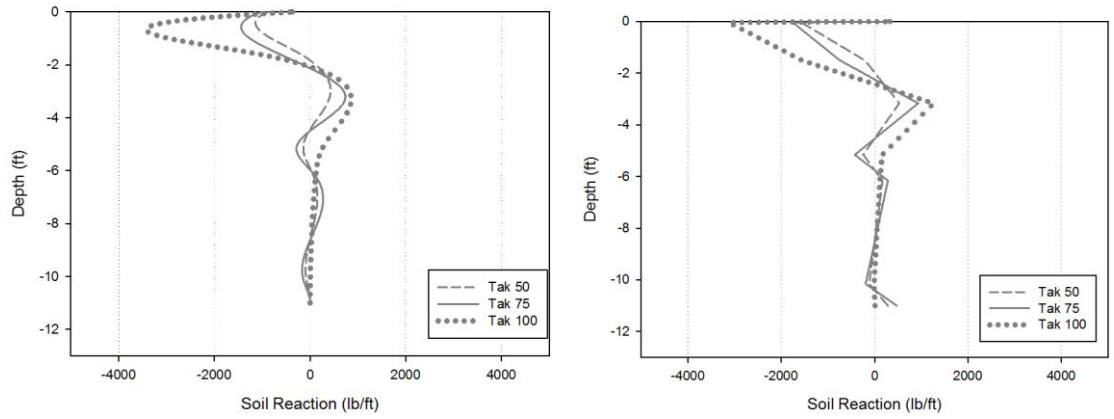

Figure 53. Comparison of soil reaction for P2 Takatori (a) From quartic spline approximation and cubic spline interpolation of boundary points (b) from cubic spline interpolation

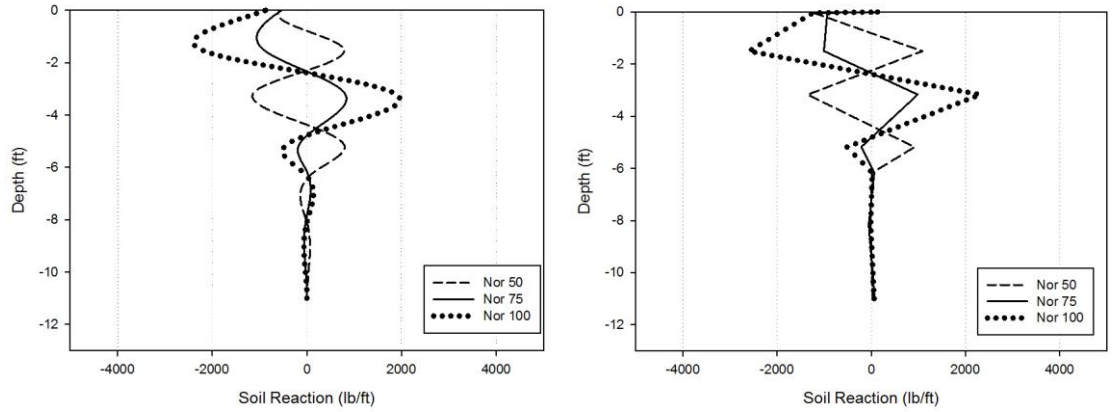

Figure 54. Comparison of soil reaction for P4 Northridge (a) From quartic spline approximation and cubic spline interpolation of boundary points (b) from cubic spline interpolation

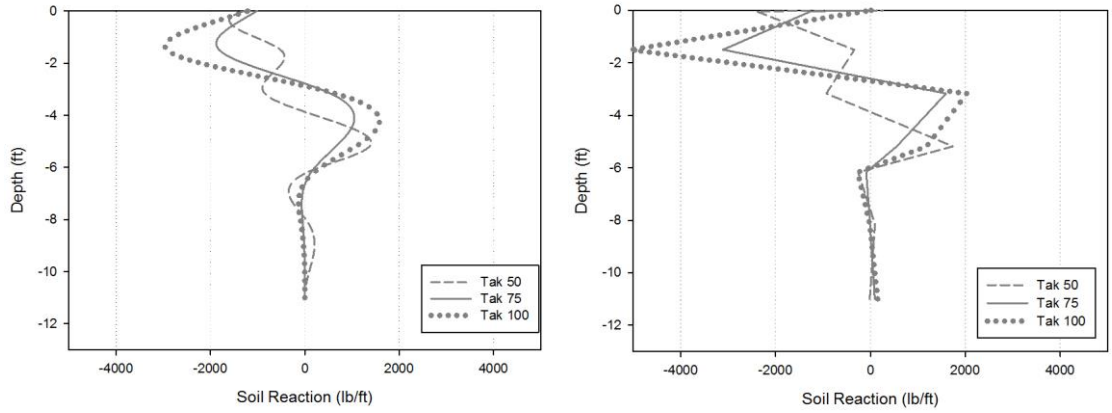

Figure 55. Comparison of soil reaction for P4 Takatori (a) From quartic spline approximation and cubic spline interpolation of boundary points (b) from cubic spline interpolation

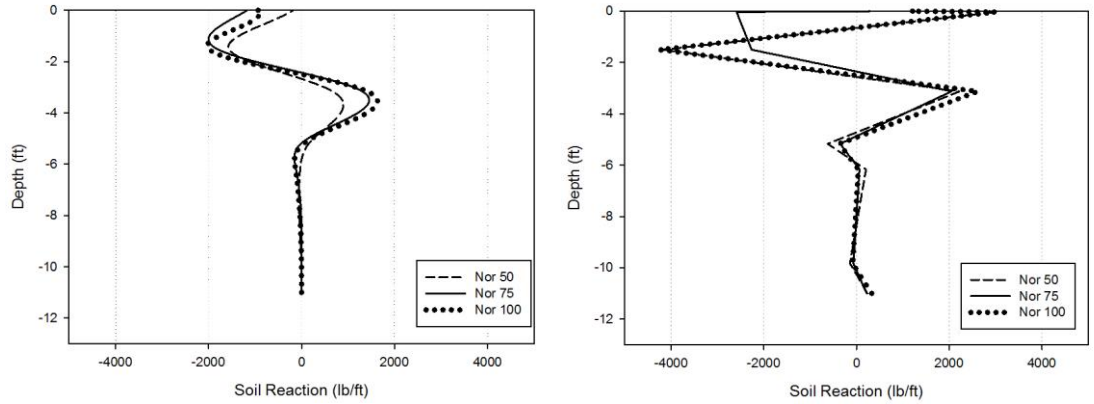

Figure 56. Comparison of soil reaction for P5 Northridge (a) From quartic spline approximation and cubic spline interpolation of boundary points (b) from cubic spline interpolation

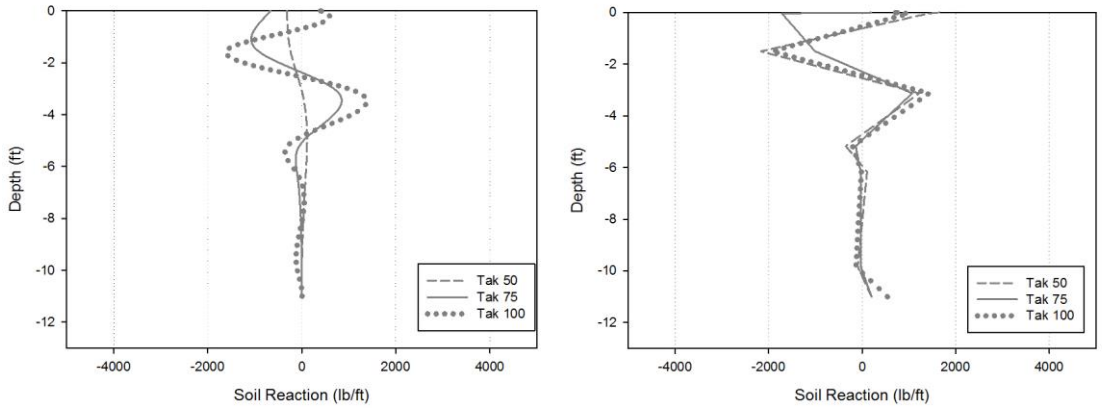

Figure 57. Comparison of soil reaction for P5 Takatori (a) From quartic spline approximation and cubic spline interpolation of boundary points (b) from cubic spline interpolation

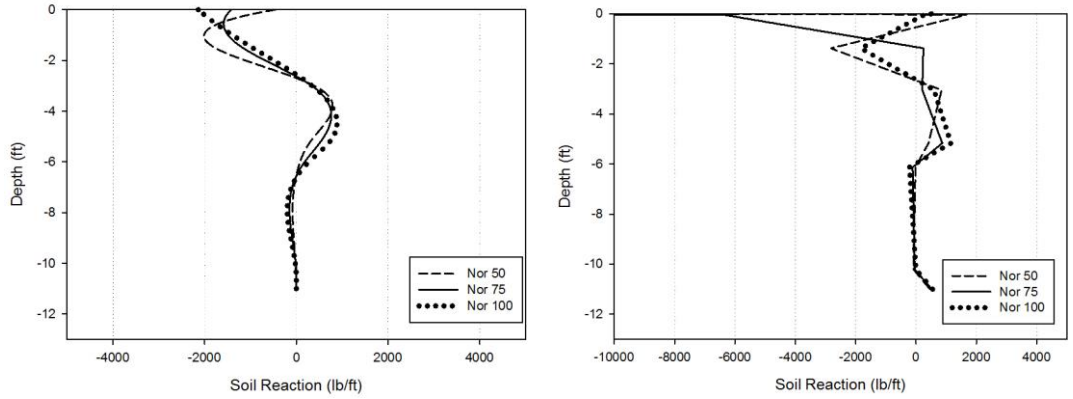

Figure 58. Comparison of soil reaction for P6 Northridge (a) From quartic spline approximation and cubic spline interpolation of boundary points (b) from cubic spline interpolation

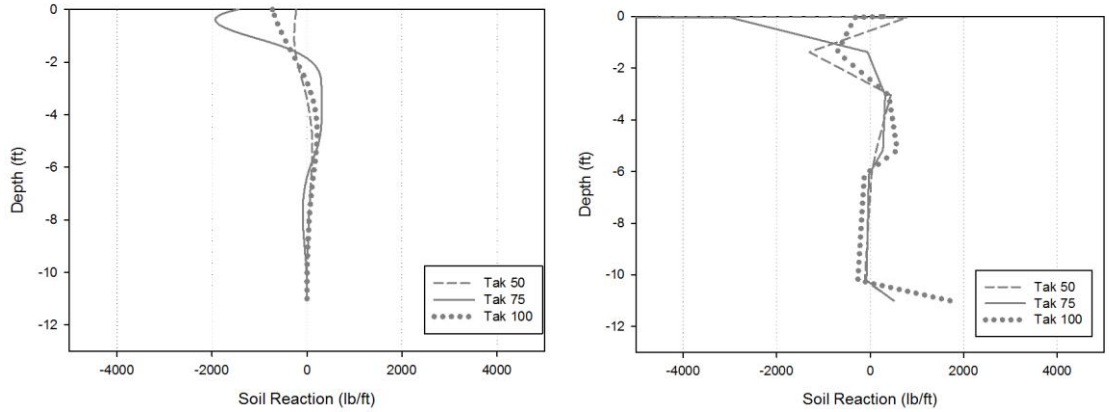

Figure 59. Comparison of soil reaction for P6 Takatori (a) From quartic spline approximation and cubic spline interpolation of boundary points (b) from cubic spline interpolation

4.3. Effect of the shape of the pile shaft

The influence of the shape of the shaft was analyzed using the results of pile 6 (square shaft with a cross sectional area of 2.44 in^2) and pile 2 (circular shaft with a cross sectional area of 2.16 in^2). However, the inertial weights that were incorporated at the top of the pile heads were significantly different; Pile 2 (P2) used two concrete weights

with a total weight of 1,652 lbs, while Pile 6 (P6) used one concrete weight with a total weight of 955 lbs. As discussed before, the weights on all the 3.5-inch piles were supposed to be the same, but, due to having to move the placement of the two center piles due to a central accelerometer cable, the second weight on the center piles had to be taken off to avoid pile weights bauzing into each other. As discussed before, the weights on all the 5.5-inch piles were supposed to be the same, but, due to having to move the placement of the two center piles due to a central accelerometer cable, the second weight on the center piles had to be taken off to avoid pile weights bumping into each other. Figure 60 and Figure 61 present the maximum bending moments for P2 and P6 during the Takatori and Northridge earthquakes, respectively. The behavior of the helical pile with a square shaft was highly influenced by the frequency content of the ground motion. At low frequency contents (Takatori), it was observed that P6 (Square) presented lower bending moment than P2, (Figure 60), but matched the bending moment of P2 in the Northridge 100% shake, even though the weight was significantly less (Figure 61). The frequency content o f both shakes were different and the natural frequency of the square pile 6 (4.0 Hz) was much closer to that of the Northridge shake. P6, therefore, was probably close to resonance in the Northridge earthquake.

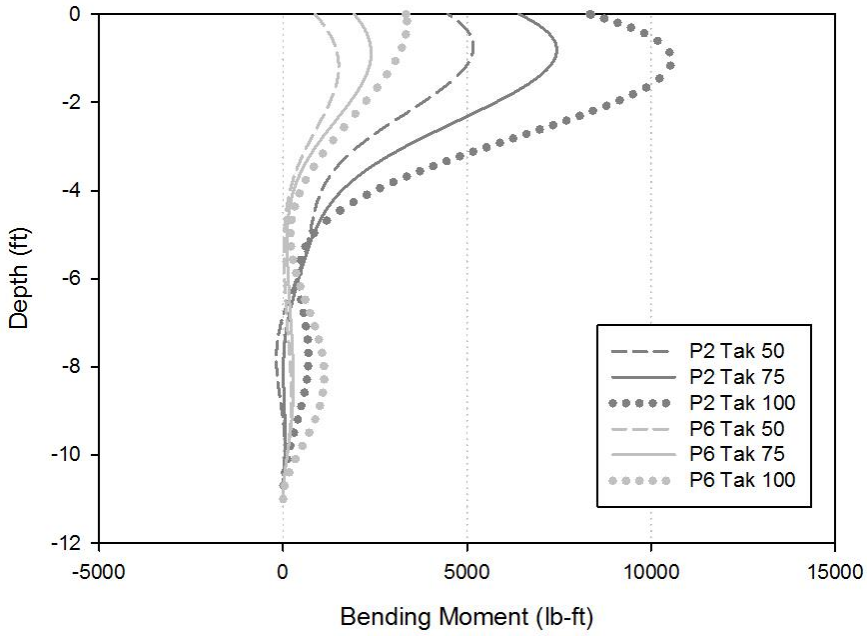

Figure 60. Comparison between the maximum bending moments of P6 (square shaft) vs P2(circular shaft) for the Takatori (Low Frequency) shakes

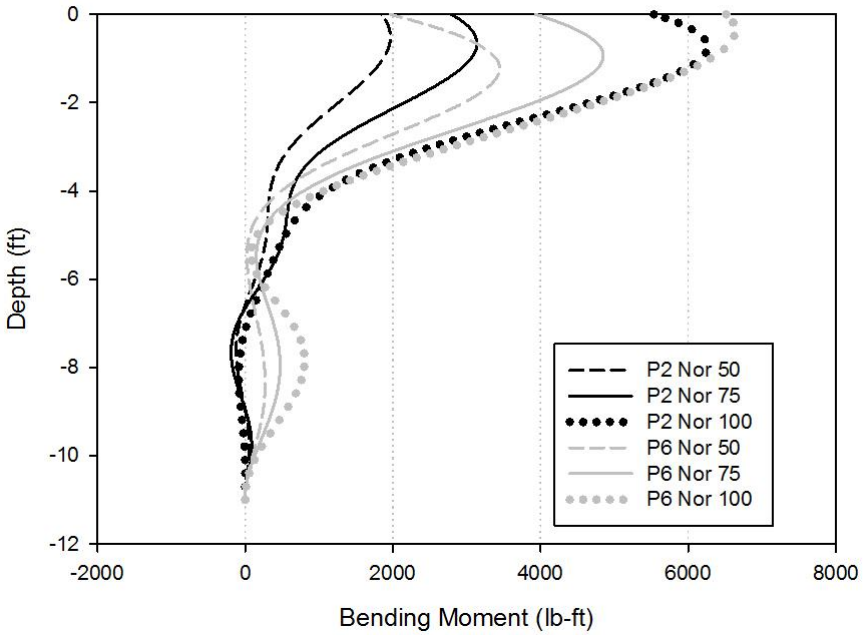

Figure 61. Comparison between maximum bending moments P6(square shaft) vs P2(circular shaft) for the Northridge (Higher Frequency) shakes

The relationship between the frequency content of the ground motion and the behavior of the helical pile with a square shaft can be easily determined at the same ground motion acceleration, (0.5 g), therefore, a comparison between the behavior of the piles at Northridge 100% and Takatori 75%, that presented the same peak acceleration of 0.5g, is illustrated in Figure 62.

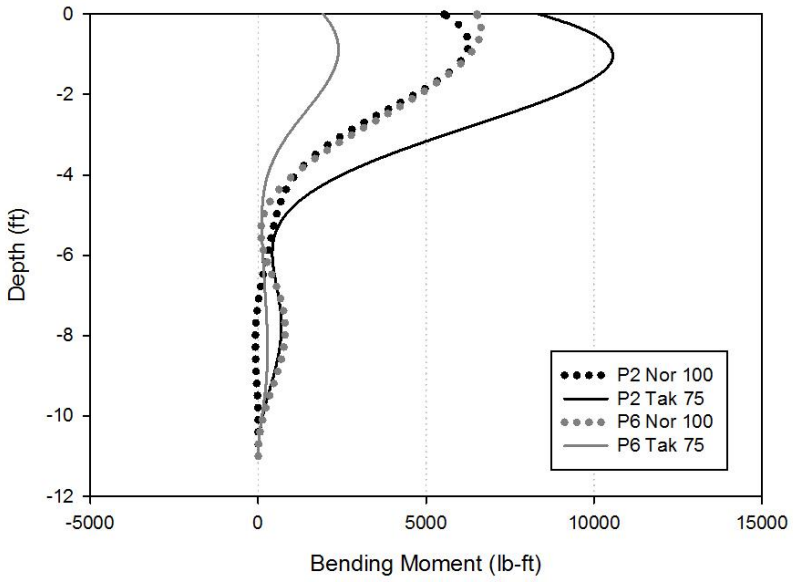

Figure 62. Comparison between maximum bending moments P6(square shaft) vs P2(circular shaft) for Northridge 100% and Takatori 75%

From Figure 62, it can be seen that the maximum bending moment of P6 increased approximately 95% with an increase in the frequency content, while the maximum bending moment of P2 decreased around 14% with an increase in the frequency content. P2 and P6 showed almost the exact same bending moment curves in the higher frequency shake (Northridge), even with different weights. However, during the Takatori earthquake even with the same peak acceleration, P2 (circular shaft) showed a much

greater bending moment curve. This difference in behavior is attributed to frequency content.

In addition to the comparisons between bending moments, a comparison between the calculated pile deflections was conducted. In Figure 63 and Figure 64 it can be seen that the maximum deflection of the pile 2 (circular) under 100% amplitude of the Takatori earthquake was around 1.7 times higher than the deflections obtained in P6 (square) for the same ground motion. The maximum deflections of P2 were always greater than the maximum deflections of P6 for all of Takatori shakes. The circular pile was more affected by lower frequency. The opposite can be seen with the Northridge earthquake. The maximum deflections of P6 (Square) under the Northridge higher frequency earthquake were greater than the maximum deflections of P2 (circular) for the Northridge earthquake with intensities of 100% and 75%. In general, the square pile was more affected by the higher frequency earthquake than the lower frequency earthquake and showed higher deflections. It is important to highlight that the natural frequency of P6 was 3.78 Hz, and the natural frequency of P2 was 2.33 Hz, therefore, it seems that the loading frequency of the Northridge earthquake better matched the natural frequency of the square-shaft helical pile, P6, while the Takatori earthquake had frequency content closer to the natural frequency of the circular-shaft pile (P2).

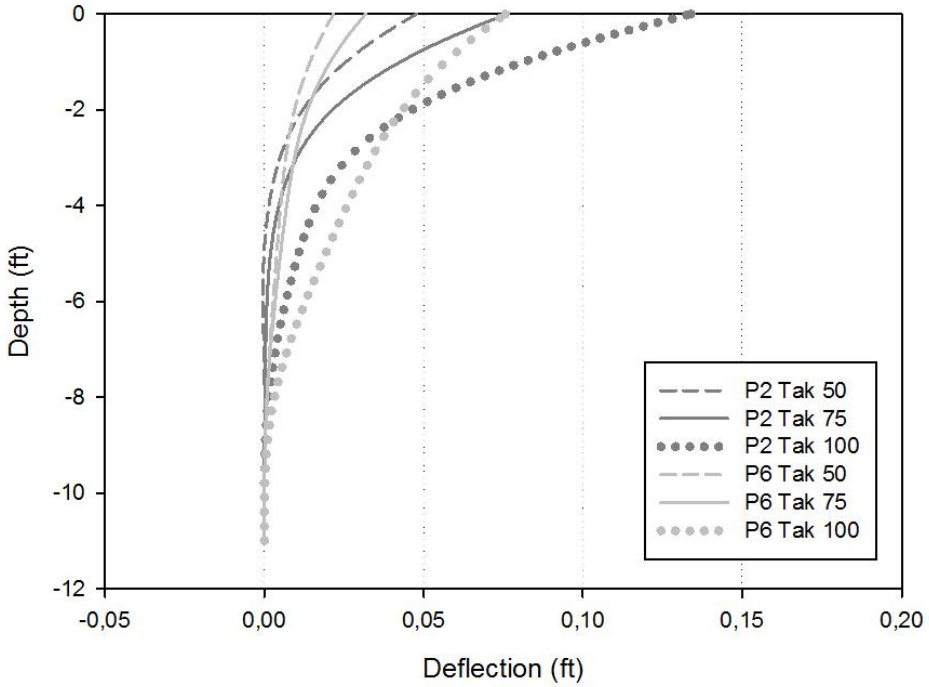

Figure 63. Comparison between the maximum pile deflection of P6 (square shaft) vs P2(circular shaft) for the Takatori shakes

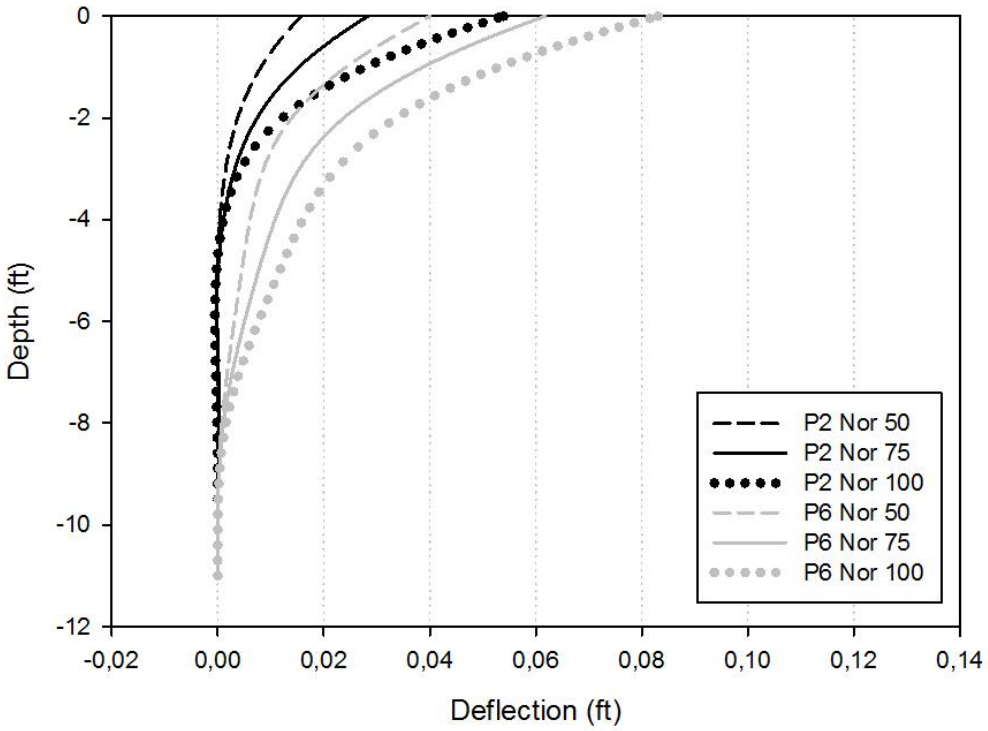

Figure 64. Comparison between the maximum pile deflection of P6 (square shaft) vs P2(circular shaft) for the Northridge shakes

Figure 65 and Figure 66 pull out the behavior of P2 and P6 under the 100% shakes to show clearly the difference in behavior between earthquake records; P6 (square) shows higher deflections than P2 (circular) under the higher frequency record (Northridge) but lower deflections than P2 under the Takatori shake.

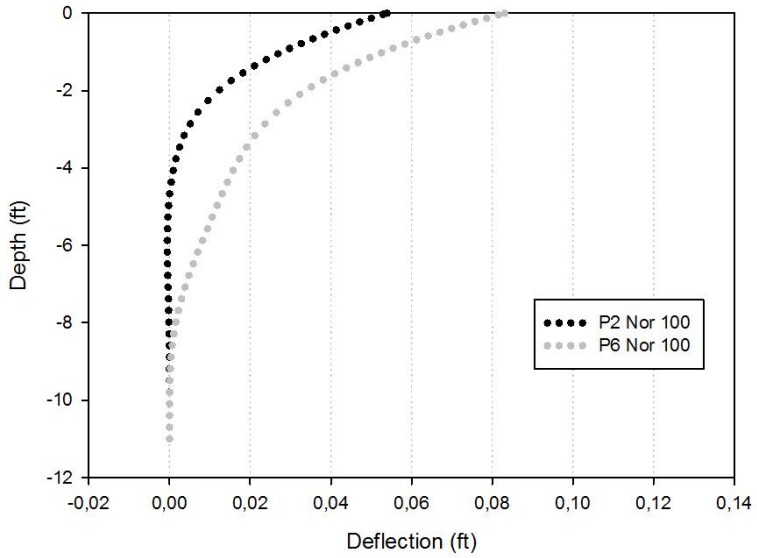

Figure 65. Comparison between maximum pile deflection of P6(square shaft) vs P2(circular shaft) for Northridge 100%

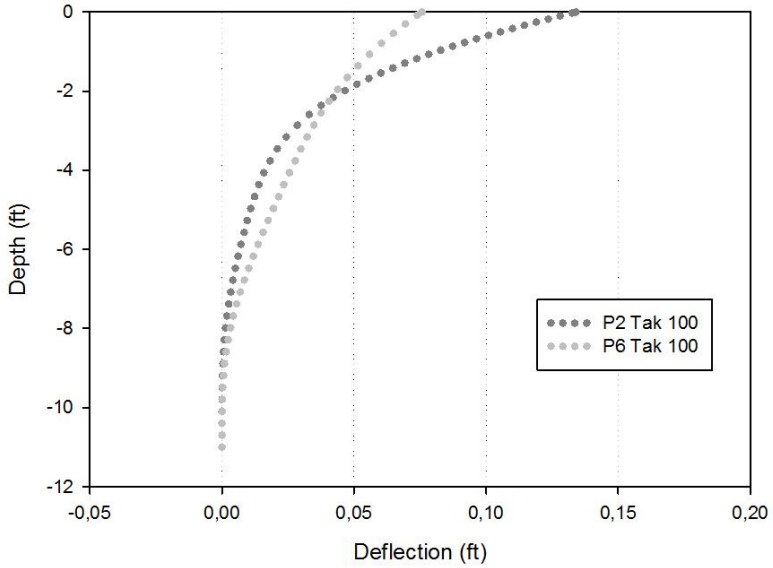

Figure 66. Comparison between maximum pile deflection of P6(square shaft) vs P2(circular shaft) for Takatori 100%

When analyzying these same piles under the same peak acceleration of 0.5 g, it can be seen that P2 shows higher deflection than the square pile (Figure 67).

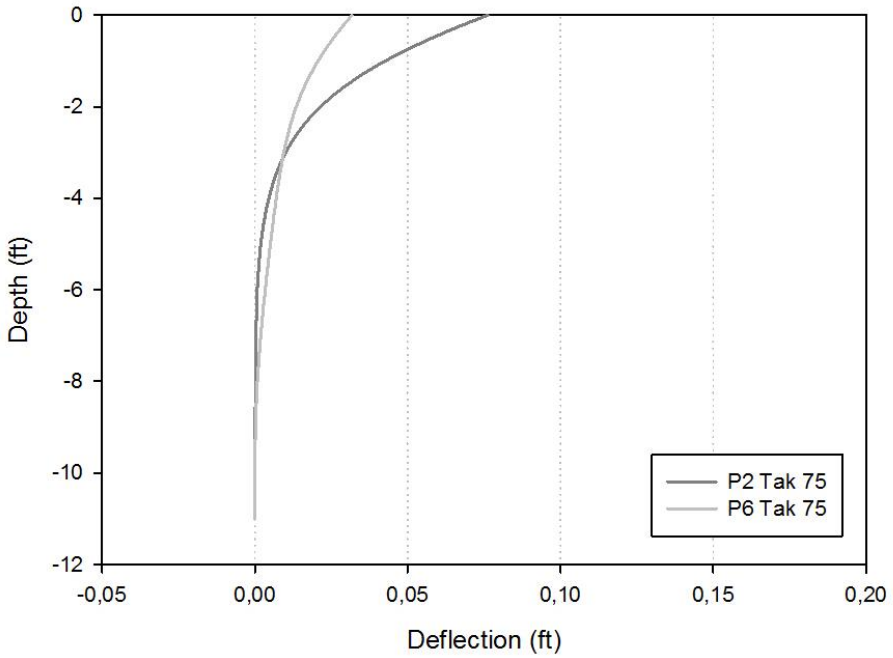

Figure 67. Comparison between maximum pile deflection of P6(square shaft) vs P2(circular shaft) for Takatori 75%

4.4. Effect of the helix configuration

To evaluate the influence of different helix configurations, the performance of P1, P2 and P4 were compared. P2 (single helical pile) and P4 (double helical pile) had double-bolt couples and P1 (single helical pile) had a threaded couple. The single helical piles had a helix of 10 inch of outside diameter, while the double helical piles had an 8-inch diameter bottom helix and a 10-inch diameter top helix. It was observed that the performance of the double helical pile (P4) and the performance of the single helical pile with the same length (P2) were fairly close during the Takatori 100% earthquake (Figure 68) but the

maximum bending moment of P2 was greater than the bending moment of P1 and P4 for the Northridge 100% earthquake (

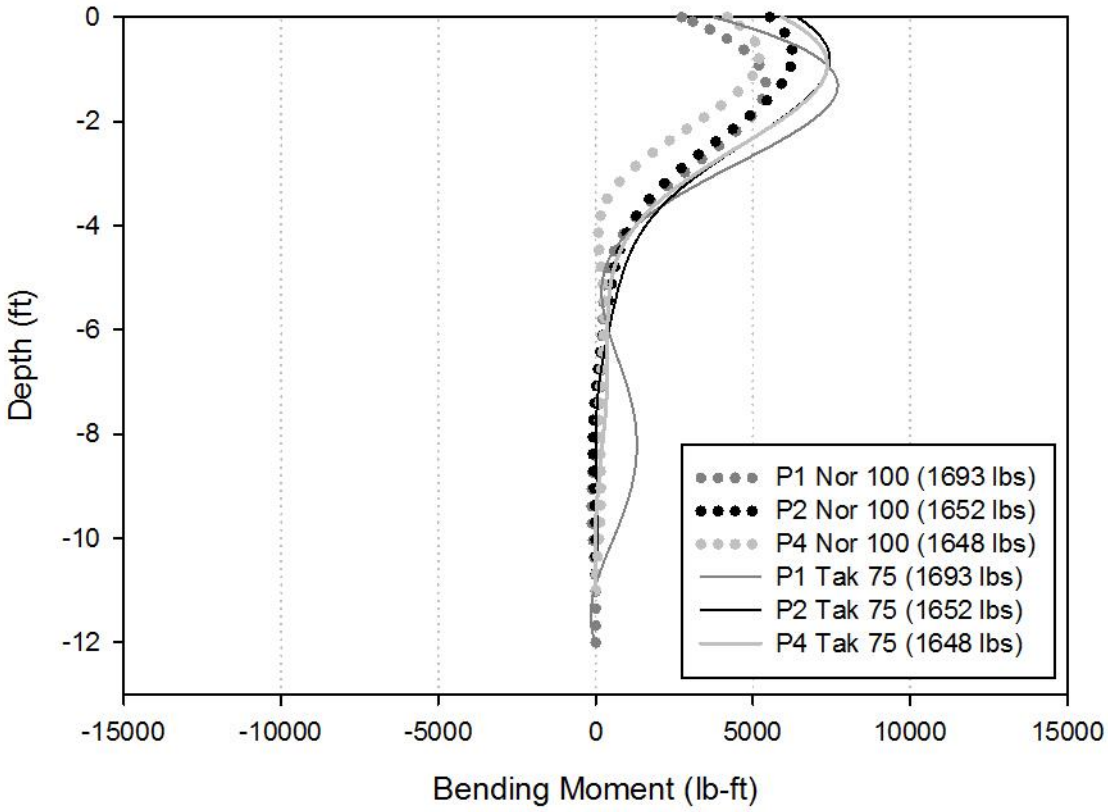

Figure 69). Looking at another shake, it was observed that P1 presented a slightly higher bending moment at a lower elevation than P2 and P4, which had similar bending moment magnitudes and locations to each other (Figure 69) during the Takatori 75% shake. This was similar to what was seen during the Takatori 100% shake (Figure 68).

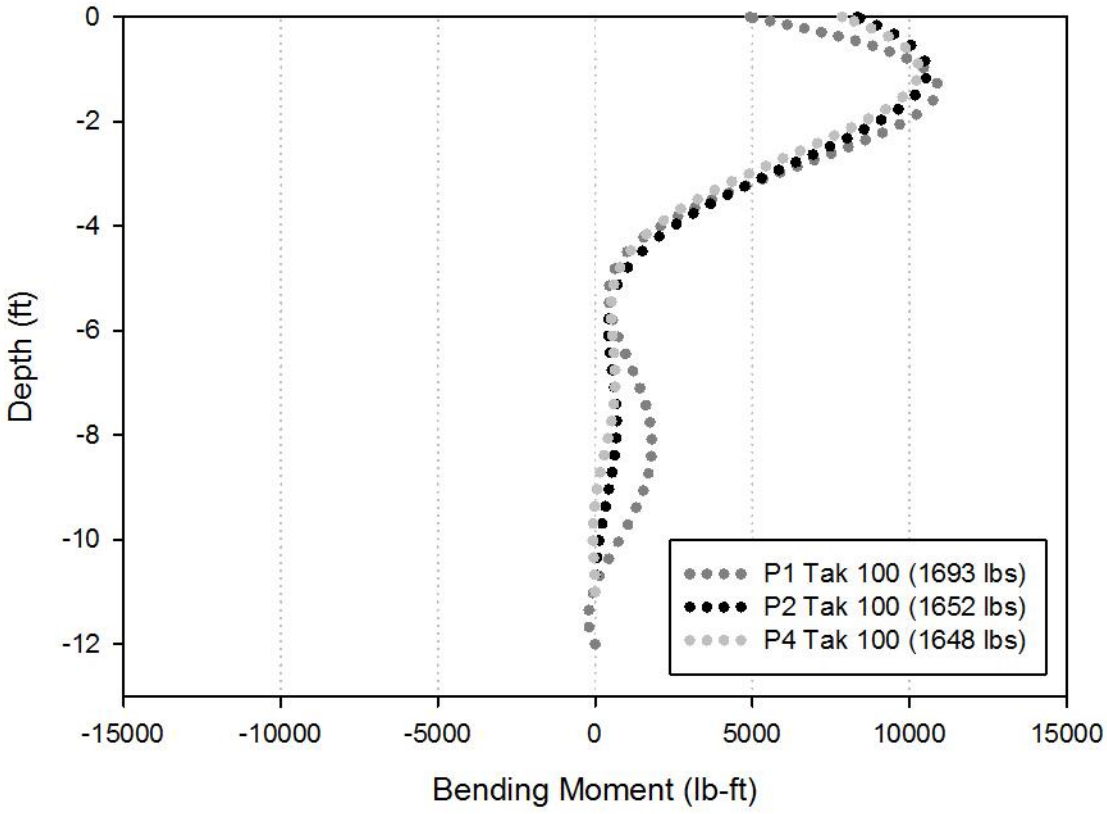

Figure 68. Comparison between maximum bending moments P1, P2 (single helix) vs P4 (Double helix) for Takatori 100%

In order to compare the effect of the frequency content of the earthquakes with the performance of the piles, Figure 69 was created. It was found that all the bending moments were higher for the Takatori earthquakes than for the Northridge earthquakes, but in general, the double helical pile presented lower bending moments than the single helical piles.

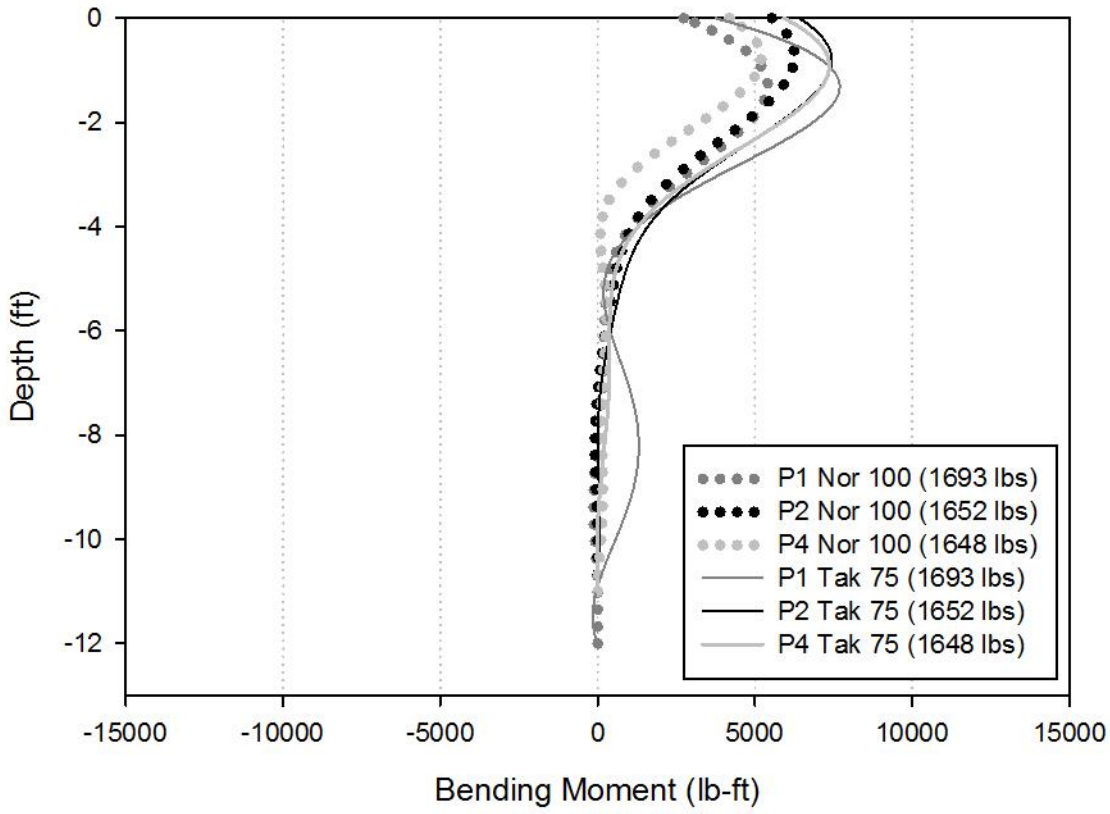

Figure 69. Comparison between maximum bending moments P1, P2 (single helix) vs P4 (Double helix) for Northridge 100% and Takatori 75%

The maximum deflection curves for P2 and P4 were similar during Northridge 100% (Figure 70), Takatori 100% (Figure 71) and Takatori 75% (Figure 72), but the double helix (P4) presented a lower maximum deflection for both the 100% shakes, probably because its natural frequency was slightly lower than that of P2 due to the lower inertial weight. On the other hand, when comparing the deflection of P1 (1 foot longer than P2 or P4) it seems that the influence of the helix depends on the type of ground motion. During Takatori 100%, (which was an earthquake with a peak acceleration of 0.67g with energy content concentrated in the frequency range between 0.5 Hz and 1.5 Hz) P1 presented a higher maximum deflection than P4. This occurred again during Takatori

75%. However, during Northridge 100%, P4 exhibited a higher maximum deflection than P1. Northridge 100% and Takatori 75% have the same peak acceleration of 0.5g, but with energy content concentrated in different frequency ranges.

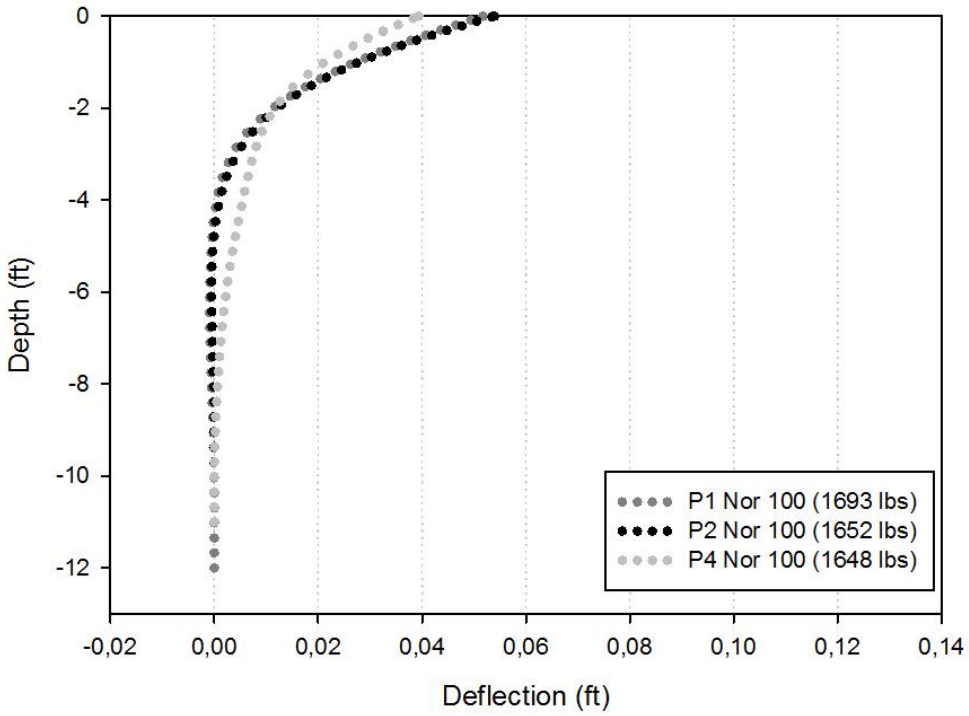

Figure 70. Comparison between maximum deflections P1, P2 (single helix) vs P4 (Double helix) for Northridge 100%

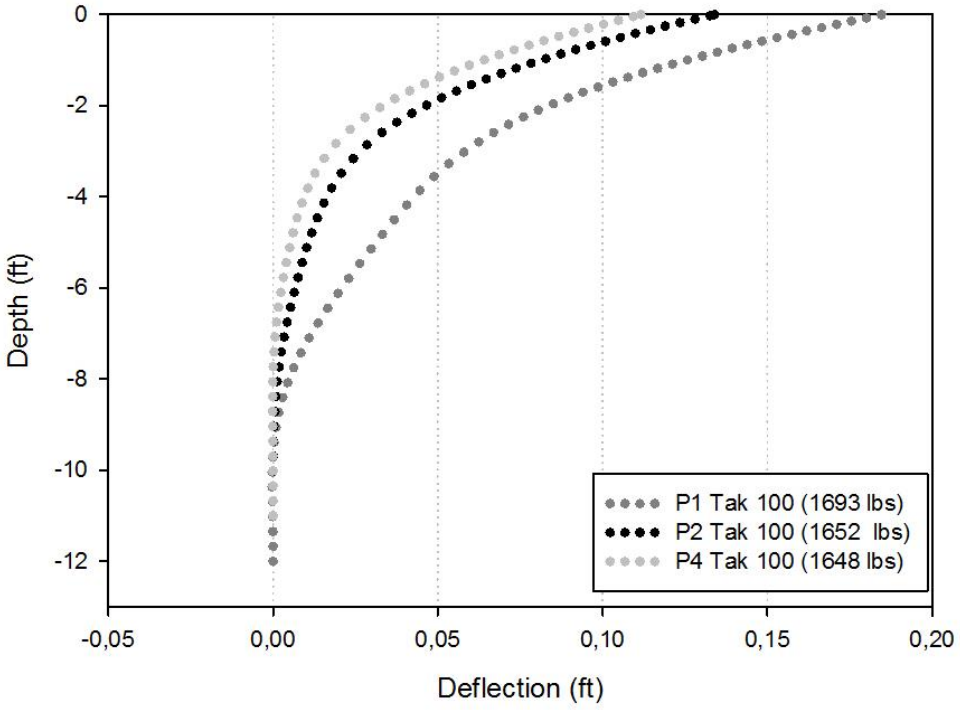

Figure 71. Comparison between maximum deflections P1, P2 (single helix) vs P4 (Double helix) for Takatori 100%

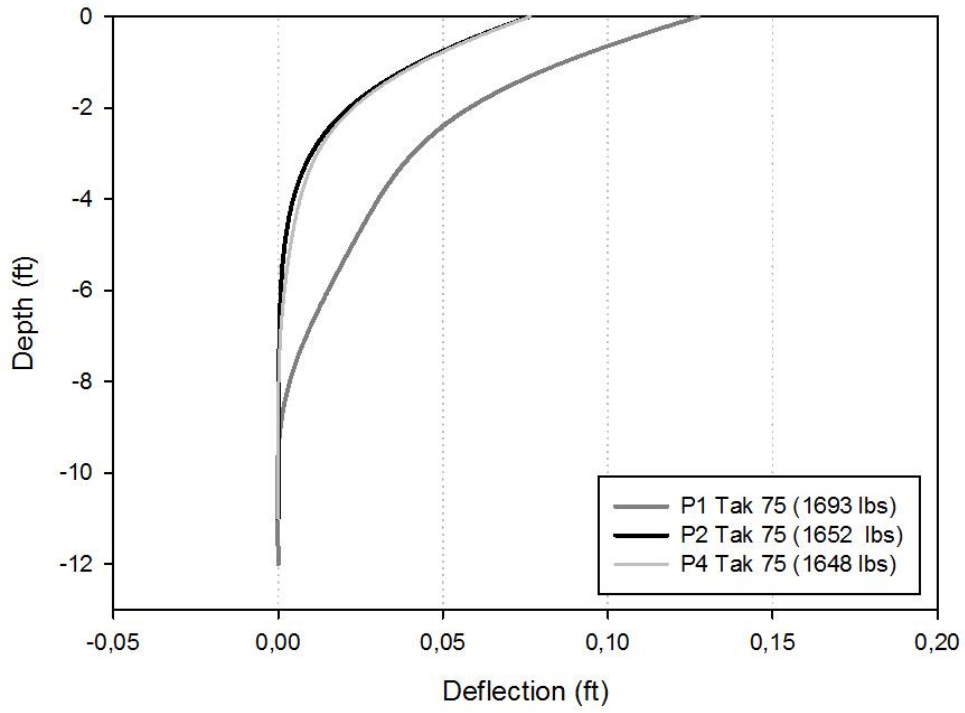

Figure 72. Comparison between maximum deflections P1, P2 (single helix) vs P4 (Double helix) for Takatori 75%

4.5. Effect of the installation method

The performance of P5 (push pile) and P2 was compared in order to better understand the influence of the installation method in the dynamic behavior of deep foundations. While the comparison cannot be direct because the inertial weight of the helical pile was twice the inertial weight that the push pile resisted, observations can be made on the behavior based on frequency contents. Under the Northridge earthquake P5 (push pile) showed almost the same bending moment curve as P2, but under the Takatori 75% and 100% earthquakes, P5 showed significantly less bending moment, while P2 increased slightly. It is noted that during the Northridge earthquake the natural frequency of P5 (4.05 Hz) may be at resonant frequency with that of the earthquake. In addition, it was concluded that the bending moment values increased as the intensity of the acceleration increased.

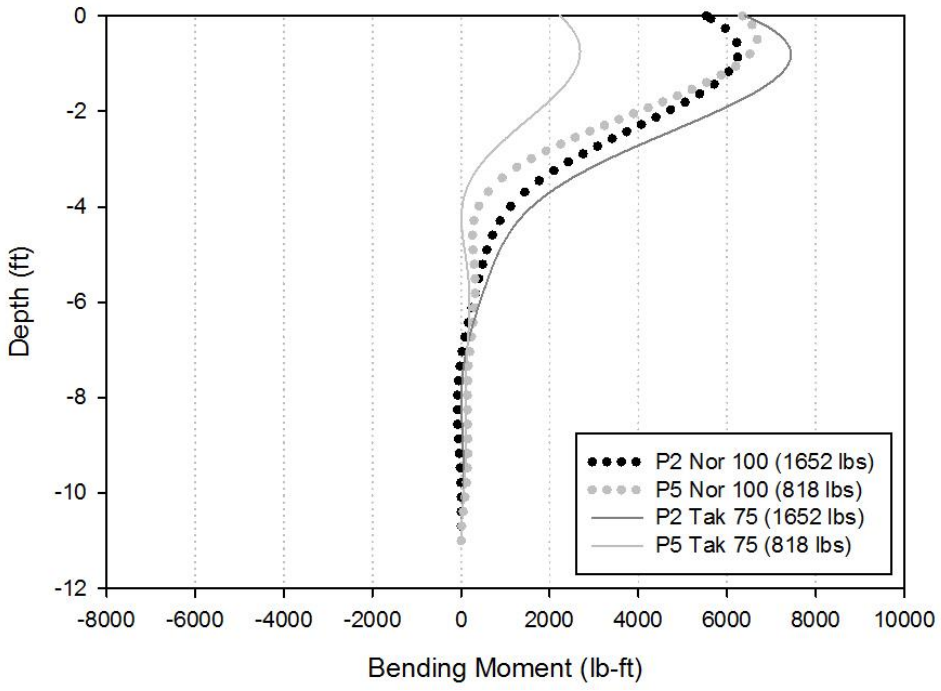

Figure 73. Comparison between maximum bending moments P2 (single helical pile) vs P5 (Push pile) for Northridge 100% and Takatori 75%

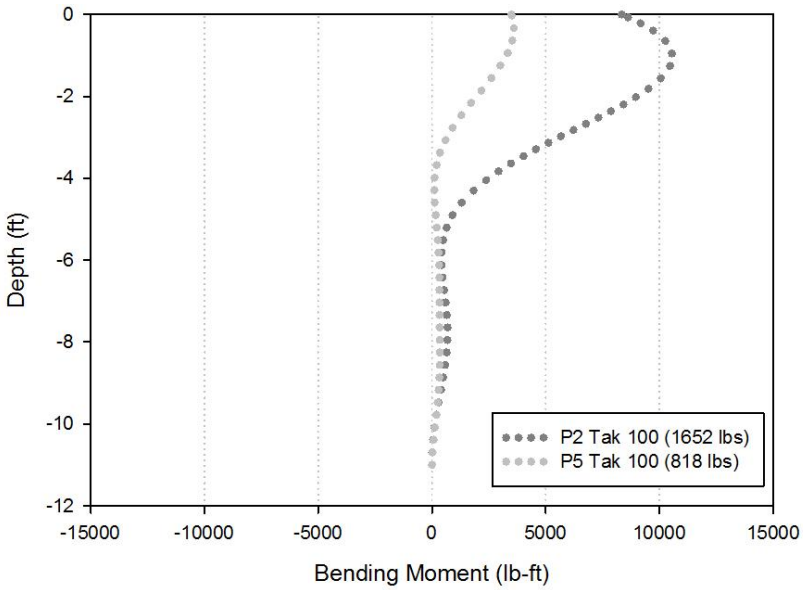

Figure 74. Comparison between maximum bending moments P2 (single helical pile) vs P5 (Push pile) for Takatori 100%

It was observed that the deflection of P2 was similar to the push pile during the Northridge shake (Figure 75), but considerably greater than the deflection of the push pile for both Takatori shakes (Figure 76 and Figure 77). The driven pile, with the shorter, smaller weight was more affected by the higher frequency Northridge earthquake than the lower frequency Takatori earthquake.

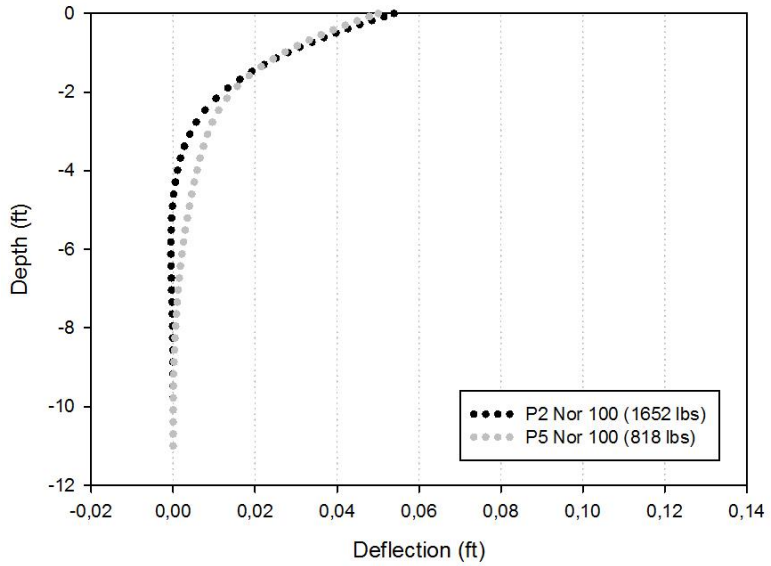

Figure 75. Comparison between maximum pile deflections, between P2 (single helical pile) vs P5 (Push pile) for Northridge 100%

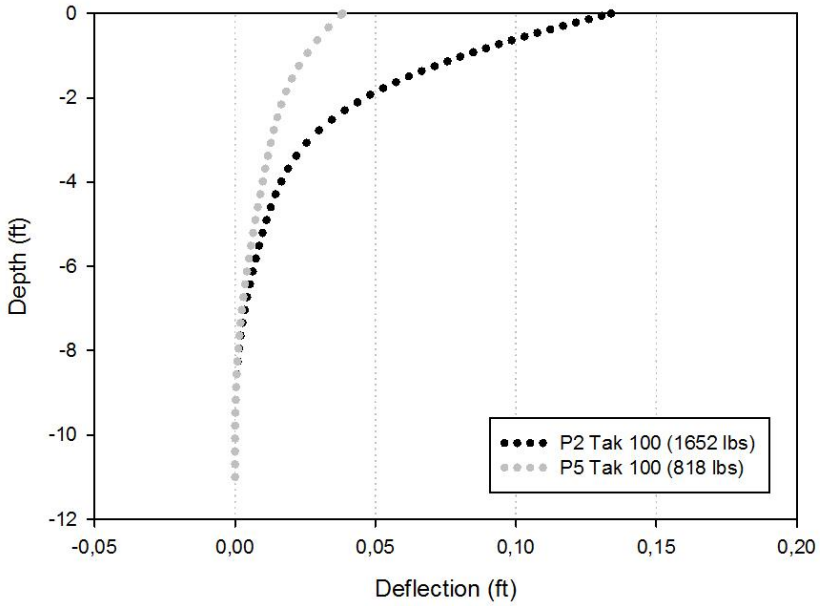

Figure 76. Comparison between maximum pile deflections, between P2 (single helical pile) vs P5 (Push pile) for Takatori 100%

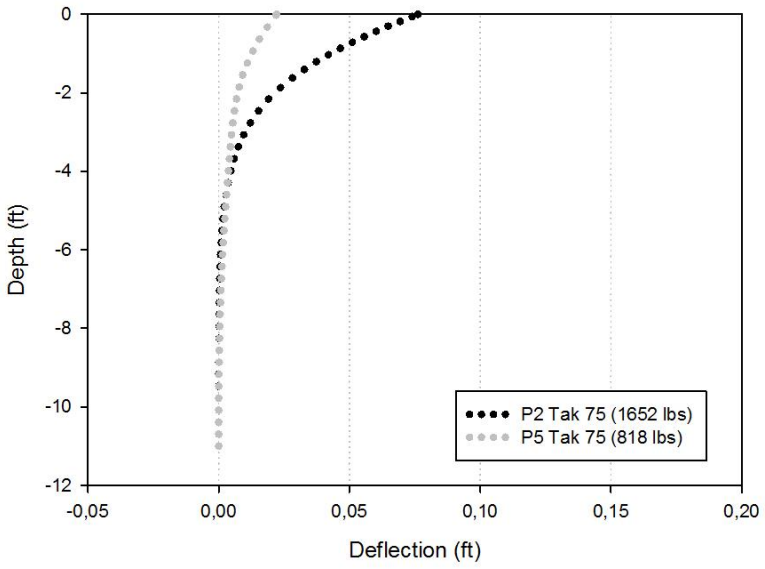

Figure 77. Comparison between maximum pile deflections between P2 (single helical pile) vs P5 (Push pile) for Takatori 75%

4.6. Effect of the load intensity

It is important to highlight that the results of soil reactions (p) are highly dependent on the fitting procedures that were employed to interpolate or approximate the bending moment curves. A slight deviation in the curvature of the fitted bending-moment curve can be magnified through the double differentiation process. As it was described in the computations section, a code in MATLAB was generated to optimize the location of the two interior knots of the 5^{th} order approximation splines. The code was created in order to optimize the fitting procedures at the top portion of the pile, as the goal of the research was to compute the p-y loops from 1.25D to 7D. In addition, the code was programmed in order to optimize its processing time to comply with the project deadlines. Nevertheless, the soil reaction that was obtained at the pile tip was greater than zero, which could be attributed to the greater curvature that the fitted bending-moments profiles presented at the bottom pile section and that were mentioned in section 3.8.2. According to (Degny, 1985), in order to fit bending moment records that were obtained from dynamic tests, the soil reaction curves at the pile tip were forced to approach zero using a smoothing –spline methodology, which was conducted at the bottom portion of the pile using the software that they developed. The same approach was undertaken to create an improved profile of soil reaction.

A complete report of the test results is included in Appendix A to D, and it was observed that as the intensity of the acceleration increases, the bending moment of all the piles increased and the deflection increased as well (except for P4, double helical pile, and P1 during the Northdridge shakes). It was also observed that at greater intensities of ground

motions, the absolute shear force at the upper portion of the piles-soil interface (1.25D to 7D) increases. This was observed for all piles but P4, double helical pile, during the Northridge shakes, the push-pile, P5, during both Northridge and Takatori earthquakes and P6, the square-shaft helical pile, for both Northridge and Takatori ground motions. On the other hand, the absolute value of the soil reaction at the top portion of the soil-pile interface, for all the piles analyzed, increased as the intensity of the ground motion increased.

4.7. Comparisons between p-y loops

The dynamic p-y hysteretic loops obtained for the upper portions of the pile (1.25D to 7D) are shown in Figure 78 and Figure 79 for piles 1 and 2, respectively. It was observed a hysteretic reduction of damping with respect to depth for both piles. It was observed that the Takatori shakes presented higher deflections and soil reactions than the values presented for the Northridge earthquake. It can also be seen that P1 shows more non-linearity in the hysteresis than P2, which suggests that P1 exhibit a higher pile-soil damping (area under the curve). It is unclear at this time why that may be, but my thought is that the type of couple and its inherent stiffness played a role.

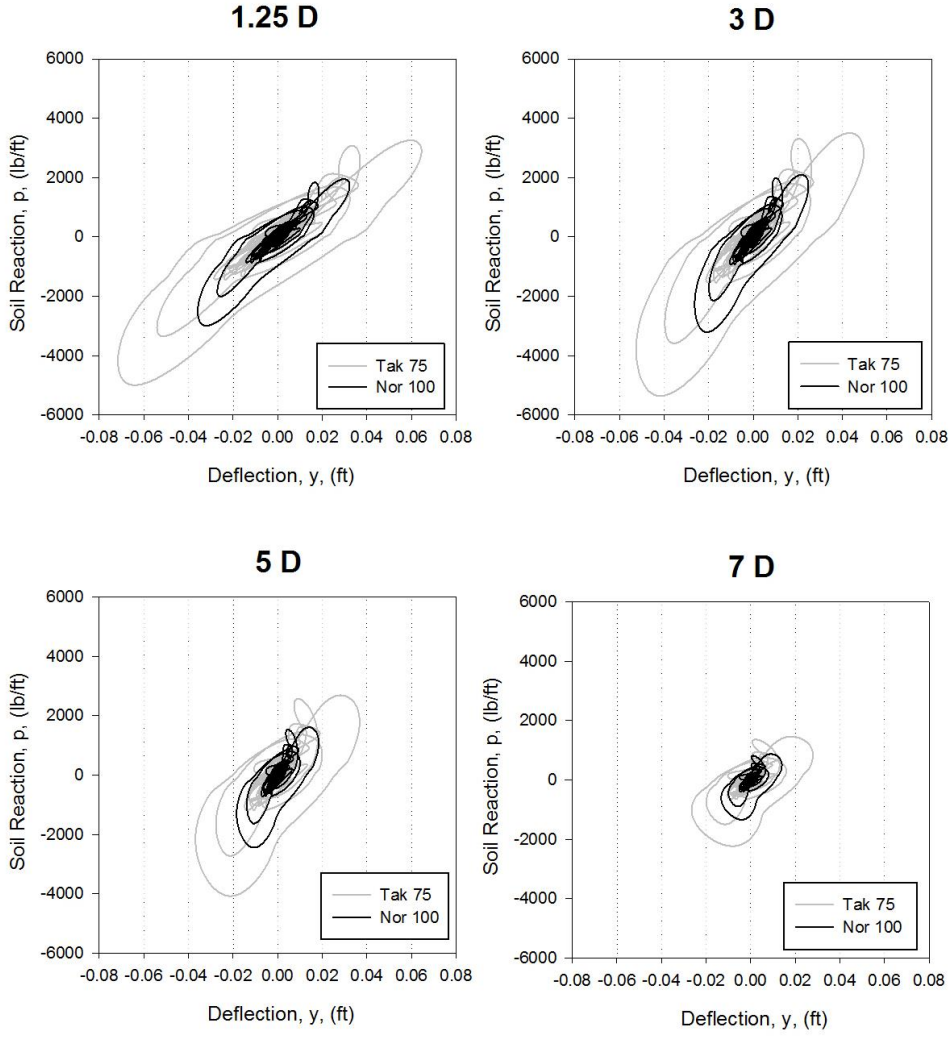

Figure 78. p-y loops for P1 Takatori 75% and Northridge 100%

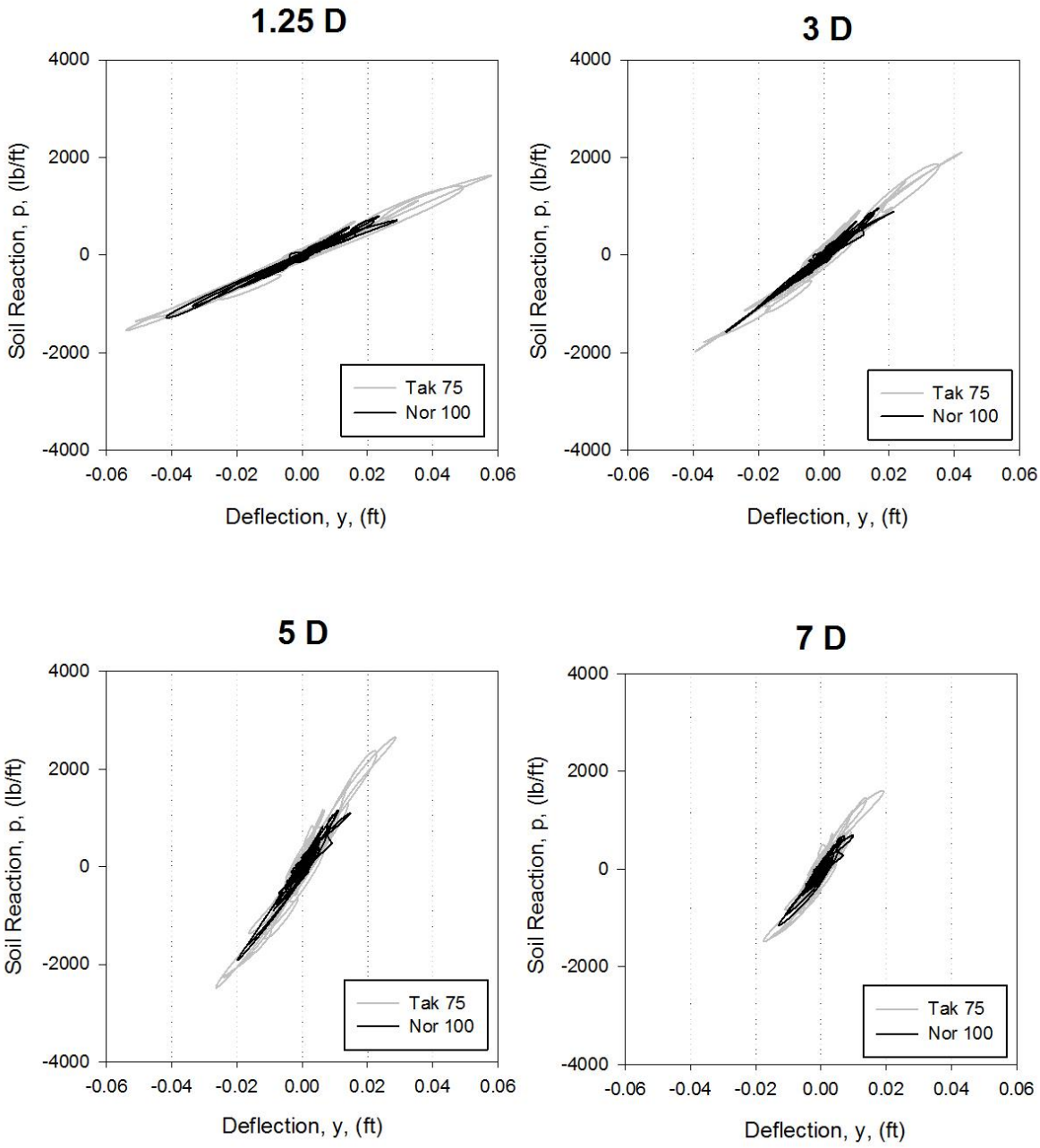

Figure 79. p-y loops for P2 Takatori 75% and Northridge 100% T0

5. Summary and Conclusions

The primary objectives of this research project included 1. Reporting and documenting the general performance of single helical piles in dense sand subjected to two major earthquakes events (Takatori and Northridge), 2. Quantifying the influence of the number of helices of screw anchors on their dynamic lateral resistance, 3. Quantifying the influence of shaft geometry on seismic performance, and 4. Quantifying the influence of pile type and installation method on seismic performance. A large-scale shake table experimental test was undertaken to produce results that would fulfill these objectives.

5.1. Conclusions

Some conclusions can be summarized as follows:

- It was observed that the dynamic performance of the piles was primarily influenced by their natural frequency, and therefore the resonant frequency generated with the frequency of the earthquake. The natural frequency of the square helical pile was higher than the natural frequency of the circular helical pile.
- For ground motions with frequency ranges between 0.5 Hz to 5 Hz and peak accelerations between 0.25g to 0.67g, the single helical pile presented a stiffer behavior compared with the double helical pile, which may be attributed to the higher soil disturbance produced during the installation of the double helical pile.

- Under ground motions characterized by a low frequency content (up to 1.5 Hz), the square-shaft helical pile outperformed the response of the circular-shaft helical pile for all the accelerations tested.
- Under seismic conditions, it was observed a hysteretic reduction of the damping response of single helical piles with respect to the depth of the soil. This reduction was independent of the length of the pile, for the geometries tested. The reduction in the damping response of the helical piles under dynamic loadings is consistent with previous results conducted in other pile types (Hajialilue-bonab, et al., 2007). This results are consistent with the calculated deflections at higher depths of embedment.
- The single-helix helical pile with embedment depth of 11 feet and double thru-bolt couple (P2) presented the same damping response of the single-helix helical pile with embedment depth of 12 feet and a threaded couple (P1) for depths from 1.25 D to 7D.

5.2. Recommendations

This was the first true seismic test on helical piles and the results generated thus far show that helical piles in dense sand performed extremely well under multiple earthquake sequences. While much data and insight has been achieved through this test, there is much more information to be gathered through further analysis of this data as well as

additional testing. Some potential research efforts that would help in explaining questions raised through this study are:

- Analysis of the axial load distribution during shaking to assess the helical plate influence on capacity.

- It is recommended to perform test in other soil types and other conditions. It would be recommendable to perform other tests in sands using lower relative densities to evaluate the influence of the density of the soil in the seismic performance of the soil-pile system.

- It is recommended to calculate additional p-y loops at the bottom portions of the piles using the MATLAB code created with the present research, in order to evaluate the change in the dynamic performance of the pile with depth.

- It is recommended to calculate additional p-y loops using the MATLAB code created with the present research at different ground motion intensities, in order to evaluate the dynamic performance of the piles with greater accelerations and the change in their performance.

- It is recommended to calculate additional p-y loops for the other piles tested; P3, P4, P5, P6, P7, P8, P9 and P10 using the MATLAB code created with the present research, in order to compare the dynamic performance of the piles throughout

the sand depth and the influence of the different geometries tested in the general shape of the p-y loops.

- It is recommended to conduct further research in order to study the influence of the location of the strain gauges into the accuracy of the available fitting methods to calculate dynamic p-y curves.

- It is recommended to conduct further tests of helical piles under earthquake motions in order to determine the influence of the double helix in the general seismic behavior of the piles.

- It is recommended to conduct further tests on helical and driven piles under seismic conditions using the same inertial weights in order to conduct direct comparisons between their performances.

Bibliography

Abdelghany, Y. (2008). *Monotonic and cyclic behaviour of helical screw piles under axial and lateral loadings.* London, Ontario, Canada: The University of Western Ontario.

Abdelghany, Y., & El Naggar, M. (2011). Steel Fibers Reinforced Grouted and Fiber Reinforced Polymer Grouted Screw Piles - An Innovative Deep Foundations Seismic Systems. *Proceedings of the 2011 Pan-Am CGS Geotechnical Conference, GEO11 - Paper 1043* (pp. 1-10). Toronto, ON, Canada: GEO11.

Abdoun, T., & Dobry, R. (2002, October). Evaluation of Pile Foundation Response to Lateral Spreading. *Soil Dynamics and Earthquake Engineering, 22*(9-12), 1051-1058.

Allotey, N., & El Naggar, M. H. (2008, September). A numerical study into lateral cyclic nonlinear soil–pile response. *Canadian Geotechnical Journal, 45*(9), 1268-1281.

American Society of Civil Engineers (ASCE). (2005). *Minimum Design Loads for Buildings and Other Structures.* American Society of Civil Engineers (ASCE).

Ashford, S. A., Rollins, K. M., & Baez, J. I. (2000). Comparison of Deep Foundation Performance in Improved and Non-improved Ground using Blast-induced Liquefaction. *Soil Dynamics and Liquefaction*, 20-34.

Basack, S., & Bhattacharya, A. K. (2009, January). Influence of Lateral Cyclic Load on Pile Foundation with Emphasis on Disturbance at Ground Surface . *EJGE, 14*, 1-11.

Basack, S., & Dey, S. (2011). Pile Subjected to Lateral Cyclic Loading in sand. *Proceedings of Indian Geotechnical Conference, December 15-17, 2011*, (pp. 1-4). Kochi.

Bea, R. G., Audibert, J., & Dover, A. R. (1980). Dynamic response of laterally and axially loaded piles". *Proceedings of the 12th OTC conference, Paper OTC 3749*, pp. 129-139. Houston, TX.

Beim, J., & Luna, S. (2012, July). Results of Dynamic and Static Load Tests on Helical Piles in the varved clay of Massachusetts. *DFI Journal, 6*(1), 58-67.

Bergdahl, U., & Hult, G. (1981). Load Test on Friction Piles in Clay . *Proceedings of the 10th international conference on soil mechanics and foundation engineering, 2*, pp. 625-630. Stockholm, Sweden.

Bhattacharya, S., Tokimatsu, K., Goda, K., Sarkar, R., Shadlou, M., & Rouholamin, M. (2014, October). Collapse of Showa Bridge during 1964 Niigata earthquake: A quantitative reappraisal on the failure mechanisms. *Soil Dynamics and Earthquake Engineering, 65*, 55–71.

Bogard, D., & Matlock, H. (1998). Static and cyclic load testing of a 30-inch diameter pile over a 2.5-year period. *Proceedings 30th annual Offshore Technology Conference 4-7 May, 1998, 1*, pp. 455-468. Houston, TX.

Bogard, J. D., & Matlock, H. (1990a). In-Situ Pile Segment Model Experiments at Empire, Louisiana. *22nd Annual Offshore Technology Conference.* Houston, TX.

Bogard, J. D., & Matlock, H. (1990b). Application of Model Pile Tests to Axial Pile Design. *22nd Annual Offshore Technology Conference.* Houston, TX.

Bogard, J. D., & Matlock, H. (1991). In-Situ Model Pile Experiments at West Delta 58A. *23rd Annual Offshore technology conference* .

Broms, B. (1972). *Bearing capacity of cyclically loaded piles* . Swedish Geotechnical Institute.

Buhler, R., & Cerato, A. (2010). Desing of dynamically wind-loaded helical piers for small wind turbines. *ASCE Journal of Performance of Constructed Facilities, 24*(4), 417-426.

Cannon, J. (2000). The application of high strain dynamic pile testing to screwed steel piles. *Sixth International Conference on the Application of stress-wave theory to piles.* (pp. 393-398). Sao Paulo, Brazil: Nivaa and J. Beim Eds. .

Chan, & Hanna. (1980). Repeated loading on single piles in sand. *Journal of the geotechnical engineering division, 102*(2), 171-180.

Chen, R.-p., Sun, Y.-x., Zhu, B., & Dong Guo. (2015). Lateral cyclic pile-soil interaction studies on a rigid model monopile. April. *ICE Proceedings Geotechnical Engineering, 168 (2)*, pp. 120-130.

Clemence, & Smithling. (1984). Dynamic uplift capacity of helical anchors in sand. In 1.-1. M. 1984 (Ed.), *Proceedings of the Fourth Australia - New Zealand Conference on Geomechanics. V1*, pp. 88-93. Perth, Western Australia: Publ Barton: Inst of Engineers.

Clemence, S. P., & Pepe, F. (1984). Measurement of Lateral Stress Around Multi-Helix Anchors in Sand. *Geotechnical Testing Journal, 7*(3), 145-152.

Cox, W. R., Cameron, K., & Clarke, J. (1993). Static and Cyclic axial load tests on two 762mm diameter pipe piles in clay. In J. Clarke (Ed.), *Proceedings of the*

conference recent large-scale fully instrumented pile tests in clay. London, UK: Thomas Telford.

Degny, E. (1985). *SLIVALIC5 - Programme de lissage par spline quintique.* Ministère de l'Urbanisme du Logement et des Transports, France.

Dilley, L., & Hulse, L. (2007). *Foundation Design of Wind Turbines in Southwestern Alaska, a Case Study.* Institute of the North. Anchorage, Alaska: The Artic Energy Summit.

Dobry, R., Vicente, E., O'Eourke, M., & Roesset, J. (1982). Horizontal stiffness and damping of single piles. *Journal of the Geotechnical Engineering DIvision, 108*(GT3), 439-459.

Doherty, P. (2009). Cyclic axial loading of offshore piles- an issue of concern? *DFI 34th annual conference on deep foundations on October 21-23, 2009* (p. 13). Kansas, MO: Deep Foundation Institute Organization.

Doyle, E. H., & Pelletier, J. H. (1985). Behavior of a large scale pile test in silty clay. *Proceedings of the 11th International Conference in Soil Mechanics Foundation Engineering.* San Francisco, CA.

El Naggar, M., & Abdelghany. (2007). Seismic helical screw foundations systems. *Proceedings of the 60th Canadian Geotechnical Conference.* Ottawa.

El Sharnouby, M. (2012, October). Monotonic and Cyclic Behaviour of Steel Fibre-Reinforced and FRP-Steel Fibre-Reinforced Helical Pulldown Micropiles. London, Ontario, Canada.

El Sharnouby, M. M., & El Naggar, M. H. (2011). Monotonic and Cyclic Axial Full - Scale Testing of Reinforced Helical Pulldown Micropiles. *2011 Pan-Am CGS Geotechnical Conference*, (p. 6). Toronto, ON, Canada.

El Sharnouby, M. M., & El Naggar, M. H. (2011). Monotonic and cyclic lateral full scale testing of reinforced helical pulldown micropiles. *Deep Foundations Institute*, 9.

El Sharnouby, M. M., & El Naggar, M. H. (2012 (b)). Field investigation of axial monotonic and cyclic performance of reinforced helical pulldown micropiles. *Canadian Geotechnical Journal, 49*, 560 – 573.

El Sharnouby, M., & El Naggar, M. (2012(a)). Axial Monotonic and cyclic performance of fibre-reinforced polymer (FRP)- steel fibre-reinforced helical pulldown micropiles (FRP-RHPM). *Canadian Geotechnical Journal, 49*, 1378-1392.

Elkasabgy , M., El Naggar, M., & Sakr, M. (2011). Field and theoretical dynamic response of vertically loaded helical and driven steel piles. *Proceedings of the 2011 Pan-Am CGS Geotechnical Conference.* Toronto, Ontario, Canada.

Elkasabgy, M., & El Naggar, M. (2013). Dynamic response of vertically loaded helical and driven steel piles. *Canadian Geotechnical Journal, 50,* 521–535.

Elkasabgy, M., El Naggar, M., & Sakr, M. (2010). Full-Scale vertical and horizontal dynamic testing of a doubel helix screw pile. *GeoCalgary 2010,* (pp. 352-359). Calgary, Alberta.

Fox, P. J., Sander, A. C., Elgamal, A., Greco, P., Isaacs, D., Stone, M., & Wong, S. (2015, January). Large Soil Confinement Box for Seismic Performance Testing of Geo-Structures. *Geotechnical Testing Journal, 38*(1), 72-84.

Gallagher, K. A., & St. John, H. D. (1980). Field scale model studies of piles as anchorages for buoyant platforms. *Procedure of European Off-shore Petroleum Conference.* London, UK.

Gazetas, G., & Dobry, R. (1984). Horizontal response of piles in layered soils. *Journal of Geotechnical Engineering, 110*(1), 20-40.

Gerber, T. (2003). *P-y curves for liquefied sand subject to cyclic loading based on testing of full-scale deep foundations.* Provo, UT: Brigham Young University.

Ghaly, A., & Hanna, A. . (1991). Experimental and theoretical studies on installation torque of screw anchors . *Canadian Geotechnical Journal, 28*(3), 353-364.

Grosch, J., & Reese, L. C. (1980). Field tests of small-scale pile segments in a soft clay deposit under repeated axial loading. *Proceedings of the 12th OTC conference* , (pp. 143-151). Houston, TX.

Gudehus, G., & Hettler, A. (1981). Cyclic and monotonous model tests in sand. *Proceedings of the 10th International Conference on Soil Mechanics and Foundation Engineering, 2*, pp. 211-214. Stockholm.

Guo, W. D. (2006). On limiting force profile, slip depth and response of lateral piles. *Computers and Geotechnics, 33*(1), 47-67.

Guo, W. D., & Zhu, B. T. (2005). Static and cyclic behavior of laterally loaded piles in calcareous sand. In S. a. Gourvence (Ed.), *Frontiers in Offshore Geotechnics: ISFOG 2005,* (pp. 373–379). London.

Hajialilue-bonab, M., Levacher, D., & Chazelas, J.-L. (2007). Experimental evaluation of static and dynamic p-y curves in dense sand. *4th International Conference on Earthquake Geotechnical Engineering,* (pp. 1-8).

Hamada, M. (1992a.). *Large ground deformations and their effects on lifelines: 1964 Niigata Earthquake.* Case studies of liquefaction and lifeline performance during past earthquakes. Buffalo, NY: National center for earthquake engineering research.

Hamada, M. (1992b.). *Large ground deformations and their effects on lifelines: 1983 Nihonkai-chubu earthquake.* Case studies of liquefaction and lifeline performance during past earthquakes. Buffalo, NY: National center for earthquake engineering research.

Hamada, M. (2000). Performances of foundations against liquefaction-induced permanent ground displacements. *12th WCEE 2000*, (p. 8).

Hamada, M., Saito, K., Yasuda, S., & Isoyama, R. (1988). Earthquake damage by liquefaction-induced permanent ground displacement. *Proceedings of the ninth world conference on earthquake engineering, August 2-9, VIII*, pp. 213-218. Tokyo-Kyoto, Japan.

Hamada, M., Wakamatsu, K., & Yasuda, S. (1992a.). *Liquefaction-induced ground deformations during the 1923 kanto earthquake.* Case Studies of Liquefaction and lifeline performance during past earthquakes. Buffalo, NY: National center for earthquake engineering research.

Hamada, M., Yasuda, S., & Wakamatsu, K. (1992b.). *Large ground deformations and their effects on lifelines: 1948 Fukui Earthquake.* Case studies of liquefaction and lifeline performance during past earthquakes. Buffalo, NY: National center for earthquake engineering research.

Holmquist, D., & Matlock, H. (1976). Resistance-displacement relationships for axially-loaded piles in soft clay. *Proceedings of the 8th offshore technology conference.* Houston, TX.

Hussein, M., Tobita, T., & Susumu, I. (2010). Experimental and FE Analysis of seismic soil-pile-structure interaction in sand. *Annuals of Disas. Prev. Res. Inst., Kyoto University, No. 53 B*, pp. 299-306. Kyoto.

Huybrechts, N., & Legrand, C. (1998). Static and Dynamic pile loading tests on different types of driven piles in Limelette (B). *Proceedings- Seventh International Conference & Exhibition on piling and deep foundations. Vienna, Austria* (pp. 1.20.1-1.20.10). Vienna, Austria: DFI.

International Code Council. (2014). *International Building Code (IBC).* Washington, DC: International Code Council.

Jaime, A., Romo, M., & Resendiz, D. (1990). Behavior of friction piles in Mexico City clay. *Journal of Geotechnical and Geoenvironmental Engineering, 116*, 915-931.

Japan Society of Civil Engineers. (1966). *Report on the 1964 Niigata Earthquake.* Research commitee on the 1964 Niigata Earthquake, Tokyo, Japan.

Kanai, S. (2007). A seismic retrofitting application by means of multihelix micropiles. *23th U.S. - Japan Bridge Engineering Workshop.* Tsukuba.

Kawamura, S., Nishizawa, T., & Wada, H. (1985). Damage to piles due to liquefaction found by excavation tweenty years after earthquakes. *Nikkei Architecture*.

Kishida, H. (1996). Damage to reinforced concrete buildings in Niigata City with special reference to foundation engineering. *Soils anf Foundations, 6*(1), 71-88.

Komatsu, A. (2007). Development on battered pile with screw pile method (NS-ECO pile). In Y. K. Francis (Ed.), *Proceedings of the International Workshop on Recent Advances of Deep Foundations (IWDPF07)*, (pp. 253–257). Yokosuka, Japa.

Kraft, L. M., Cox, W. R., & Verner, E. A. (1981). Pile load test: cyclic loads and varying load rates. *Journal of the Geotechnical Engineering Division, 107*, 1-19.

L. Rasmussen, K., Hansen, M., Kirk Wolf, T., Ibsen, L. B., & Roesen, H. R. (2013). *A Literature Study on the Effects of Cyclic Lateral Loading of Monopiles in Cohesionless Soils.* Aalborg, Department of Civil Engineering. Aalborg: Aalborg University.

Lai, J., Zheng, Y., Liu, Y., & Lee, Y. (2014). Analysis of shaking table model test on embedded anti-slide piles under earthquake. *EJGE, 19*, 3963-3976.

Livneh, & El Naggar, H. (2008). Axial testing and numerical modeling of square shaft helical piles under compressive and tensile loading. *Canadian Geotechnical Journal. , Vol. 45*(No. 8), 1142-1155.

Lutenegger, A. J. (2015). *Technical bibliography on Design, Construction and Performance of Screw-Piles and Helical Anchors.* University of Massachusetts, Department of Civil and Environmental Engineering. Amherst,MA: International Society for Helical Foundations (ISHF).

Marsafawi, H., Han, Y., & Novak, M. (1992). Dynamic experiments on two pile groups. *Journal of Geotechnical Engineering, 118*(4), 576-592.

Martin, G., & Lam, I. P. (1995). Seismic design of pile foundations: structural and geotechnical issues. *Proceedings: third international conference on recent*

advances in geotechnical earthquake engineering and soil dynamics. April 2-7,1995, III, pp. 1491-1515. St. Louis, Missouri.

Matlock, H. (1970). Correlations for design of laterally loaded piles. *In Proceedings, 2nd offshore technology conference* (pp. 577-593). Houston, TX: April 22-24, Paper No. OTC 1204.

Mcanoy, R., Chasman, A. C., & Purvis, D. (1982). Cyclic tensile testing of a pile in glacial till. In I.O.C. (Ed.), *Proceedings recent developments in the design and construction of offshore structures conference.* London, UK: IN Engineers.

McCabe, B. (2002). *Experimental investigations of pile group behaviour in soft silt.* (T. C. Dublin, Ed.) Dublin , Ireland: University of Dublin.

Michaelides, O., Gazetas, G., Bouckovalas, G., & Chrysikou, E. (1997). Approximate non-linear dynamic axial response of piles. *Geotechnique, 48*(1), 33-53.

Mooney, J., Adamczak, S., & Clemence, S. (1985). Uplift capacity of helical anchors in clay and silt. *Proceedings, Uplift Behaviour of Anchor Foundations in Soil, American Society of Civil Engineers*, 48-72.

Mylonakis, G., & Gazetas, G. (1999). Lateral vibration and internal forces of grouped piles in layered soil. *Journal of geotechnical and geoenvironmental engineering, 125*(1), 16-25.

New Zealand Police . (2012, February 9). *New Zealand Police*. Retrieved November 21, 2016, from List of deceased: http://www.police.govt.nz/major-events/previous-major-events/christchurch-earthquake/list-deceased

Nogami, T., Otani, J., Konagai, K., & Chen, H. (1992). Nonlinear Soil-Pile Interaction Modelfor Dynamic Lateral Motion. *Journal of Geotechnical Engineering , 118*(1), 89-106.

Novak, M. (1991). piles under dynamic loads. *Proceedings of the 2nd internationalconference on recent advances in geotechnical earthquake engineering and soil dynamics* (pp. 2433-2456). St. Louis, Mo: March11-15.

Novak, M., & El Sharnouby, B. (1983). Stiffness constant for single piles. *Journal of Geotechnical Engineering, 109*(7), 961-974.

Novak, M., & Sheta, M. (1980). Approximate approach to contact problems of piles. *Proceedings of Specialty Session, ASCE National Convention on Dynamics Response of Pile Foundations: Analytical Aspects* (pp. 53-79). New York: ASCE.

Parsad, Y.V.S.N., and Rao, S.N. (1996). Lateral capacity of helical piles in clays. *ASCE Journal of Geotechnical Engineering, 122*(11), 938–941.

Perko, H. (2007, December). Creating Acceptance for Helical Foundations. *Structure Magazine*, 49-50.

Perko, H. (2009). *Helical piles: a practical guide to design and installation.* Hoboken, NJ.: John Wiley & Son, Inc.

Perko, H. (2009). *Helical piles: a practical guide to design and installation.* New York, NY, United States: John Wiley & Sons.

Poulos, H. G. (1982). *Influence of cyclic loading on axial pile response.* University of Sydney, School of Civil Engineering, Sydney, Australia.

Prasad and Rao, N. (1994). Pullout behaviour of model pile and helical pile anchors subjected to lateral cyclic loading .

Prasad, Y. S., & Rao, S. N. (1994). Pullout behaviour of model pile and helical pile anchors subjected to lateral cyclic loading. *Canadian Geotechnical Journal, Vol. 31*, 110-119.

Puech, A., & Jezequel, J. F. (1980). The effects of long time cyclic loading on the behaviour of a tension pile . *12th offshore technology conference.* Houston, TX.

Puri, V. K., Stephenson, R. W., Dziedzic, E., & Goen, L. (1984). Helical anchor piles under lateral loading. Laterally loaded deep foundations: Analysis and performance. *American society for testing and materials.*, 194-213.

Qin, H., & Dong Guo, W. (2016, February 09). Response of static and cyclic laterally loaded rigid piles in sand. *Marine Georesources & Geotechnology, 34*(2), 138-153.

Rao, N. S., & Prasad, Y. S. (1993). Estimation of Uplift capacity of Helical anchors in clay. *Journal of Geotechnical Engineering, 119 (2)*, 352-357.

Rao, N., & Prasad. (1993). Uplift behavior of Pile Anchors subjected to lateral cyclic loading. *J. Geotech. Engrg. , 119*, pp. 786-790.

Raongjant, W., & Meng, J. (2011, September). Experimental investigation on seismic behavior of single piles in sandy soil. *Earthquake engineering and Engineering vibration, 10*, 417-422.

Read, A., & Sritharan, S. (1993). Reconnaissance report on the Ormond Earthquake - August 10,1993. *Bulletin of the New Zealand National Society for earthquake engineering. 26*, pp. 292-308. Bulletin of the New Zealand National Society for Earthquake Engineering.

Rollins, K., Hales, L., Ashford, S. A., & Camp, W. (2006). p-y curves for large diameter shafts in liquefied sand from blast liquefaction tests. *Seismic*

Performance and simulation of pile foundations in liquefied and laterally spreading ground , 11-23.

Rupiper. (2000). Personal communication. (Perko, Interviewer) San Jose, CA.

Sakr, M. (2009). Performance of helical piles in oil sand. *Canadian Geotechnical Journal, 46*(9), 1046 – 1061.

Sakr, M. (2009). Performance of Helical piles in oil sand. *Canadian Geotechnical Journal, Vol. 46*, 1046-1061.

Sakr, M. (2013). Comparison between high strain dynamic and static load tests of helical piles in cohesive soils. *Soil Dynamics and earthquake engineering, 54*, 20-30.

Sakr, M. (2014, October). Relationship between installation torque and axial capacities of helical piles in cohesionless soils. *Canadian Geotechnical Journal, 52*, 747-759.

Sander, A. C., Fox, P. J., Elgamal, A., Pradel, D. E., Isaacs, D., Stone, M., & Wong, S. (2013). Seismic testing program for large-scale MSE Retaining walls at UCSD. *Geo-Congress 2013* (pp. 1188-1195). ASCE.

Schiavon, J. (2016). *Comportamento de ancoragens helicoidais submetidas a carregamentos ciclicos.* Sao Carlos, Brazil: Universidade de Sao Paulo.

Seed, H. B., & Reese, L. C. (1955). The action of soft clay along friction piles. *Transaction of the American Society of Civil Engineers*, 731-754.

Silva, Foray, Rimoy, Jardine, Tsuha, & Yang. (2013). Influence of cyclic axial loads in the behaviour and response of driven piles in sand. *Proceedings of the 18th international conference on soil mechanics and geotechnical engineering*, (pp. 2403-2406). Paris, France.

Steenfelt, J. S., Randolph, M. F., & Wroth, C. P. (1981). Model tests on instrumented piles jacked into clay. *Proceedings of the 10th International Conference on Soil Mechanics and Foundation Engineering*, *2*, pp. 857-864. Stockholm.

Sun, K., & Pires, J. (1993). Simplified Approach for Pileand Foundation Interaction Analysis. *Journal of Geotechnical Engineering*, *119*(9), 1462-1479.

Swan, C. (2016). *Engineering- Foundations of structures* . Retrieved November 6, 2016, from The University of Iowa: http://user.engineering.uiowa.edu/~swan/courses/53139/notes/changes-in-soil-during-pile-driving.pdf

Tabesh, A., & Poulos, H. G. (1999). The Effect of Soil Yielding on Internal Pile Response. In S. e. Pinto (Ed.), *Proceedings of the 2nd International Conference on Earthquake Geotechnical Engineering. 1*, pp. 327-333. Rotterdam: A.A. Balkema.

Tsuha, C. A. (2012). Evaluation of the efficiencies of helical anchors plates in sand by centrifuge model tests. *Canadian Geotechnical Journal*, 1102-1114.

Unsever, Y., Kawamori, M., Matsumoto, T., & Shimono, S. (2013). Cyclic horizontal load tests of single pile, pile group and piled raft in model dry sand. *Conference: 18th Southeast Asian Geotechnical Conference (18SEAGC) & Inaugural AGSSEA Conference (1AGSSEA)* (pp. 1-6). Research publishing.

Van Weele, A. F. (1979). Pile Bearing capacity under cyclic loading compared with that under static loading. *Proceedings of the 2nd International conference in behavior of Offshore structures*, (pp. 475-488). London.

Velez, A., Gazetas, G., & Krishnan, R. (1983). Lateral Dynamic Response of Constrained Head Piles. *Journal of Geotechnical Engineering, 109*(8), 1063-1081.

Victor, R., & Cerato, A. (2008). Helical Anchors as Wind Tower Guyed Cable Foundations. In B. M. Brown M. J. (Ed.), *Proceedings of the 2nd British Geotechnical Association (BGA) International Conference on Foundations, 1*, pp. 343-356. Dundee, Scotland.

Wakamatsu, K., Yoshida, N., Suzuki, N., & Tazoh, T. (1992). *liquefaction-induced large ground deformations and their effects on lifelines during the 1990 Luzon, Phillipines earthquake).* Case studies of liquefaction and lifeline performance during past earthquakes. Buffalo, NY: National center for earthquake engineering research.

Wichtmann, T. (2005). *Explicit accumulation model for non-cohesive soils under cyclic loading.* Bochum: DES INSTITUTES FÜR GRUNDBAU UND BODENMECHANIK DER RUHR-UNIVERSITÄT BOCHUM.

Willis, D. (n.d.). *How to design Helical Piles per the 2009 International Building Code.* Ram Jack Foundation Solutions, System Distribution. Ada, OK: Ram Jack .

Wood, J. (2015). Principal at Piletech. (D. A. Cerato, Interviewer)

Yoshida, N., & Hamada, M. (1990). Damage to foundation piles and deformation pattern of ground due to liquefaction-induced permanent ground deformations. *Proceedings of the 3rd Japan-U.S. workshop on earthquake resistance design of lifeline facilities and countermeasures for soil liquefaction*, (pp. 147-161). San Francisco, CA.

Zeevaert, L. (1983). *Foundation engineering for difficult subsoil conditions.* New York, NY: Van Nostrand Reinhold Company Inc.

Appendix A. Bending moment curves by intensity

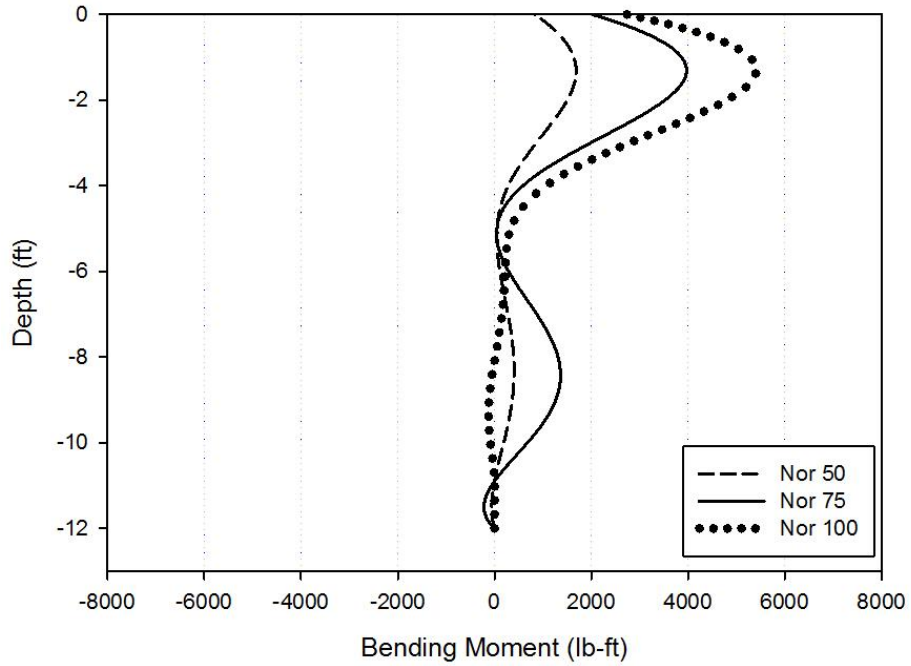

Figure 80. P1 (3.5” O.D. single bolt couple, single helix): Bending Moments for the Northridge shakes

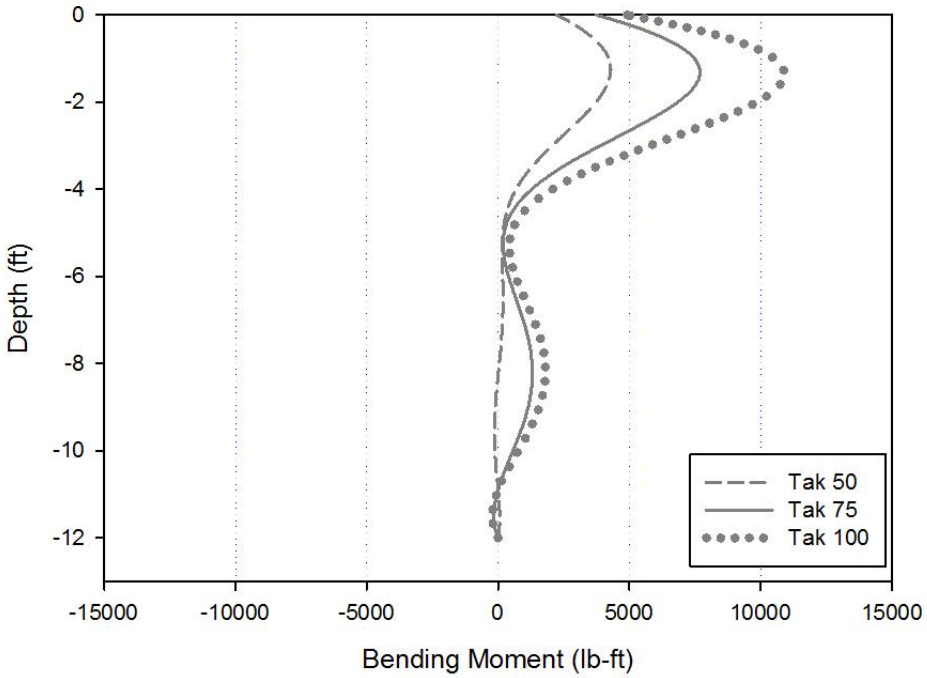

,Figure 81. P1 (3.5” O.D. single bolt couple, single helix): Bending Moments for the Takatori shakes

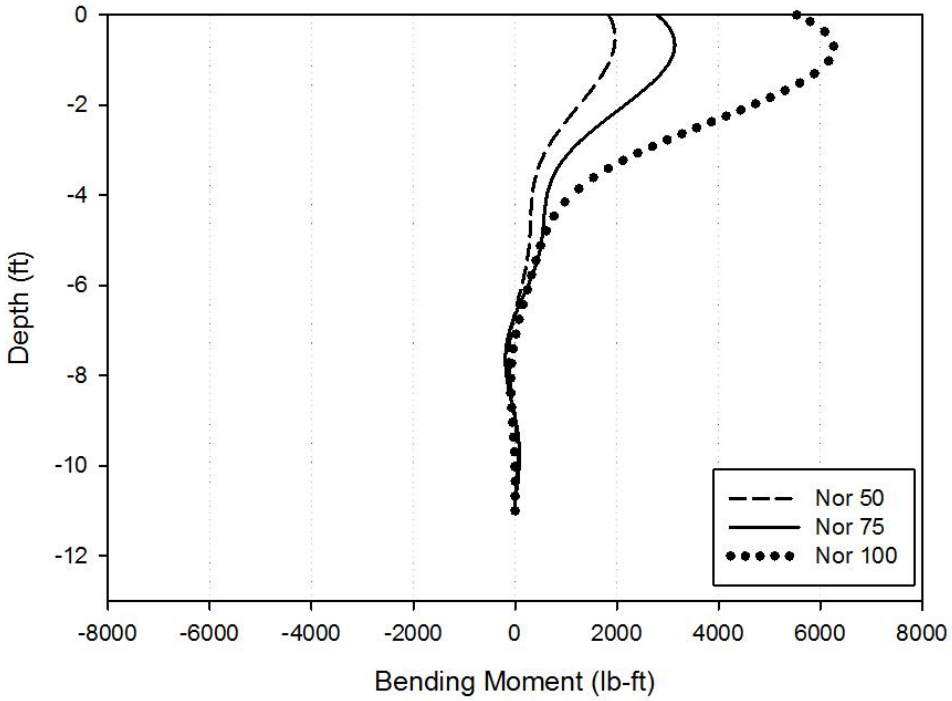

Figure 82. P2 (3.5" O.D. double-bolt couple single helix): Bending Moments for the Northridge shakes

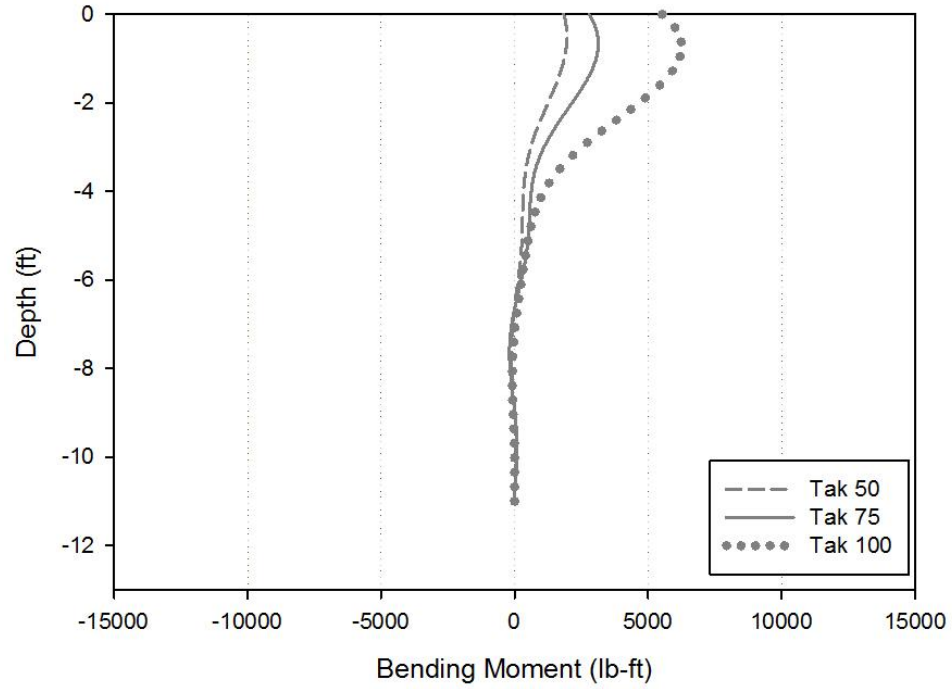

Figure 83. P2 (3.5" O.D. double-bolt couple single helix): Bending Moments for the Takatori shakes

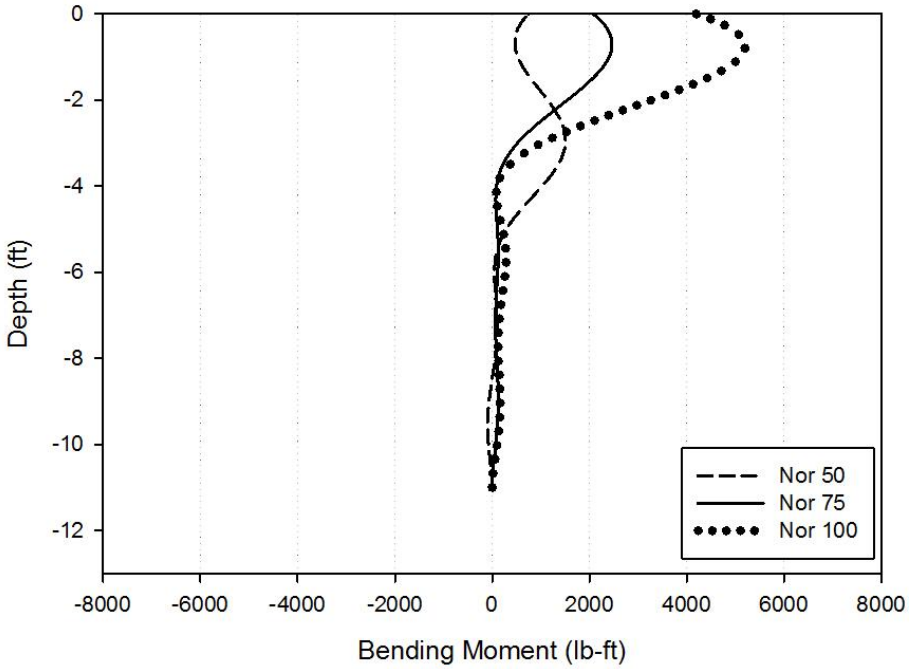

Figure 84. P4 (3.5" O.D. double-bolt couple double helix): Bending Moments for the Northridge shakes

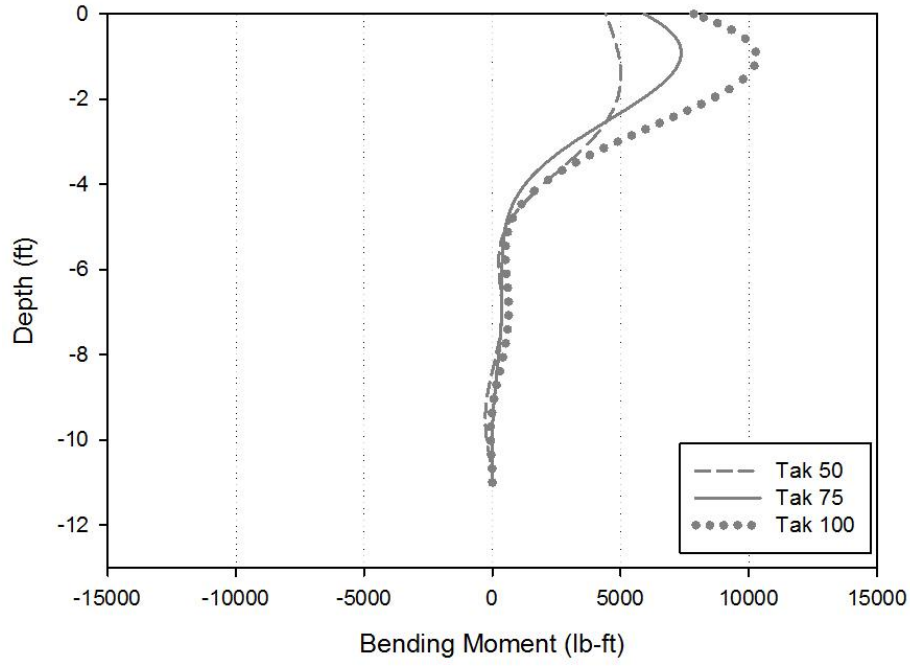

Figure 85. P4 (3.5" O.D. double-bolt couple double helix): Bending Moments for the Takatori shakes

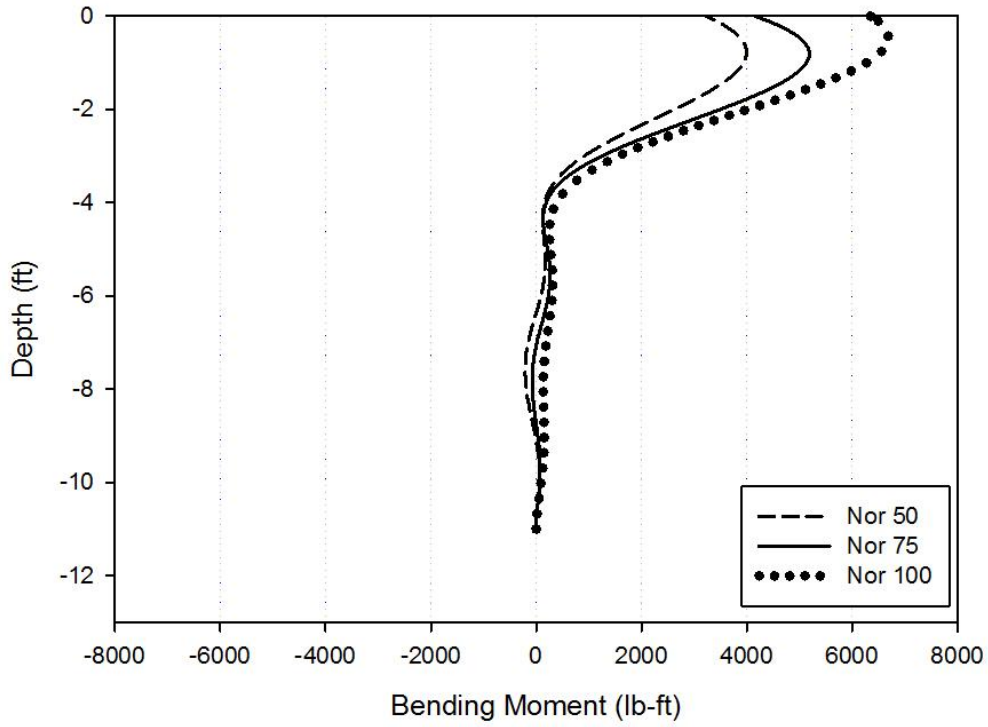

Figure 86. P5 (3.5" O.D. push pile): Bending Moments for the Northridge shakes

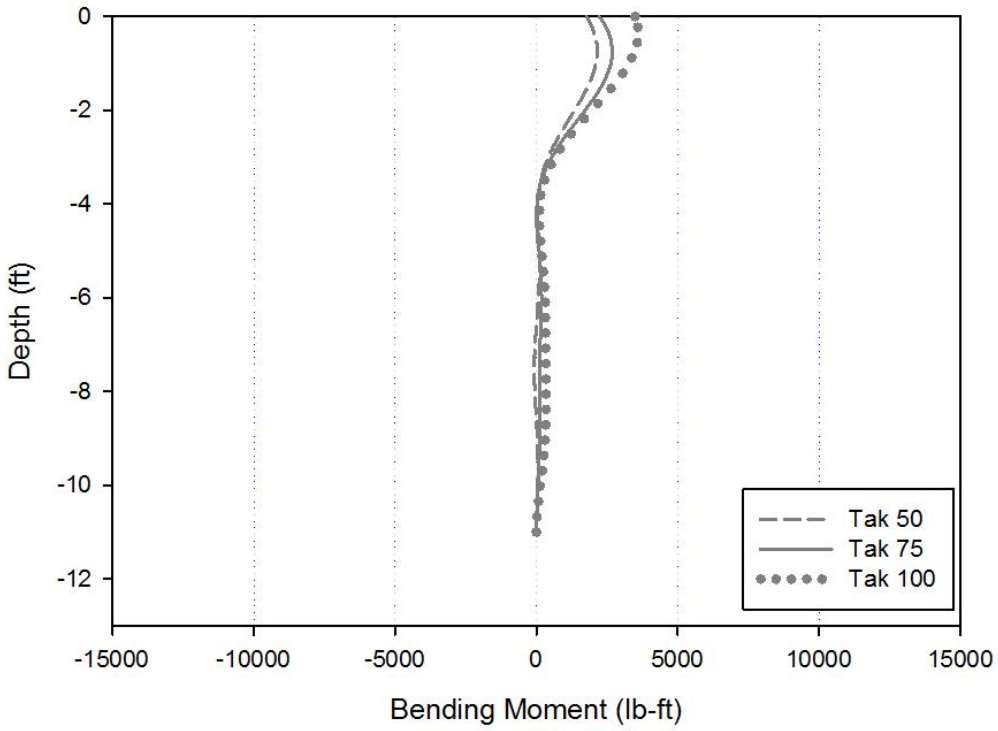

Figure 87. P5 (3.5" O.D. push pile): Bending Moments for the Takatori shakes

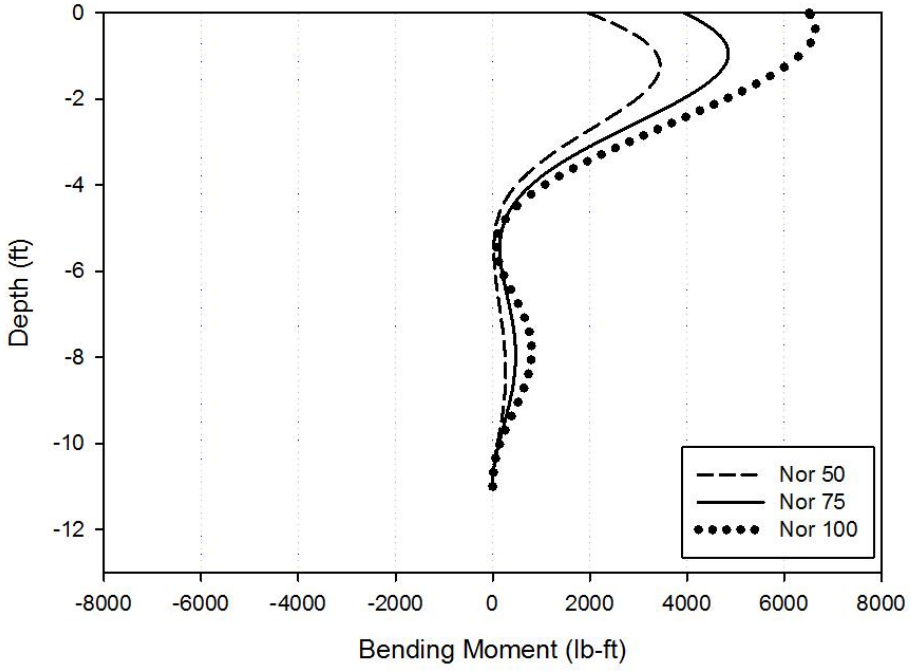

Figure 88. P6 (3.0" square shaft with a single bolt couple single helix): Bending Moments for the Northridge shakes

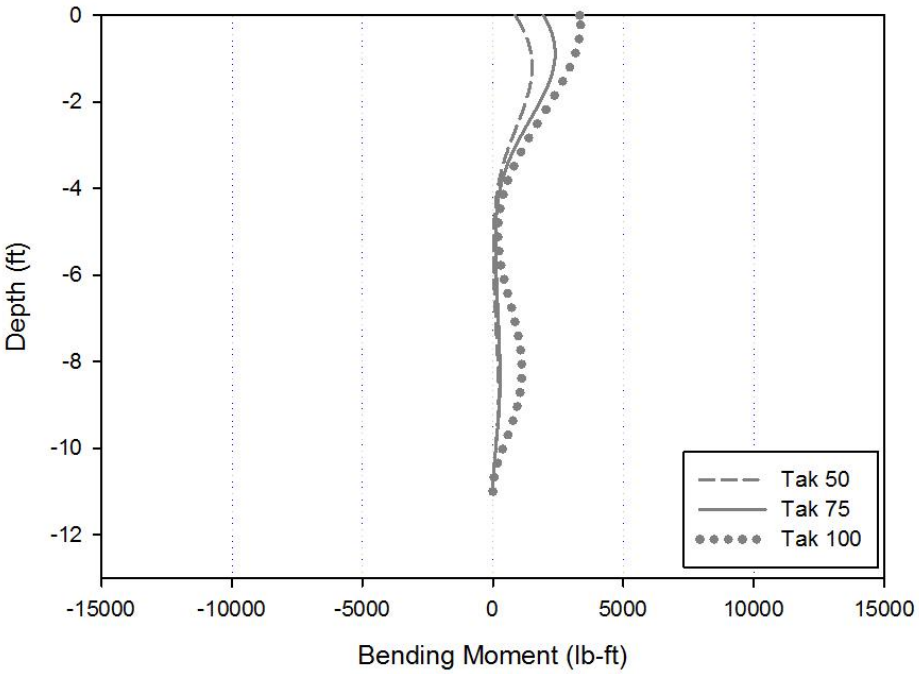

Figure 89. P6 (3.0" square shaft with single-bolt couple single helix): Bending Moments for the Takatori shakes

Appendix B. Pile deflection by intensity

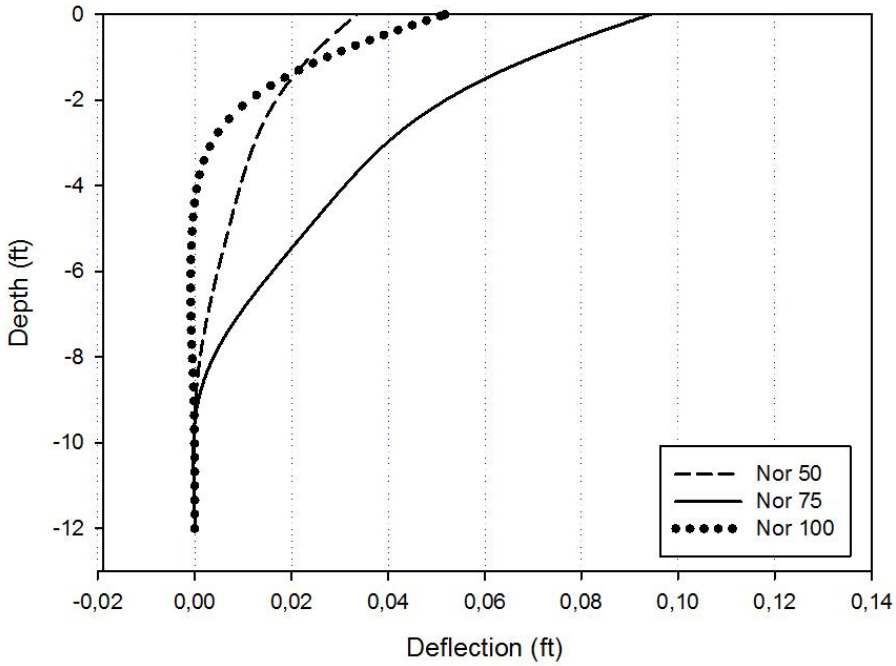

Figure 90. P1 (3.5" O.D. single-bolt couple single helix): Pile deflection for the Northridge shakes

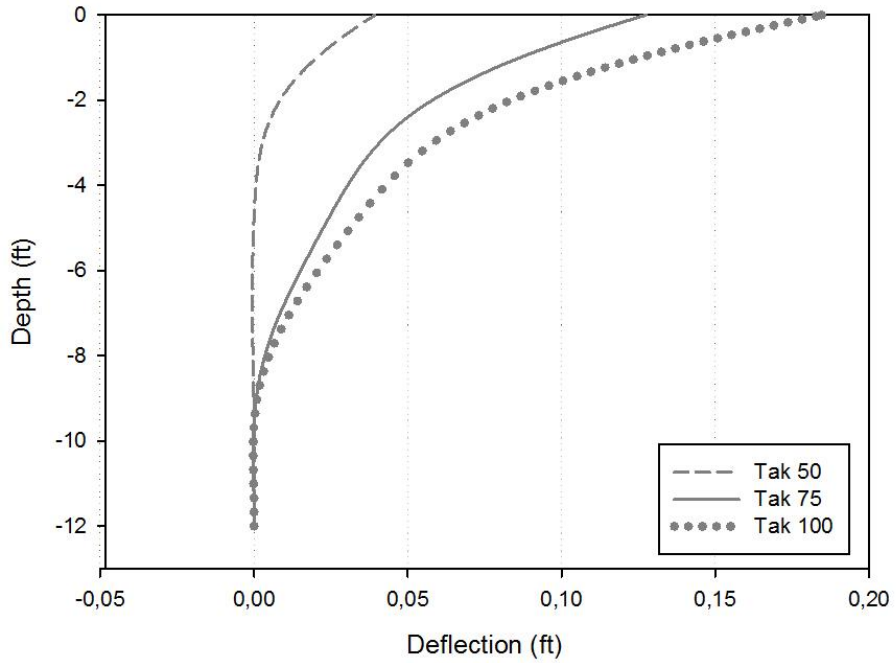

Figure 91. P1 (3.5" O.D. single-bolt couple, single helix): Pile deflection for the Takatori shakes

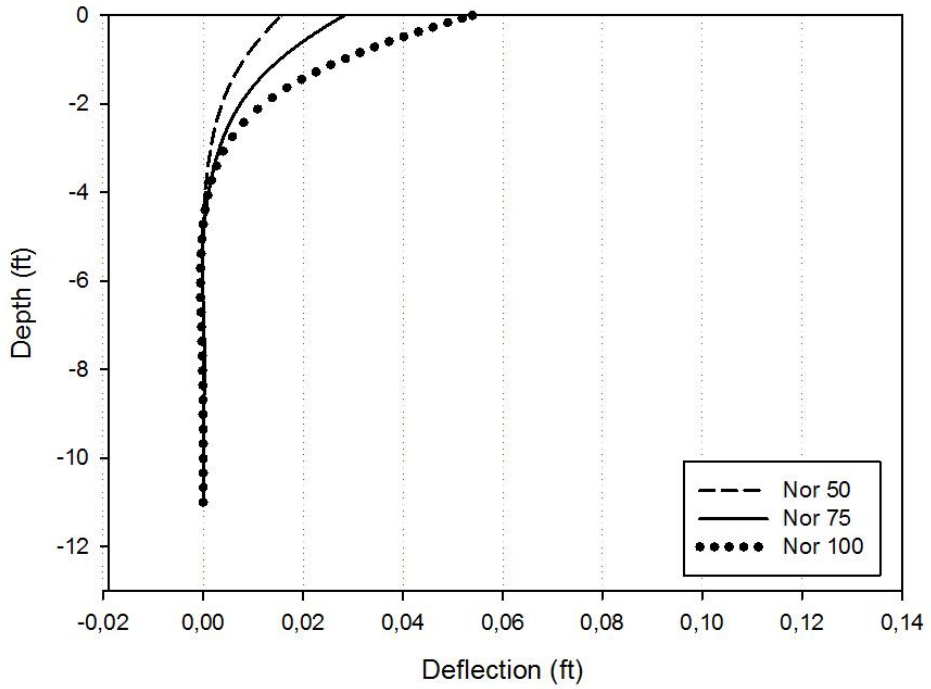

Figure 92. P2 (3.5" O.D. double-bolt couple single helix): Pile deflection for the Northridge shakes

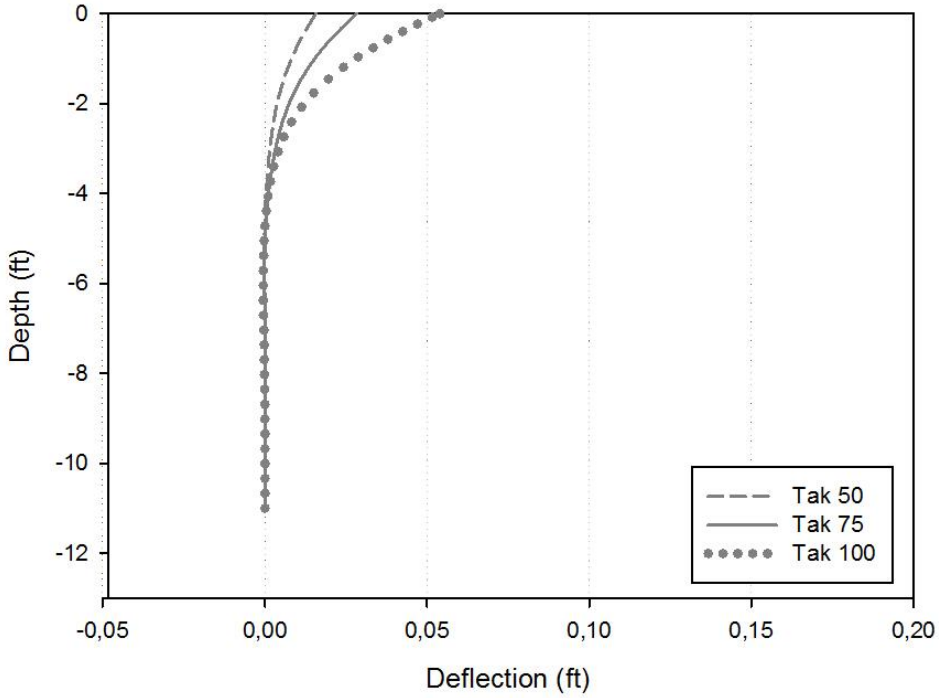

Figure 93. P2 (3.5" O.D. double-bolt couple single helix): Pile deflection for the Takatori shakes

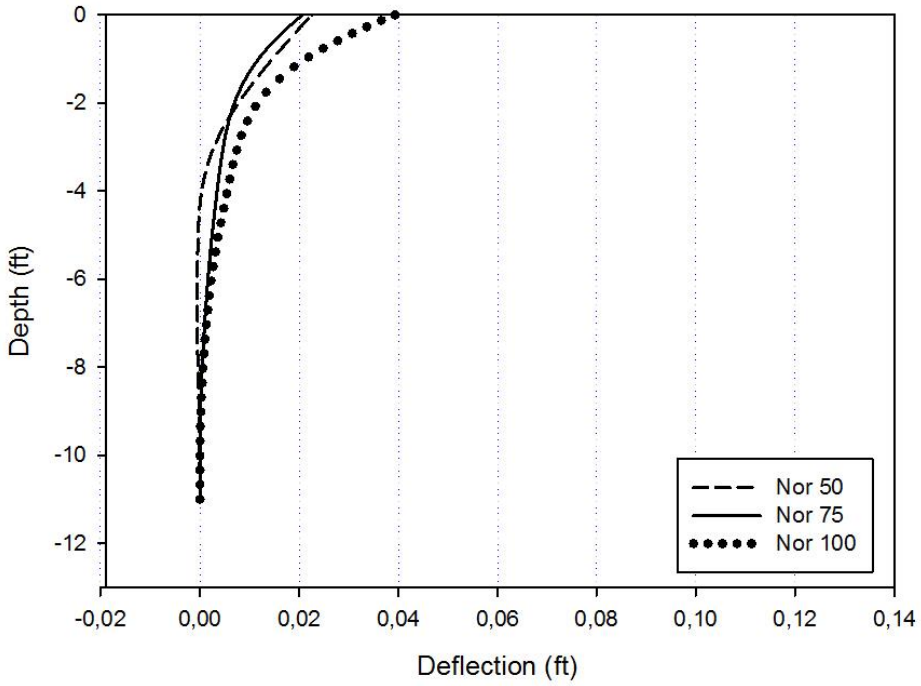

Figure 94. P4 (3.5" O.D. double thru-bolt couple double helix): Pile deflection for the Northridge shakes

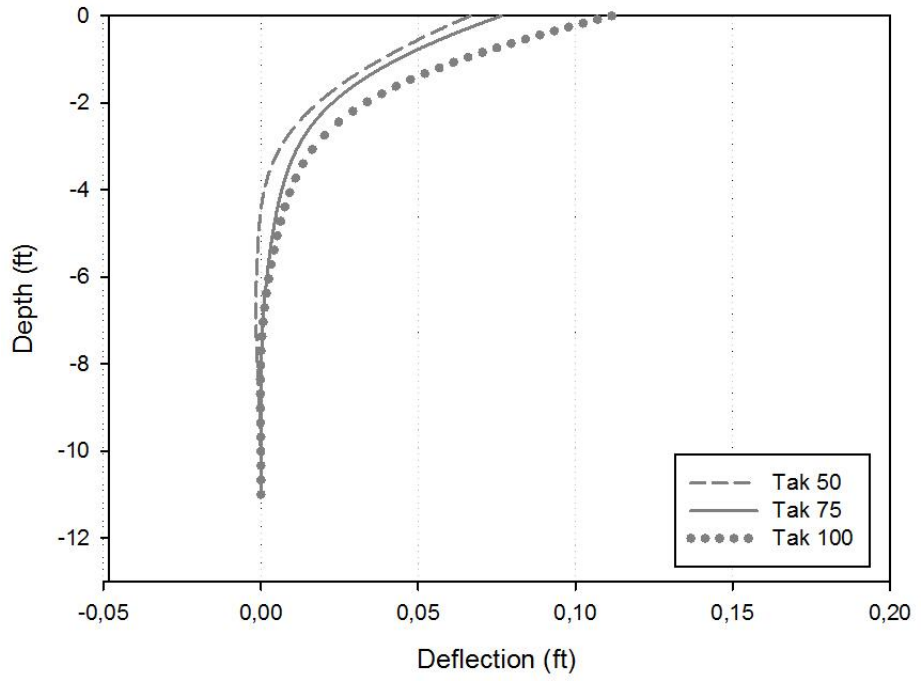

Figure 95**. P4 (3.5" O.D. double thru-bolt couple double helix): Pile deflection for the Takatori shakes**

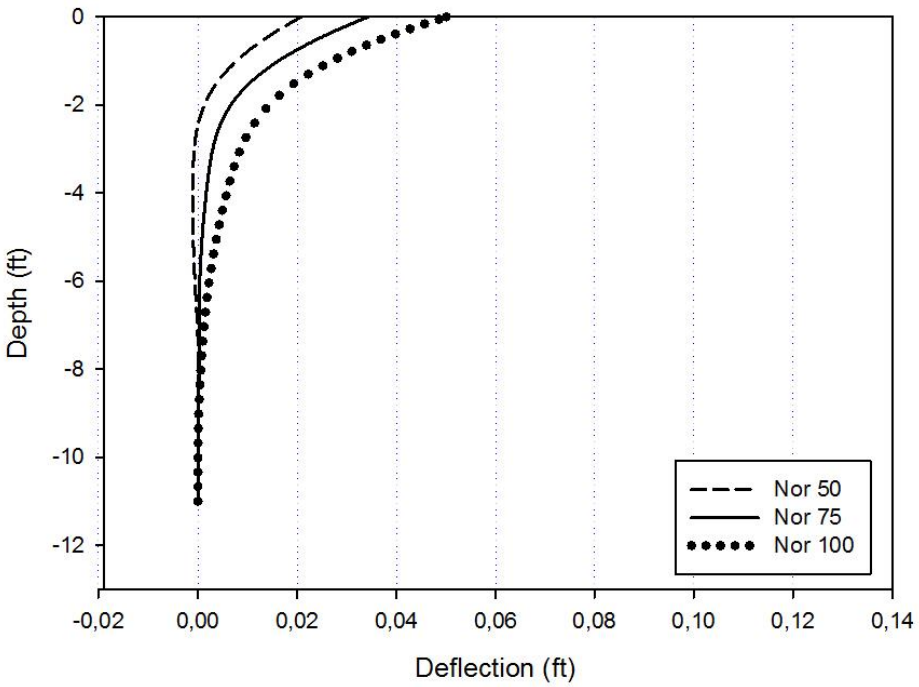

Figure 96. P5 (3.5" O.D. push pile): Pile deflection for the Northridge shakes

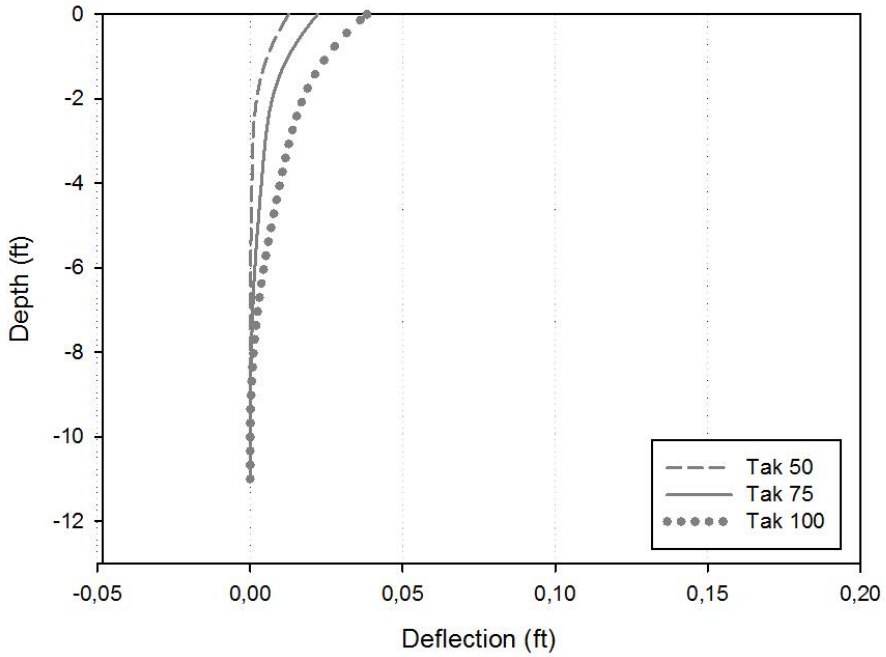

Figure 97. P5 (3.5" O.D. push pile): Pile deflection for the Takatori shakes

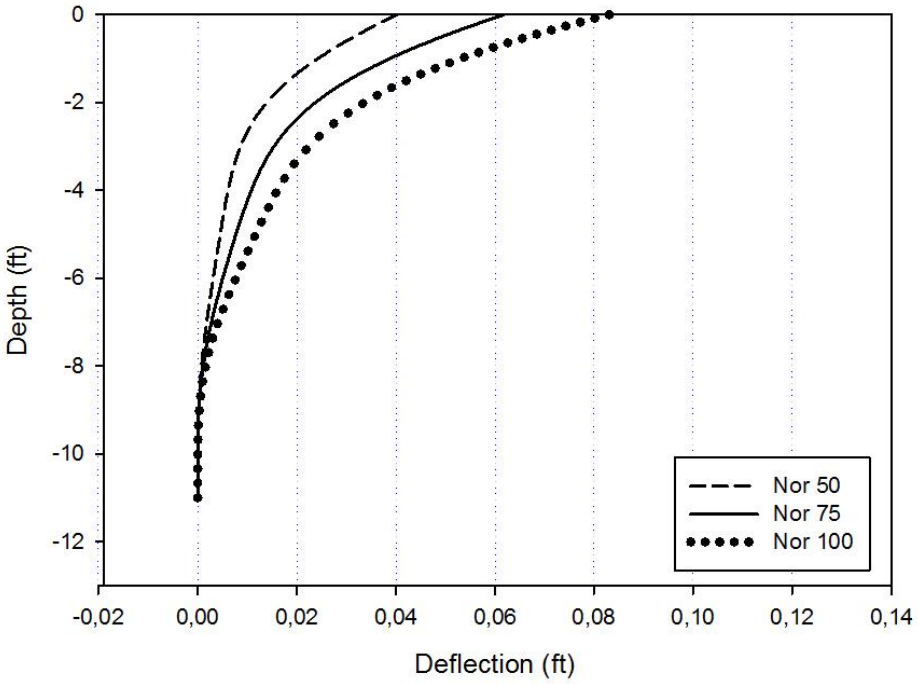

Figure 98. P6 (3.0” square shaft with thru-bolt couple single helix): Pile deflection for the Northridge shakes

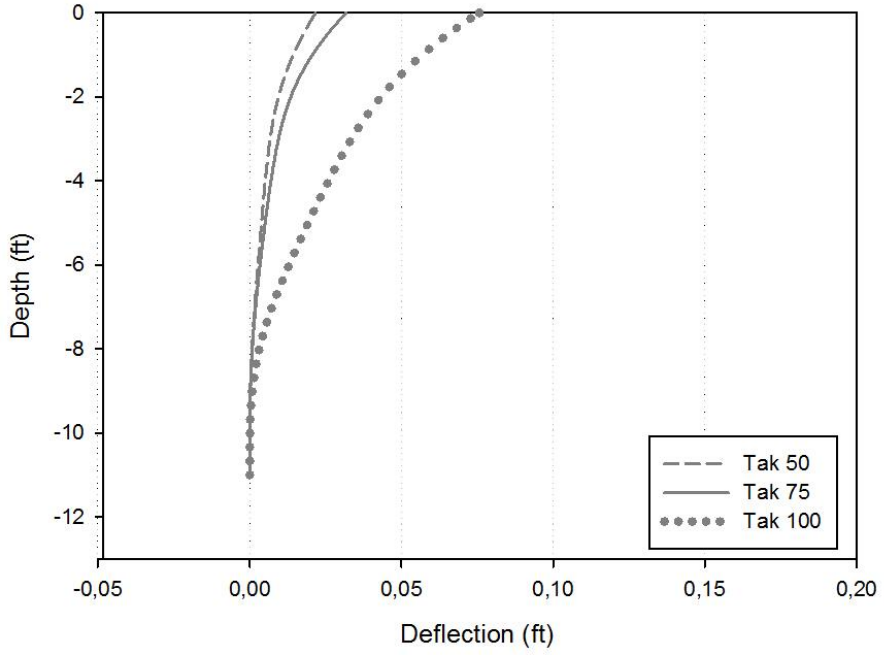

Figure 99. P6 (3.0” square shaft with thru-bolt couple single helix): Pile deflection for the Takatori shakes

Appendix C. Shear by intensity

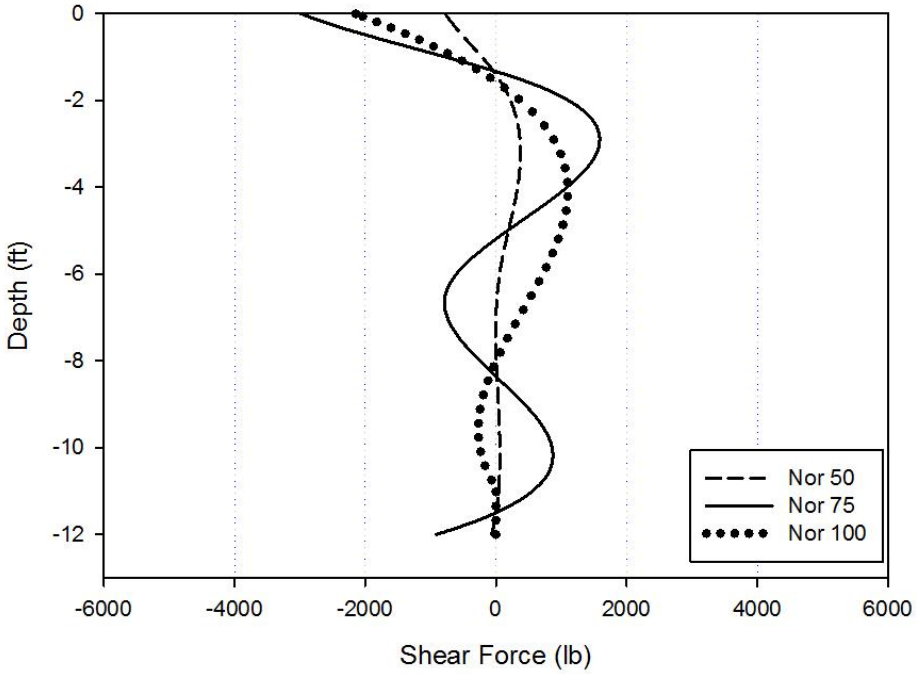

Figure 100. P1 (3.5" O.D. single-bolt couple single helix): Shear Force for the Northridge shakes

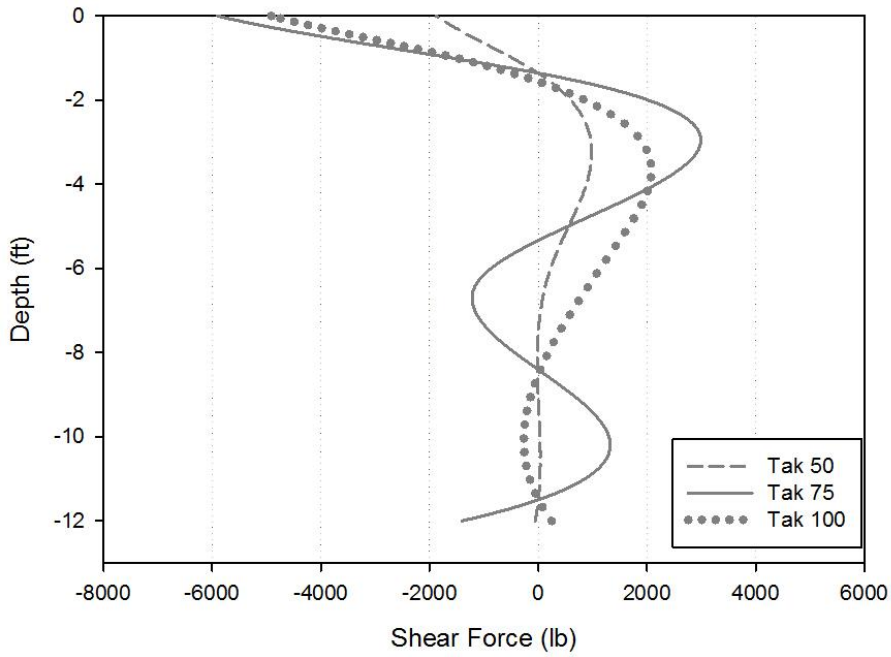

Figure 101. P1 (3.5" O.D. single-bolt couple single helix): Shear Force for the Takatori shakes

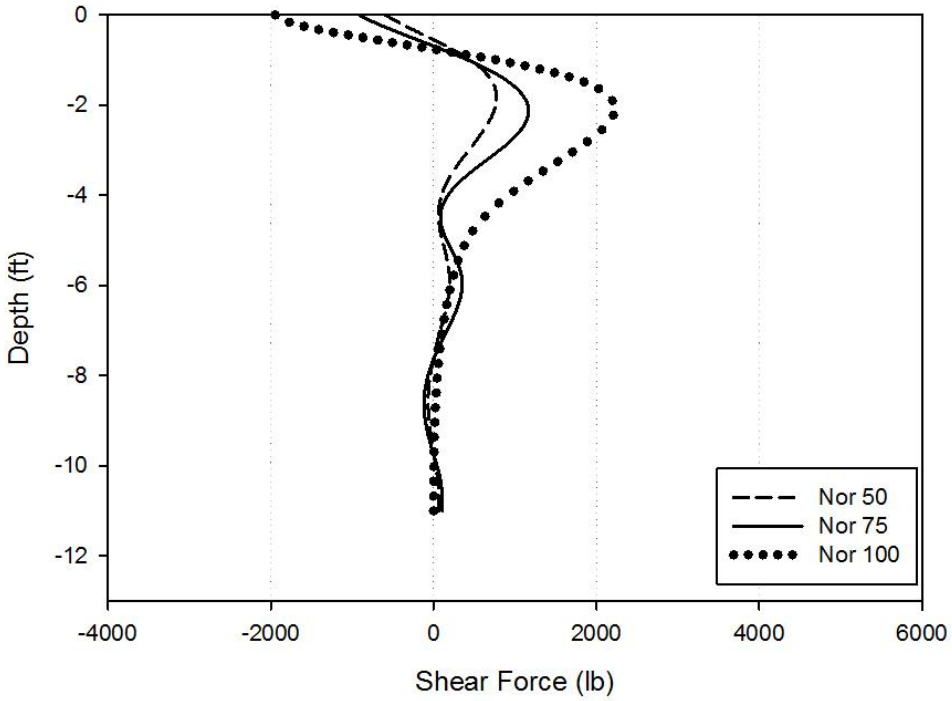

Figure 102. P2 (3.5" O.D. double-bolt couple single helix): Shear Force for the Northridge shakes

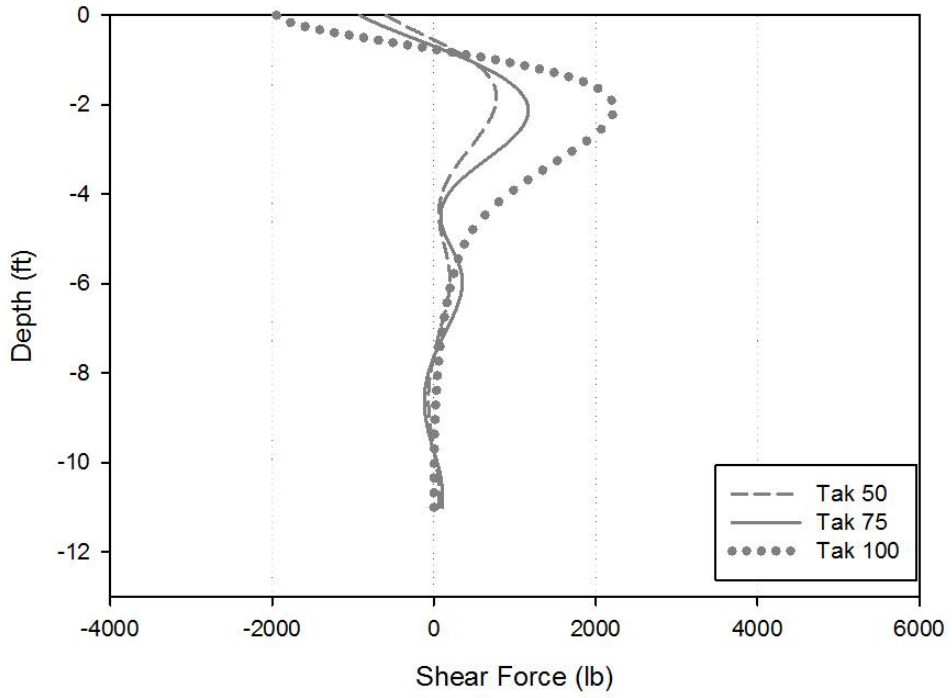

Figure 103. P2 (3.5" O.D. double-bolt couple single helix): Shear Force for the Takatori shakes

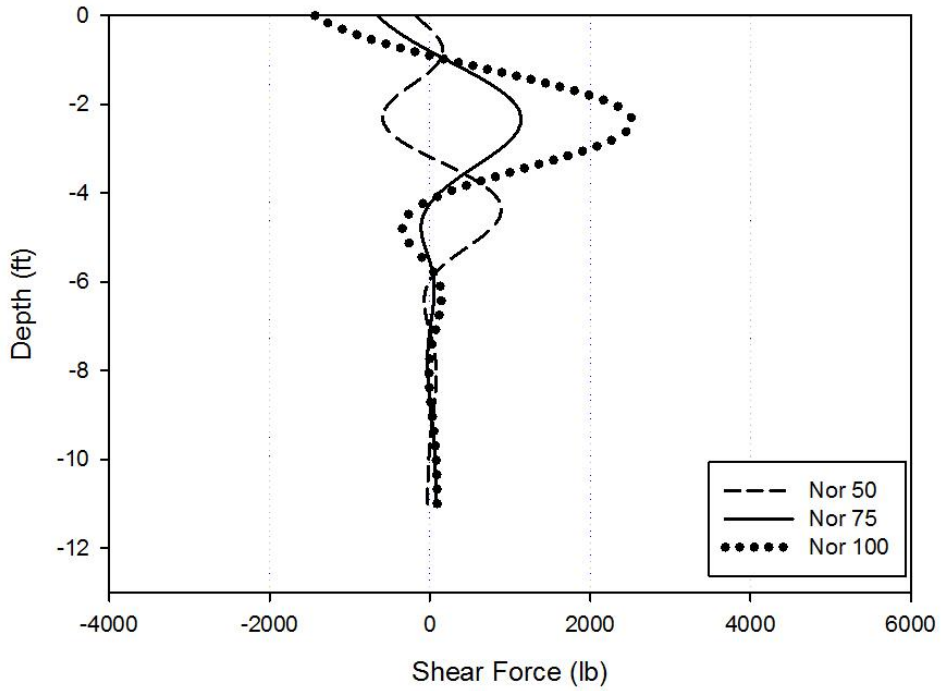

Figure 104. P4 (3.5" O.D. double-bolt couple double helix): Shear Force for the Northridge shakes

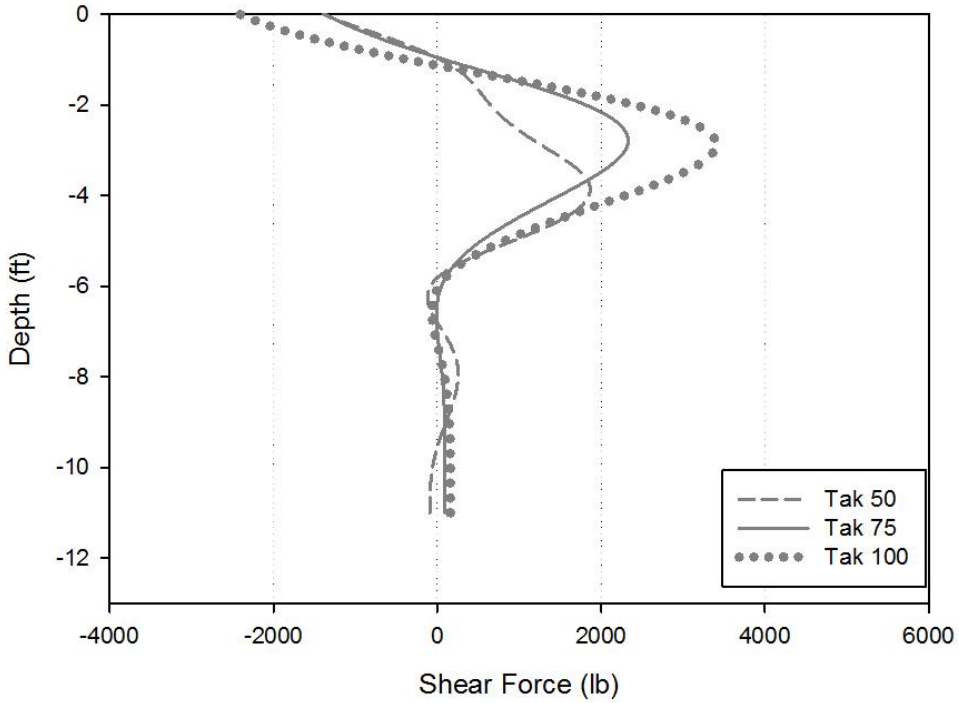

Figure 105. P4 (3.5" O.D. double-bolt couple double helix): Shear Force for the Takatori shakes

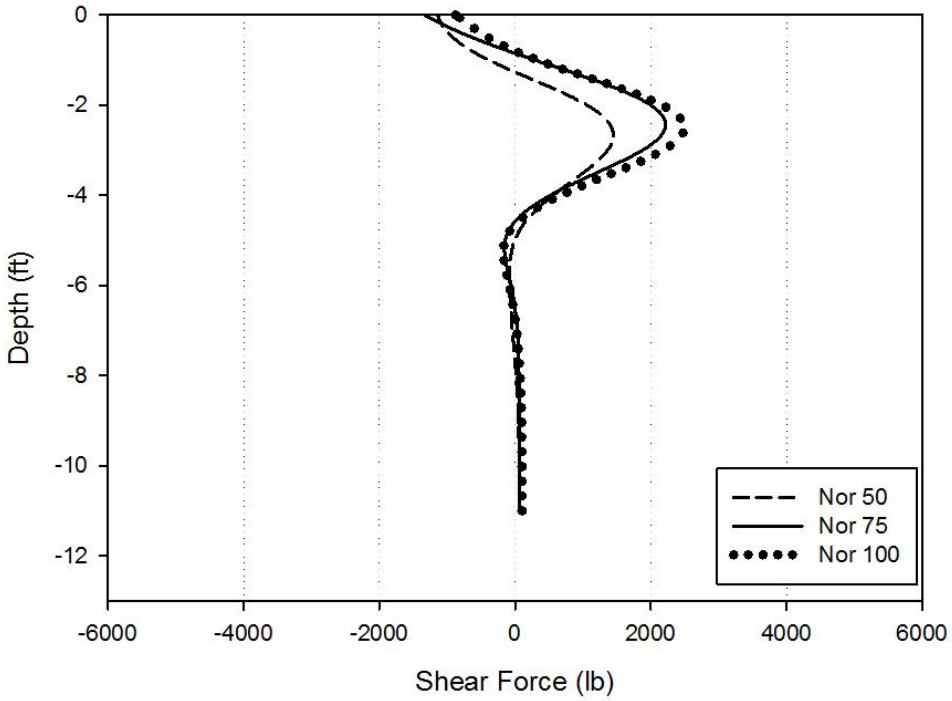

Figure 106. P5 (3.5" O.D. push pile): Shear force for the Northridge shakes

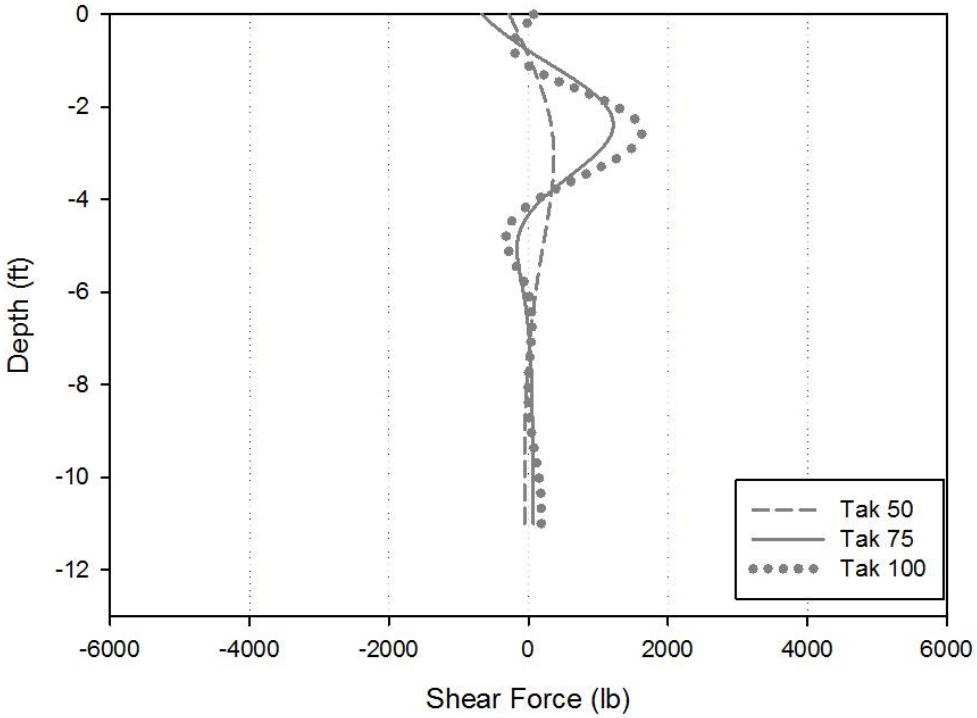

Figure 107**. P5 (3.5" O.D. push pile): Shear force for the Takatori shakes**

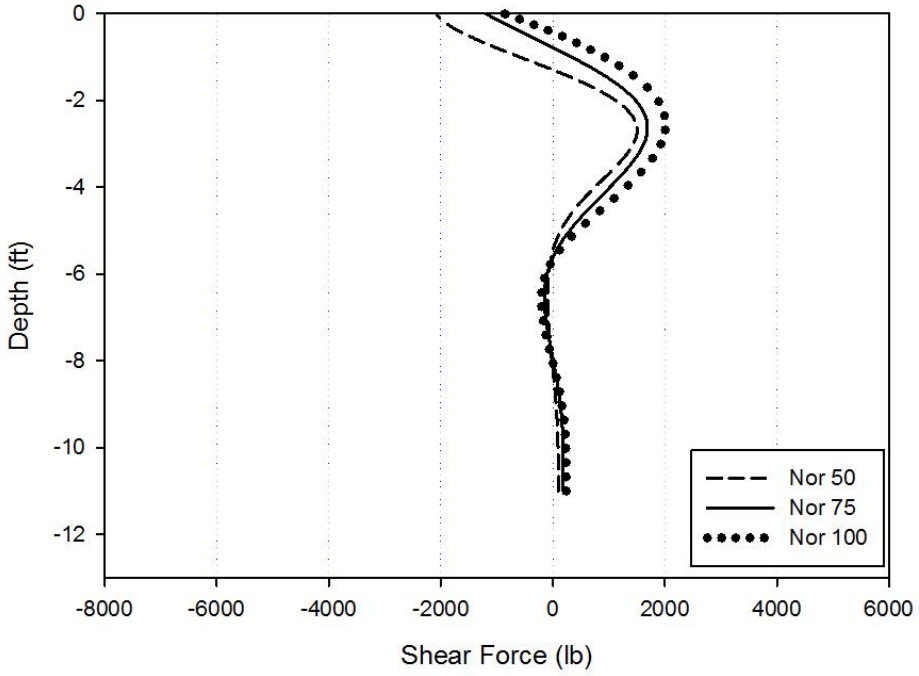

Figure 108. P6 (3.0" square shaft with thru-bolt couple single helix): Shear force for the Northridge shakes

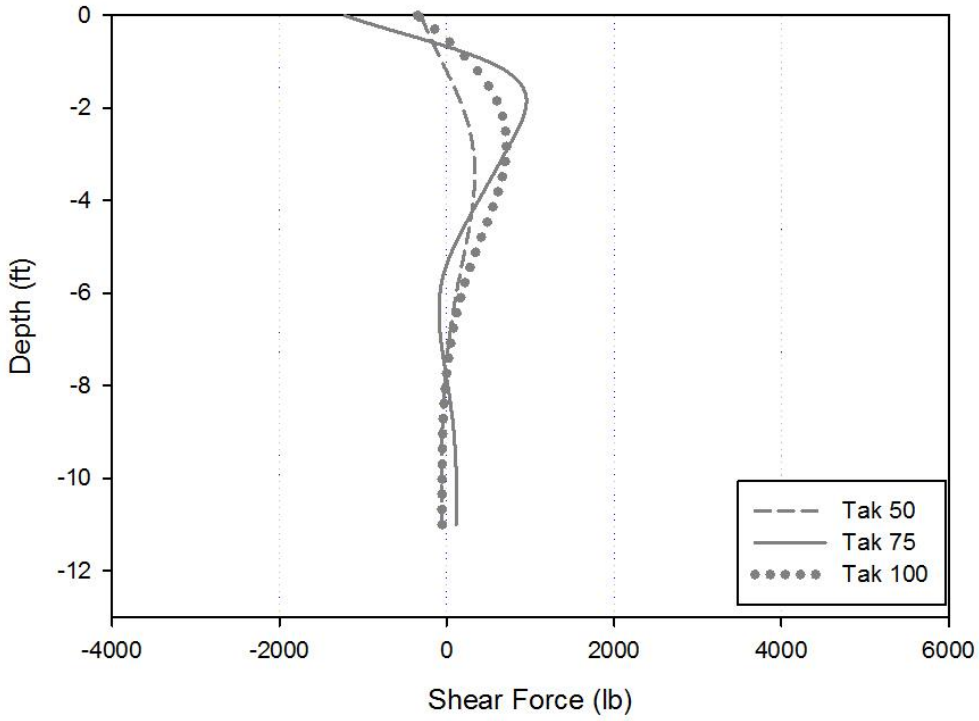

Figure 109. P6 (3.0" square shaft with thru-bolt couple single helix): Shear force for the Takatori shakes

Appendix D. Soil Reaction, p, by intensity

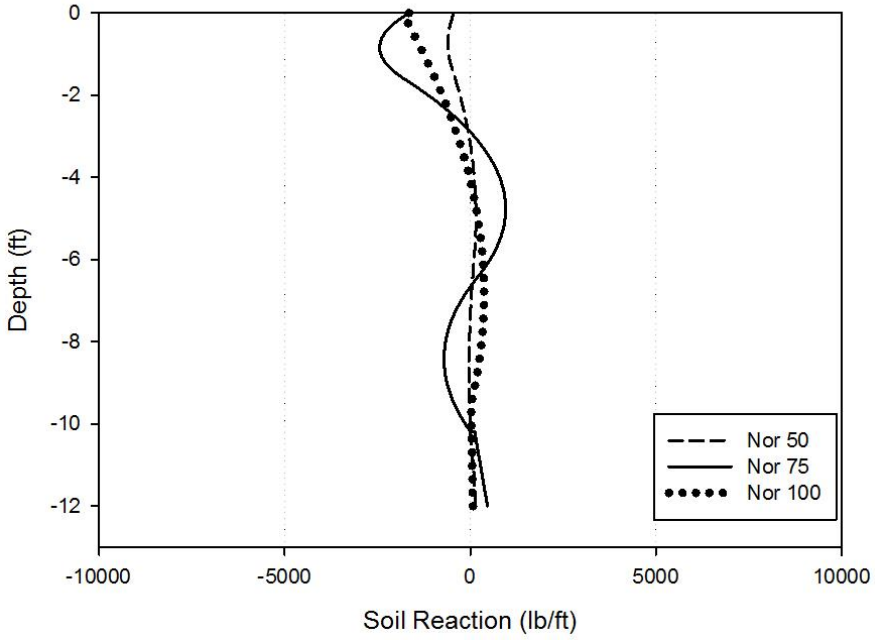

Figure 110. P1 (3.5" O.D. threaded couple single helix): Soil Reaction for the Northridge shakes

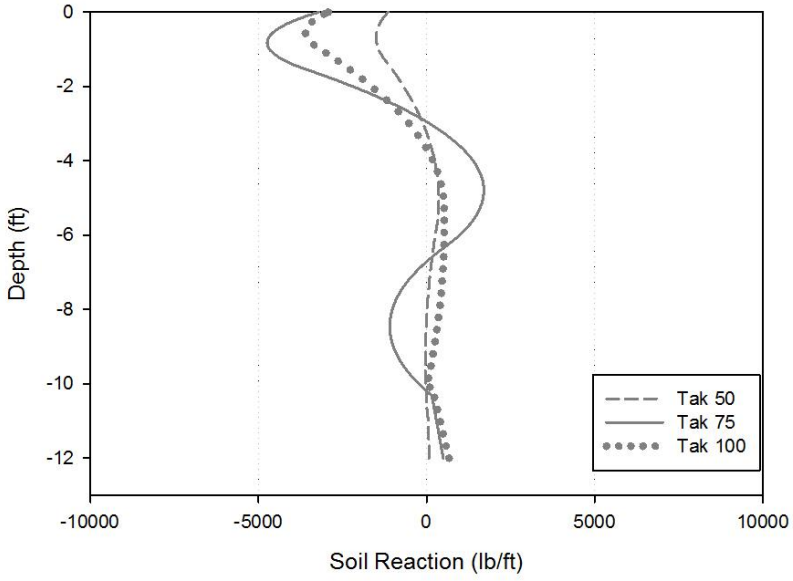

Figure 111. P1 (3.5" O.D. threaded couple single helix): Soil Reaction for the Takatori shakes

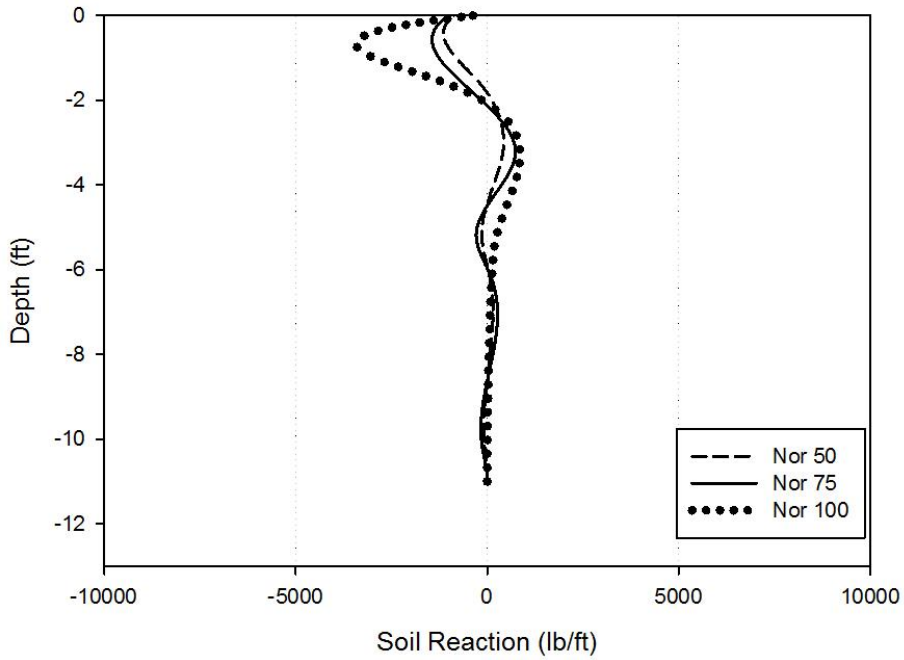

Figure 112. P2 (3.5" O.D. double thru-bolt couple single helix): Shear Force for the Northridge shakes

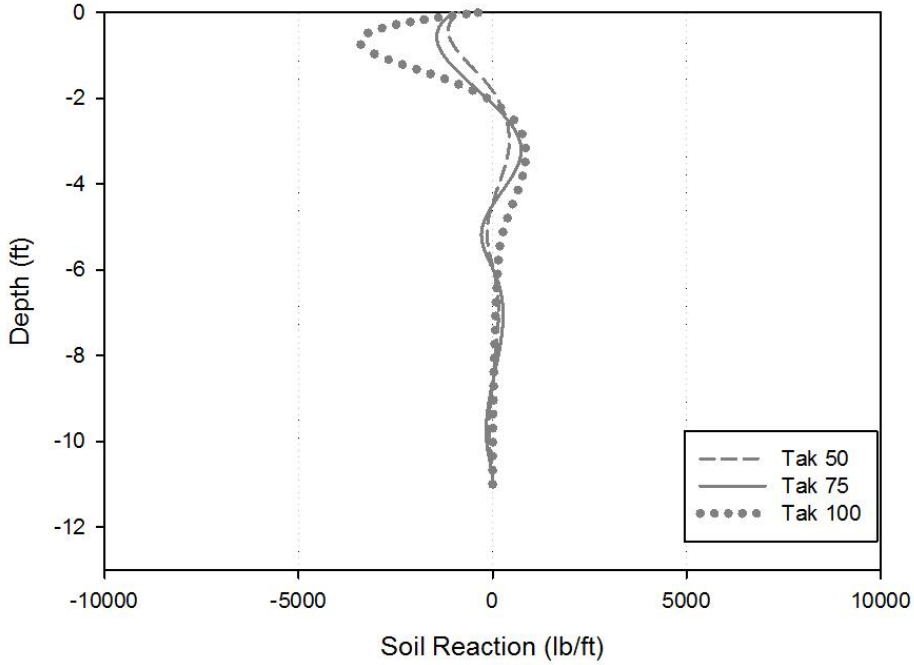

Figure 113. P2 (3.5" O.D. double thru-bolt couple single helix): Shear Force for the Northridge shakes

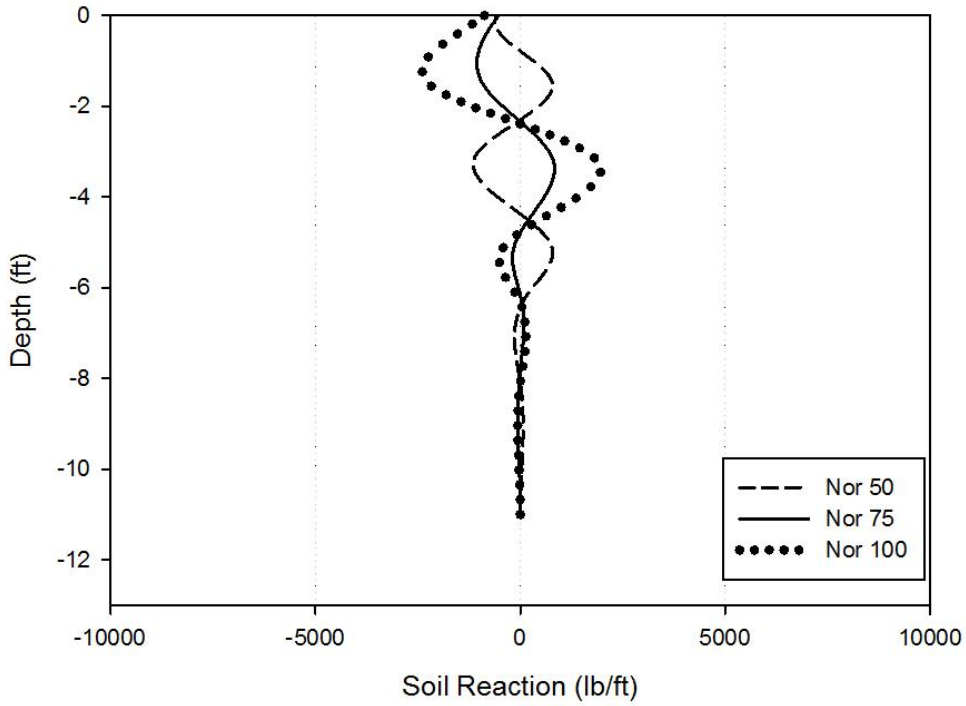

Figure 114. P4 (3.5" O.D. double thru-bolt couple double helix): Soil Reaction for the Northridge shakes

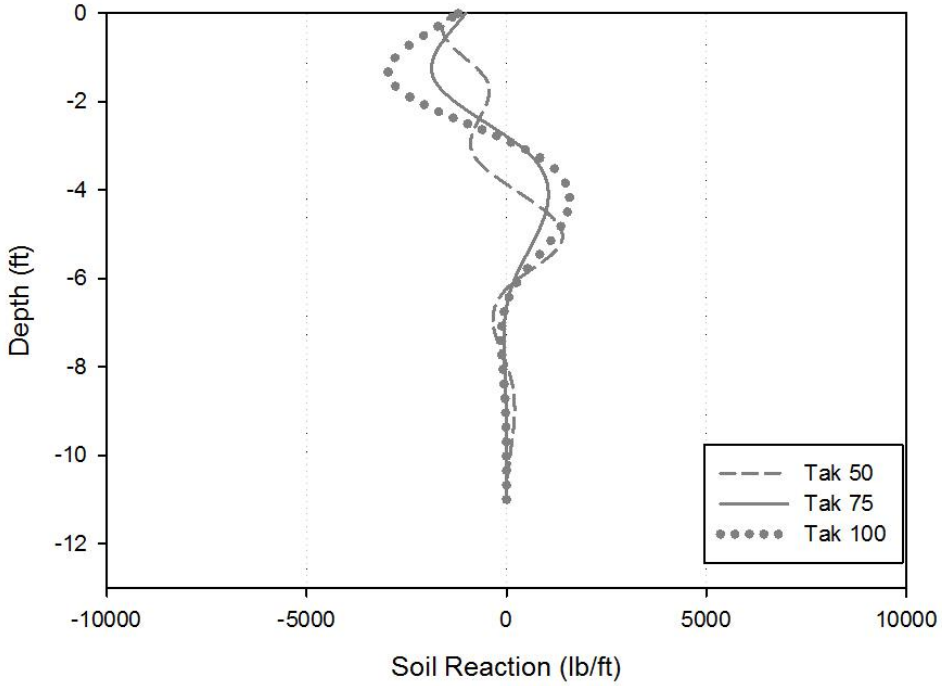

Figure 115. P4 (3.5" O.D. double thru-bolt couple double helix): Soil Reaction for the Takatori shakes

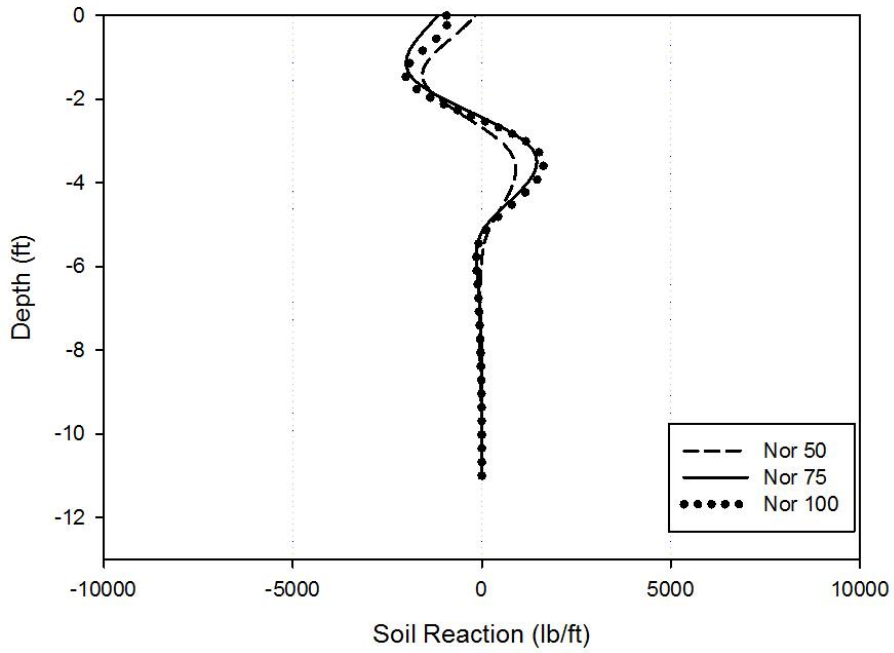

Figure 116. P5 (3.5” O.D. push pile): Soil Reaction for the Northridge shakes

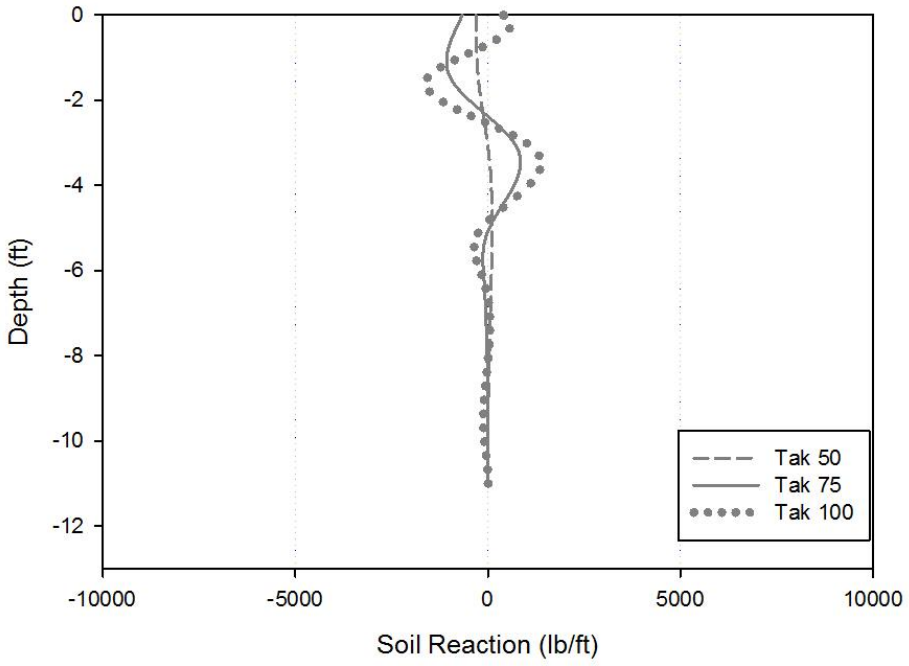

Figure 117. P5 (3.5” O.D. push pile): Soil Reaction for the Takatori shakes

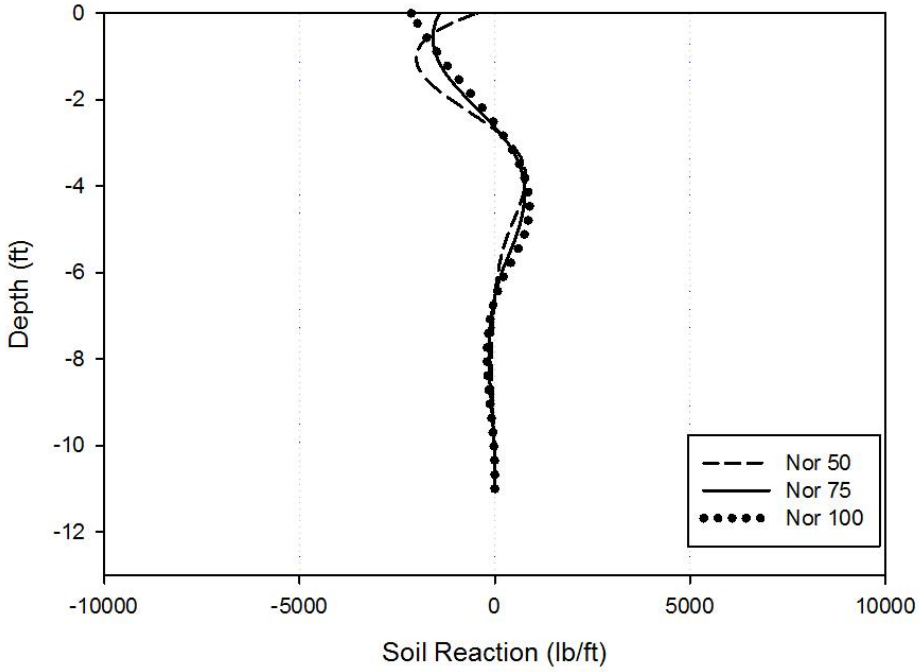

Figure 118. P6 (3.0" square shaft with thru-bolt couple single helix): Soil Reaction for the Northridge shakes

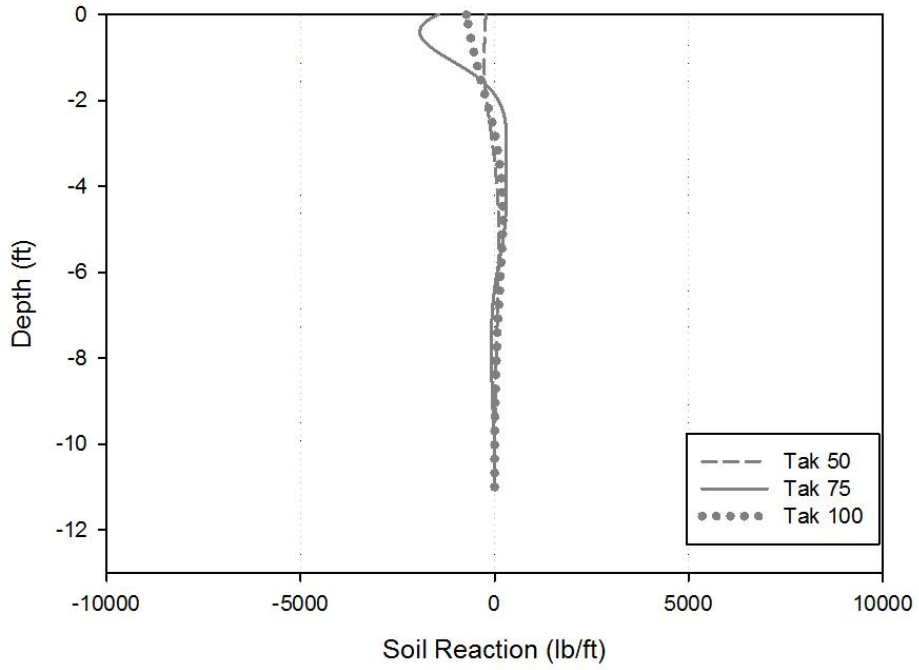

Figure 119. P6 (3.0" square shaft with thru-bolt couple single helix): Soil Reaction for the Takatori shakes

Appendix E. Literature Review

Vertical Cyclic/DyNamic Tests on Single Piles (Table 1)

(1) Elkasabgy, M. and El Naggar, M.H. (2013). Dynamic response of vertically loaded helical and driven steel piles. Canadian Geotechnical Journal. Vol. 50. Pp. 521-535.

(2) Sakr, M. (2013). Comparison between high strain dynamic and static load tests of helical piles in cohesive soils. Soil Dynamic and Earthquake Engineering, Vol. 54, pp. 20-30.

(3) White, B., Alzawi, A., Bradka, T., Phang, Y. (2013). High Strain Dynamic Load Testing on Helical Piles - Case Study. Proceedings of 1st International Geotechnical Symposium on Helical Foundations: Amherst, MA; 336-346.

(4) Elkasabgy, M. and El Naggar, M.H. (2011). Field and theoretical dynamic response of vertically loaded helical and driven steel piles. *Proceedings of the 2011 Pan-Am CGS Geotechnical Conference*, GEO11Paper574, Toronto, ON, Canada, October 2-6, 2011.

(5) Elkasabgy, M. , El Naggar, M. H. and Sakr, M. (2010). Full-Scale Vertical and Horizontal Dynamic Testing of a double helix screw pile. Geo2010 – 63rd Canadian Geotechnical Conference in Calgary. September 12, 2010 – September 16, 2010. pp. 352-359.

(6) Buhler, R. and Cerato, A.B. (2010). Design of Dynamically Wind-Loaded Helical Piers for Small Wind Turbines. ASCE Journal of Performance of Constructed Facilities. Vol. 24, No. 4, pp. 417-426.

(7) Cerato, A.B. and Victor, R. (2009). Effects of Long-Term Dynamic Loading and Fluctuating Water Table on Helical Anchor Performance for Small Wind Tower Foundations. ASCE Journal of Performance of Constructed Facilities. Vol. 23, No. 4, pp. 251-261.

(8) Cerato, A.B. and Victor, R. (2008). Effects of Helical Anchor Geometry on Long-Term Performance for Small Wind Tower Foundations Subject to Dynamic Loads. The Journal of the Deep Foundations Institute (DFI), Vol. 2, pp. 30-41.

(9) Victor, R. and Cerato, A.B. (2008). Helical Anchors as Wind Tower Guyed Cable Foundations. Proceedings of the 2nd British Geotechnical Association (BGA) International Conference on Foundations. ICOF2008. . Brown M. J., Bransby M. F.,

Brennan A. J. and Knappett J. A. (Editors). Dundee, Scotland. June 24-27, 2008. Vol. 1, pp. 343-356.

(10) Cannon, J.G. (2000). "The Application of High Strain Dynamic Pile Testing to Screwed Steel Piles." Sixth International Conference on the Application of Stress-Wave Theory to Piles, S. Niyama and J. Beim eds., September 11-13, São Paulo, Brazil, pp. 393-398.

(11) Clemence, S.P. and Pepe, F.D. Jr. (1984). Measurement of Lateral Stress Around Multi-Helix Anchors in Sand. Geotechnical Testing Journal, Vol. 7, No. 3, pp. 145-152.

(12) Abdelghany, Y. and El Naggar, M.H. (2013). Innovative Seismic Resistant Helical Screw Piles (FRP-G-HSP – Fiber Reinforced Polymer Grouted and RG-HSP Reinforced Grouted Steel Fibers Novel System) . Proceedings of the 2013 Geo Montreal Conference, Montreal, Quebec, Canada, September 29 – October 3, 2013.

(13) Abdelghany, Y. and El Naggar, M.H. (2011). Steel Fibers Reinforced Grouted and Fiber Reinforced Polymer Grouted Screw Piles–An Innovative Deep Foundations Seismic Systems. Proceedings of the 2011 Pan-Am CGS Geotechnical Conference, GEO11Paper1043, Toronto, ON, Canada, October 2-6, 2011.

(14) Abdelghany, Y. and El Naggar, M.H. (2010 a). Monotonic and Cyclic Behavior of Helical Piles Under Axial and Lateral Loading. Proceedings of the Fifth International Conference on Recent Advances in Geotechnical Earthquake Engineering and Soil Dynamics, Ed. Prakash, S., San Diego, CA, May 24-29, SPL 4.

(15) Abdelghany, Y. and El Naggar, M.H. (2010b). Full-Scale Experimental Investigations & Numerical Analysis of Different Innovative Instrumented Helical Screw Piles Under Axial & Lateral Monotonic & Cyclic Loadings. Proceedings of the 63rd Canadian Geotechnical Conference.

(16) Abdelghany, Y. (2008). Monotonic and Cyclic Behaviour of Helical Screw Piles under Axial and Lateral Loading. *University of Western Ontario - Electronic Thesis and Dissertation Repository*

(17) Beim, J. and Luna, S.C. (2012). Results of Dynamic and Static Load Tests on Helical Piles in the Varved clay of Massachusetts. DFI Journal, Vol. 6, No. 1, pp. 58-67.

(18) El Sharnouby, Mahmoud Meckkey M. (2012) "Monotonic and Cyclic Behaviour of Steel Fibre-Reinforced and FRP-Steel Fibre-Reinforced Helical Pulldown

Micropiles." University of Western Ontario - Electronic Thesis and Dissertation Repository. Paper 902.

(19) El Sharnouby, M.M. and El Naggar, M.H. (2012). Axial monotonic and cyclic performance of fibre-reinforced polymer (FRP) – steel fibre-reinforced helical pulldown micropiles (FRP-RHPM). Canadian Geotechnical Journal. Vol. 49, pp. 1378-1392.

(20) El Sharnouby, M.M. and El Naggar, M.H. (2012). Field Investigation of Axial Monotonic and Cyclic Performance of Reinforced Helical Pulldown Micropiles. *Canadian Geotechnical Journal,* Vol. 49, pp.560-573.

(21) El Sharnouby, M.M. and El Naggar, M.H. (2011). Monotonic and Cyclic Axial Full-Scale Testing of Reinforced Helical Pulldown Micropiles. *Proceedings of the 2011 Pan-Am CGS Geotechnical Conference.* GEO11Paper336, Toronto, ON, Canada, October 2-6, 2011.

(22) El Naggar, M.H. and Abdelghany,Y. (2007). Seismic helical screw foundations systems. Proceedings of the 60th Canadian Geotechnical Conference, Ottawa, October 24-26, Paper 160.

(23) El Naggar, M.H. and Abdelghany, Y. (2007). Helical Screw Piles (HSP) Capacity for Axial Cyclic Loadings in Cohesive Soils. Proceedings of the 4th International Conference on Earthquake Geotechnical Engineering. June 25-28, Thessaloniki, Greece. Paper No. 1567.

(24) Dilley, L., Hulse, L. (2007). Foundation design of wind turbines in southwestern Alaska, a case study. *In Proceedings*, *Artic Energy Summit*, Anchorage, Alaska 15-18 October 2007. pp. 1-7. Institute of the North.

(25) Clemence, S.P. and Smithling, A.P. (1984). Dynamic uplift capacity of helical anchors in sand. Proceedings of the Fourth Australia - New Zealand Conference on Geomechanics, Perth, Western Australia, 14-18 May 1984, V1, pp. 88-93. Publ Barton: Inst of Engineers, 1984.

(26) Clemence S. P., and Smithling A.P. (1983) "Dynamic uplift capacity of helical anchors in sand," Civil Engineering for Practicing and Design Engineers 2(3): 345-367.

(27) Clemence, S.P. and Veesaert, C.J. (1977). Dynamic Pullout Resistance of Anchors in Sand. *Proceedings of the International Symposium on Soil-Structure Interaction*, Roorkee, pp. 389-397.

(28) Schiavon, J. (2016). Behavior of helical anchors subjected to cyclic loadings. *A Dissertation in partial fulfillment of the requirements of the degree.* Universidade de Sao Paulo, Sao Carlos, Brazil.

(29) Tsuha, C.H.C., Aoki, N., Rault, G., Thorel, L. and Garnier, J. (2007). Physical Modeling of Helical Pile Anchors. International Journal of Physical Modelling in Geotechnics. Vol. 4, pp. 1-12.

(30) Tsuha, C.H.C. and Aoki, N. (2010). Relationship between installation torque and uplift capacity of deep helical piles in sand. Canadian Geotechnical Journal, Vol. 47, pp. 635-647.

(31) Tsuha, C.H.C., Aoki, N. Rault, G., Thorel, L. and Garnier, J. (2012). Evaluation of the efficiencies of helical anchor plates in sand by centrifuge model tests. Canadian Geotechnical Journal. Vol. 49, pp. 1102-1114.

(32) Tsuha, C.H.C., Santos T. (2012). Effect of helix configuration in uplift load capacity of helical piles on tropical soil. Universidade de Sao Paulo. Escola de Engenharia de Sao Carlos, departamento de geotecnia. pp. 171.

(33) Tsuha, C.H.C., Santos T.C., Rault G, Thorel L., Garnier J. (2013). Influence of multiple helix configuration on the uplift capacity of helical anchors. *Proceedings of the 18th International conference on soil mechanics and geotechnical engineering*, Sep. 2013. Paris, France. pp. 2893-2896.

(34) Tsuha, C.H.C., Thorel L., Rault G. (2013). A review of centrifuge model tests of helical foundations. *Proceedings of 1st International Geotechnical Symposium on Helical Foundations.* August 8-10, 2013. International Society for Helical Foundations. Amherst, MA. pp. 1-24

(35) Tsuha, C.H.C., Thorel, L., Rault, G., and Garnier, J. (2013). Evaluation of the Effect of Installation on the Helical Pile Performance in Sand by Centrifuge Tests. Proceedings of the 1st International Symposium on Helical Foundations, pp. 308-319.

Lateral Cyclic/Dynamic Tests on Single Piles (Table 2)

(36) Abdelghany, Y. and El Naggar, M.H. (2013). Innovative Seismic Resistant Helical Screw Piles (FRP-G-HSP – Fiber Reinforced Polymer Grouted and RG-HSP Reinforced Grouted Steel Fibers Novel System). Proceedings of the 2013 Geo Montreal Conference, Montreal, Quebec, Canada, September 29 – October 3, 2013.

(37) Abdelghany, Y. and El Naggar, M.H. (2011). Steel Fibers Reinforced Grouted and Fiber Reinforced Polymer Grouted Screw Piles–An Innovative Deep Foundations Seismic Systems. Proceedings of the 2011 Pan-Am CGS Geotechnical Conference, GEO11Paper1043, Toronto, ON, Canada, October 2-6, 2011.

(38) Abdelghany, Y. and El Naggar, M.H. (2010a). Monotonic and Cyclic Behavior of Helical Piles Under Axial and Lateral Loading. Proceedings of the Fifth International Conference on Recent Advances in Geotechnical Earthquake Engineering and Soil Dynamics, Ed. Prakash, S., San Diego, CA, May 24-29, SPL 4.

(39) Abdelghany, Y. and El Naggar, M.H., (2010b). Full-Scale Experimental Investigations & Numerical Analysis of Different Innovative Instrumented Helical Screw Piles Under Axial & Lateral Monotonic & Cyclic Loadings. Proceedings of the 63rd Canadian Geotechnical Conference.

(40) Abdelghany, Y. (2008). Monotonic and Cyclic Behaviour of Helical Screw Piles under Axial and Lateral Loading. *University of Western Ontario - Electronic Thesis and Dissertation Repository*

(41) El Sharnouby, M.M. and El Naggar, M.H. (2013). Lateral Static and Cyclic Behavior of the Composite Steel-Fibre Reinforced Helical Pulldown Micropiles-Innovative Foundation Solutions for Seismic Applications. *Proceedings of the 21st Symposium of the Vancouver Geotechnical Society*, 6 pp.

(42) Elkasabgy, M., El Naggar, M. H. and Sakr, M. (2010). Full-Scale Vertical and Horizontal Dynamic Testing of a double helix screw pile. Geo2010 – 63rd Canadian Geotechnical Conference in Calgary. September 12, 2010 – September 16, 2010. p.p. 352-359.

(43) El Sharnouby, M.M. and El Naggar, M.H. (2011b). Monotonic and Cyclic Lateral Full-Scale Testing of Reinforced Helical Pulldown Micropiles. Proceedings of the 36th Annual Conference on Deep Foundations, 2011, Boston, MA, USA, (DFI)

(44) Prasad, Y.V.S.N, and Rao, S.N. (1994). Pullout behaviour of model pile and helical pile anchors subjected to lateral cyclic loading. *Canadian Geotechnical Journal*, 31(1), pp 110hnic.

(45) Rao, S. and Prasad, Y. (1993). ”Uplift Behavior of Pile Anchors Subjected to Lateral Cyclic Loading.” *Journal of Geotechnical Engineering*, 119(4), 786–790.

Table 1. Previous research considering <u>vertical</u> cyclic/dynamic loading of single helical piles

Ref	Pile Type	Vertical Load Test description	Soil	Results	Recommendations/Conclusion
1	Full scale 29'-6" by 12-3/4" OD double 24" helix (interhelix spacing of 36") helical and closed-ended steel driven piles	13 **dynamic**-quadratic tests (vertical harmonic motion) of different force intensities within a frequency range that covered the piles' resonant frequencies	Silt crust underlain by a layer of clay, underlain by sand and then clay till, respectively.	Helical pile's response manifested a reduction in the resonant frequency with an increase in the excitation intensity. The dynamic load was transferred to the surrounding soil medium through the interface resistance between pile shaft and soil. Using a linear approach, the theoretically calculated values of stiffness were found to be higher than the experimental results obtained 2 weeks after installation by 145% and by 62% to 88% for the helical piles tested 9 months after installation. The theoretical nonlinear analysis provided a reasonable estimation for the pile's response curves and impedance parameters due to the weak boundary zone considered around the pile.	The measured responses of the driven piles were significantly similar to those of helical piles tested 2 weeks after installation. There was a close agreement between measured and calculated response curves. An insignificant influence of the helices on load transfer mechanism was observed. This research demonstrated the ability of existing tools to model the dynamic behavior of helical piles.
2	4 full scale 29'6" by 12-3/4" single 24" helix helical piles 2 full scale 29'6" long or 19.7'by 12-3/4" driven piles	High strain Dynamic Testing (HSDT) and static compression loading	**Silt** over a silty **clay**	The static capacities obtained from CAPWAP were lower than the capacities established from static load tests (the delivered energy to helical piles during High Strain Dynamic Test (HSDT) was low and did not mobilize end-bearing resistance). Even more, CAPWAP analysis underestimated the axial static capacity and shaft resistance of helical piles using wave equation analysis. Helical piles provided about 230% to 290% higher capacities than driven piles with similar shaft diameter and	More research regarding HSDT of helical piles is recommended and more studies are needed for HSDT with different configurations (shaft diameter, helix size, and number of helices).

Ref	Pile Type	Vertical Load Test description	Soil	Results	Recommendations/Conclusion
				embedment depths (due to the use of single or multiple helix with diameters larger than the shaft diameter).	
3	3 full scale (50 ft long by 9-5/8" O.D.) helical piles: P1: double 20" helices, P2: double 22" helices, P 3: double 24"helices	The **High strain dynamic testing** (HSDT) used a protocol of 3 or 4 impacts ranging between 2" to 18" in height.	Sandy silt crust underlain by a layer of clay, underlain by silty sand and clay till.	The majority of the resistance (60%-75% under the highest energy impact) was from end bearing on the bottom helices, which was expected due to the hard clay layer at the tip elevation. 60%-70% of the shaft resistance was indicated to occur near the bottom of the pile based on the CAPWAP analysis. The soil profile indicated the presence of extremely hard clay at the tip elevation. It was assumed that failure occurred either by shearing of the soil plug between the helices or was affected by the upper helix.	The helical pile resistance exceeded the design load. HSDT is a viable, cost effective alternative to a traditional static load tests.
4, 5	Full scale, 29'-6" by 12-3/4" O.D. close ended, double 24" helix-helical pile	**Dynamic:** Of quadratic type; applied using a Lazan mechanical oscillator; with 5 force intensities, and with an intensity range that covered the resonance frequencies of the tested pile-soil-cap systems. A rectangular steel plate was the pile cap, then 59 circular steel	**Silt**, overlying layer of **clay** , followed by **sand** , and underneath it, **clay till.** A seismic cone penetration test was conducted to determine the dynamic	The maximum displacement was 0.01 inch at the center of gravity for the static mass. The linear approach highly overestimated both the stiffness and damping of the piles due to the assumed perfect bonding between the pile and soil. No variation in the stiffness and damping characteristics were observed for different excitation intensities, and the stiffness was not sensitive to frequency changes, especially at low frequencies.	The responses of driven piles were close to those of helical piles; therefore, their performance characteristics are similar for all the pile geometries considered. The nonlinear approach provided a reasonable estimation for impedance parameters and response curves, which confirmed the influence of soil disturbance due to pile installation process on the dynamic response of helical piles. The pile-soil separation length predicted by the nonlinear approach was 1.54 -1.85 times the shaft radius.

Ref	Pile Type	Vertical Load Test description	Soil	Results	Recommendations/Conclusion
		plates were added simulating a superstructure.	properties of the soil. Poison's ratio 0.4 to 0.47.	The damping coefficient of piles rapidly increased as the frequency approached zero. The damping ratios ranged from 6.85% to 7.57%. The vertical response for the adopted 5 excitation intensities was linear with clear resonance peaks. The resonance frequency was linear for the low excitation intensities as resonant frequency ranged from 37-38 Hz. The resonant frequency decreased from 37 to 35 Hz as the excitation intensity (defined as $m_e * e$, where m_e is the oscillator eccentric rotating mass and e is the eccentricity) increased from 0.87 to 1.52 lb-ft indicating a slight nonlinear response of the soil-pile system.	
6	7 full scale 10' by 1-3/4" (SS 175) square piles: 6 with triple 8-10-12" helices and 1 with double 8-10" helices.	Long term dynamic vertical: working load was applied first (2-4 kips) at 5 Hz and then shock wind loads were applied at 1 Hz. In two piles the difference between the maximum and minimum load was kept constant at 2 kips, maximizing the load span. Initially an 18-20 kips span, followed by 10-20, 2-10, 2-15 and 2-20 kips. Displacement was determined to be	Layered soil composed of a lean clay overlying layers of sand.	The dynamic span has a greater effect on a helical pile performance than the maximum load applied, for loads lower than 50% the predicted ultimate static uplift capacity. The capacity of two anchors with similar torque installation values and different water content (2% change) was not affected when the water table level was not changed and under the same loading and soil conditions. A three helix anchor performed better than the two helix anchor. Between the cylindrical shear, bearing plate, Helicap® and torque correlation	Large span dynamic loads will reduce uplift capacity of helical piles. Piles in soils with increased water content showed equal capacity to comparable piers in drier soils. Nevertheless, there is an indication of increased displacement at lower loads in increased water content conditions. More testing is necessary to determine the relationship between water content increase and helical pile performance. Fewer number of helices increase the possibility of local bearing capacity failure at each helix, based on a single 2 helix pier test.

Ref	Pile Type	Vertical Load Test description	Soil	Results	Recommendations/Conclusion
		stopped if over 30-s there was no variation. Failure was determined when at a constant load the anchor continued to displace.		methods to predict uplift capacities, Helicap® predicts the actual dynamic failure span magnitudes of dynamically loaded piles more closely. The torque correlation method exhibited more consistent results than the soil mechanics approaches and could be reduced by 3 to account for the dynamic loading effects.	It would be improbable to see significant movement in a single wind load event, piers could be monitored for displacement and the guy wires tightened over the lifetime of the tower to compensate for any movement.
7,8	8 Full scale, depths of embedment of: 10', 14', 16', 21.5', 23' and 25' by 1-3/4" Square shaft helical anchors. 3 with quadruple 8-10-12-14" helices, 2 with triple 8-10-12" helices and 3 with double 8-10" helices. All adjacent piles were spaced 5D of the largest helix with a minimum of 5 ft	A 1 year monitoring program was executed on a wind tower to determine loadings from working and extreme conditions. 5 anchors Cyclically/dynamically loaded in uplift for 2 to 4 weeks followed by a post-dynamic static test. 3 piles were only tested statically to compare their performance. Dynamic test were conducted under a sustained-repeated loading condition.	Layered soil composed by a lean clay overlying layers of sand, then silty clay and weathered shale, respectively	Wind vibrations occurred between 3 and 5 Hz, and average working loads were 1,000-3,000 lbs per guyed cable. The maximum load was on the south cable during a 50 mi/hr wind gust was 8,000 lbs. Depending on the soil type, the soil could fill the voids around the helices during dynamic loading, which would prevent the anchor from returning to its original position. A 3-helix anchor with a predicted capacity of 29,700 lbs performed well in minimizing long term creep, An anchor with a capacity of 30,000 lbs and FS of 2 experienced half of the total displacement during seating loads, nevertheless over 100% of the displacement was recovered after that the load was released. Even if there is disturbance during installation, once the anchor is cycled several times to a seating load there is	More tests are needed to confirm that the resistance to long term creep is more correlated to the number of helices than it is to the factor of safety. More tests are needed to confirm if a 2-helix does not have enough surface area to dissipate dynamic loads and are more susceptible to creep. Would be beneficial to test the effect of using larger helices to determine the general cyclic resistance. The optimum geometry to use on dynamically loaded guyed cable foundation is the 3-helix pile. All anchors showed movement during seating loadings due to installation disturbance of an inclined anchor. A dynamic anchor preloading program should be implemented to achieve the desired lifetime performance A rise of 13 ft in water table from below to above all the helices lowered the predicted anchor capacity, therefore all anchors

Ref	Pile Type	Vertical Load Test description	Soil	Results	Recommendations/Conclusion
		predicted ultimate uplift capacity and sustained for 10-15 minutes on the short term testing and 1-24 hours on the long term testing up to failure. **Dynamic** testing was long term and lasted for 2-4 weeks applied in a sustained-repeated loading condition.		capacity. The 4-helix has the lowest uplift capacity. For cyclic loading, the frequency used did not affect the load-versus time behavior, therefore a 10 Hz frequency could be used when constructing long-term load-displacement comparisons. After the dynamic testing was applied the static testing showed a higher ultimate capacity than the initially predicted.	
10	Full scale 26' by 3.5" with a single 14" helix & 6.6" OD with double or quintuplet 27.5" plates (Case 1), 26' by 8.6" OD with double 33.5" helices (square plate with rounded corners) (Case 2) and 8-16' by 3.5" with single 13.5" helix and 4.5" with 17.5" Square helix plates (Case 3).	High strain dynamic test (HSDT) that started with low blows, which then increased over time until shaft stresses reached yield stress. On case 2 a static load test was conducted after the dynamic test.	**Case 1**: moderate to medium sand. **Case 2**: clayey sand. **Case 3**: stiff clay	Case 1: The test was conducted at more than 2 times the working load. CAPWAP models show resistance concentrated at the helices locations. Results show considerable resistance and elasticity which persisted over a longer time. Case 2: Static and dynamic test passed the initial elastic behavior of the pile, the dynamic test mobilized more resistance and the test was limited only by stresses in the pile shaft Case 3: CAPWAP results demonstrated 120% to 170% of the required ultimate resistance, showing that a factor of safety of 2.5 was unnecessary. Suggested a factor of safety of 0.8.	Installation torque does not give a good indication of pile capacity (From testing of high capacity piles on Redlands Mater Hospital, Brisbane: where a pile was tested at two penetrations and the torque resistance was "quite" high during installation, and during testing it was very high with a corresponding low mobilized resistance), but high strain dynamic testing gave a better quantitative indication of pile resistance (the initial CAPWAP analysis found mobilized resistance close to the requirement, for half of the test. Results showed 120 to 170% of the required ultimate resistance from Case method approach). *Nevertheless, it is important to note that the helices had no true helical shape and they may no screw into the soil but rather auger, which could create certain disturbances

Ref	Pile Type	Vertical Load Test description	Soil	Results	Recommendations/Conclusion
11	One-quarter scale, 1.6" long by .375" square shaft (SS 126543 AE) with triple 2-2.5-2.75" helices	9 Dynamic tests applying uplift loads until failure was reached.	Sand	High horizontal stresses developed in the sand by vibratory densification or installation of the piles, produced an increase in the at-rest stress and lateral stress, for all the soil conditions studied. The magnitude of the increase in stress depends on the density of the sand. During the installation process the sand in contact with the helices was sheared and displaced laterally in the case of deep anchors (H/D >8), densifying the sand. In the case of shallow anchors, the sand is mobilized upward.	The coefficient of lateral earth pressure at failure were 30 and 40% lower than the values determined for buried foundations on previous research due to shear disturbance during installation. Further research is needed to determine the effect of anchor type, soil conditions and in-situ stress conditions before a comprehensive application of the coefficients can be established.
12, 13, 14, 15, 16	7 plain helical screw piles (P-HSP); 4 grouted (G-HSPs); 8 fiber reinforced polymer (FRP-G-HSPs); and 4 reinforced grouted (RG-HSPs)	Axial monotonic and cyclic: an initial compression test, then 15 cycles of axial loading with increments of 10 to 15% of the proposed design load with constant time intervals of 2.5 min. A final compression test.	Cohesive soil: Silt and clayey **silt** reaching a very dense **sand** at 30ft	RG-HSPs presented the highest axial ultimate compression capacity and stiffness of all different pile types tested under 15 cyclic loads. Pile axial compression capacities are proportional to the installation torque and the torque correlation factor can be used to predict the pile capacity of the P-HSP. The shaft resistance measured on G-HSPs was around 55% of the total pile's compression resistance and on P-HSP was 14% of the total pile-s compression resistance.	RG-HSPs presented higher axial compression capacities, therefore the shaft's reinforcement increased the axial capacity of the anchors and enhanced their axial seismic performance. A design equation was generated to predict the contribution of the inter-helix to the axial capacity of the pile, assuming a tapered shear failure surface developed in that zone. RG-HSP axial capacity was more than twice the P-HSP.

Ref	Pile Type	Vertical Load Test description	Soil	Results	Recommendations/Conclusion
17	8 full scale 13.5' (3 piles)-20' (5 piles) by 2-7/8" OD helical piles. Triple 8-10-12" helices with 2D spacing and 3" pitch.	**Cyclic** loading tests, after 25-30 days **static** loading tests were conducted, using increments of 5% the failure load, each kept	Clay	A CAPWAP analysis was performed, and the a dynamic loading test is a viable alternative to determine the compressive load capacity of Helical Piles embedded in cohesive soils, with lower cost and execution time. It is necessary to perform one or more load tests on each site to determine the best correlating factor (K_s), which depend on the particular pile size and configuration, as well as the type and condition of the soil.	Further investigation is needed to determine the failure criterion that should be adopted for Dynamic Loading Test (DLT) on helical piles. Agreement between Static Loading Tests (SLT) and DLT of helical piles embedded in cohesive soils was demonstrated. Further research is needed to evaluate SLT and DLT agreement in non-cohesive soils.
18, 19	13 steel fiber-Reinforced Helical Pulldown Micropiles (RHPM) and 12 full scale Fiber-Reinforced Polymer - steel-fiber Reinforced Helical Pulldown Micropiles (FRP-RHPM) of 2.25 inch of width (SS 225) triple-helix (10"-8"-6") helices spaced	PHASE I: An axial **monotonic** load was applied with increments of 6744 lbf every 4 min, then 15 one-way compression **cyclic loads** with a mean load of 43% of the ultimate capacity, and an amplitude of 13% of the ultimate capacity were applied. Finally loading up to a displacement of 1 inch. PHASE II: static loading to 67,443 lbf then **15** one-way compression loading **cycles** , and a	stiff clayey silt till underlain by dense sand	For RHPM piles it was found that the residual deformation after cyclic loadings were between 0.004 in to 0.012 inch. RHPM presented higher stiffness and resistance at all times than plain helical piles, but at higher displacement levels (0.79 in) RHPM had resistance of 180% to 250% those of plain helical piles. RHPM: At low displacement levels (1.3% shaft diameter), the shaft resistance was 72% to 80% of the total resistance, but as the displacement level increases (20% shaft diameter), the shaft resistance decreases to 36% to 50% of the total resistance. Nevertheless RHPM piles did not experience stiffness degradation during cyclic loading.	The top helix contributed more to the cyclic loading resistance than the other helices. Cyclic loading improve the pile's axial performance and capacity by up to 15%. The load transfer mechanism within the lead section is through bearing of each helix, and for piles under high static loads all helices have equal distribution of the applied load. More research is needed to examine the effect of higher cyclic loading range on the pile capacity and performance.

Ref	Pile Type	Vertical Load Test description	Soil	Results	Recommendations/Conclusion
	3D. Depth of the piles ranged between 24 ft to 24.6 ft and the grout column ranged between 11.14 ft to 12.8 ft. In addition, one regular 24' by 1-3/4" (SS175) and 5-1/2" OD (with 10" OD grout reinforcement in upper 10') by triple 8-10-12" helices spaced 3D.	final static loading until jacking was required to maintain loading/large displacement/ load cell capacity reached		FRP-RHPMs performed as a composite foundation system. Cyclic and post-cyclic performance of FRP-RHPM depends on the initial level of loading. If the cyclic loading range was below the maximum initial static load, the loading and unloading stiffness remains constant throughout the cyclic loading, and the displacement is relatively small and occurs within the first 1 or 2 cycles. Negligible permanent displacement was reported after the cyclic loading. Post-cyclic axial stiffness was not affected by the cyclic loading. Where the cyclic loading was higher than the maximum initial static loading: the pile performance was satisfactory, no degradation in stiffness was observed, and the displacement per cycle decreased with the number of cycles. For FRP-RHPM under post-cyclic static compression loads, the top helix share is more than 50%. It was observed that cyclic loading densifies the sand in the vicinity of the helices, reducing disturbance due to installation processes.	

Ref	Pile Type	Vertical Load Test description	Soil	Results	Recommendations/Conclusion
20	11 full scale 1-3/4" (SS175) Steel Fiber Reinforced Helical Pulldown Micropiles (RHPM) with a 6" grout column in upper 12' with triple 6-8-10" helices spaced 3D.	Stage I-A: **Monotonic** compression loads, increased by 6744 lbs every 4 min. Piles were tested up to a displacement of 8% of the average helix diameter. Stage I-B: 15 **Cyclic** one-way compression loading, each cycle applied for 2 mins, the maximum and minimum load of 130% and 70% of the average cyclic load (67,443 lbf)	stiff clayey silt till underlain by dense sand	The shaft contribution to the total resistance ranged from 72% to 80% at working levels and from 36% to 50% at higher loading levels. Furthermore, the load-transfer mechanism of the lead section is through individual helix bearing. The pile performance depends on the cyclic performance of the grout shaft. The displacement during cyclic loading was less than 1.77% of the shaft diameter with no degradation in the stiffness. An average and maximum cyclic loading of more than 40% and 54% of the ultimate capacity, improved the ultimate axial stiffness and axial capacity of the pile.	For cyclic loading applications, it is favorable to use multi-helix lead sections instead of a single helix. The RHPM pile is a viable foundation system for axial monotonic and one-way cyclic applications.
21	Full scale, 23-24.6' by 1-3/4" square (SS 175) plain and reinforced grouted helical pulldown micropiles (RG-HSP) with triple 8-10-12" helices with 3" pitch and located 6", 29" and 58" from pile tip.	Monotonic compression loading followed by a minimum of 15 - one way compression **cyclic** axial loading, each cycle over 2 minutes, and then an axial compression reloading was applied.	Lead section embedded entirely in the dense sand layer, while the grout column embedded within the silty clayey till.	The stiffness for all four reinforced helical pulldown micropiles was found to be higher than that of plain helical piles: The load at 0.8 inch deflection for a reinforced piles was 80 to 124% higher than the load of a plain pile subjected to the same deflection. The stiffness and capacity of the reinforced piles were not affected by the cyclic loading. The stiffness remained constant during cyclic loading up to failure (121,400 lbs) for plain helical piles. The maximum monotonic axial load reached at the end of the test for the	Under a cyclic loading of up to 58% of the ultimate load, the RG-HSP pile performs well, with no deterioration in their performance and only presented a small displacement increase. RG-HSP is a viable deep foundation option for axial monotonic and cyclic loading applications. The peak deflection observed on reinforced piles was 0.07%-0.23% of the grout column diameter.

Ref	Pile Type	Vertical Load Test description	Soil	Results	Recommendations/Conclusion
				reinforced piles was 137 to 155% higher than that of the plain pile.	
22, 23	Full scale 7' by 1-3/4" square (SS175) plain (P-HSP) and Grouted Helical screw pile (G-HSP) with triple 8-10-12" helices with 3" pitch and located 6", 29" and 58" from pile tip.	15 **Cyclic** compression loadings followed by a monotonic compression loading to failure	Layered cohesive-frictional soil, composed mainly of clayey **silt**	15 Cycles of loading reduced the ultimate capacity of plain helical piles by less than 5%-10%, and by 18% in grouted helical piles. The load was transferred to the soil in both helical pile types tested (plain HSP and grouted helical piles), mainly through a cylindrical shear failure surface over the inter-helices soil and by the bearing capacity of the lead helix. The grout column works with the helical pile on the load transfer interaction as a composite pile. For P-HSP's, the percentage of the load transferred from the shaft on the portion above the helices increased from 10% for a plain helical pile to 45% for a grouted column shaft above the helices.	The cyclic performance is satisfactory and permits the consideration of helical piles for seismic applications. The effect of cyclic loading on the stiffness of Plain and Grouted Helical piles are negligible
24	2 Full scale, 25' by 20" OD helical piles with a single 36" plate.	**Cyclic:** 6 uplift load tests were applied. The downward load applied on the reaction pile was equal to half the test load.	Frozen soils composed of silt and organics underlying a layer of silty sand. Temperature between 30.5°F to 31.8° F	The helical pile reaction stabilized out to zero displacement or creep, within 24 hours following each loading cycle. The total anchor displacement in upward movement accumulated up to 0.0093 inch to 0.0072 inch when unloading from 200% to 0% of the design load.	The test anchor performed well under all loads and the displacement was minimal or the pier capacity exceeded the test load applied.

Ref	Pile Type	Vertical Load Test description	Soil	Results	Recommendations/Conclusion
25, 26, 27	One-quarter scale 16" by 0.375" square (SS5, model number 126543AE) single 2.5" helix helical piles	Application of prestress load, then 12 **cyclic** loading test were transferred to the anchor through a system composed by a lever arm and a steel test container of 30" in diameter. A frequency of 6 Hz was used. A post cyclic static tension test was conducted.	Fine air-dried medium-dense Sand compacted to a density of 97.5 lb/ft^3	The anchor subjected to a larger displacement amplitude of 1/15" failed after 120 cycles, while the anchor with smaller displacement (1/37") failed after 1,200 cycles. The horizontal stress increases during installation and during the application of a static prestress load. This stress decreases during cyclic loading, indicating that the sand around the pile was loosened until the active state of stress was reached and the anchor failed. For prestressed anchors with a ratio of dynamic load /effective static load ratio greater than 3%, the anchor failed earlier than a similar anchor subjected only to cyclic loading.	An increase in displacement amplitude results in a shorter anchor life. A significant reduction in the static uplift capacity occurred after cyclic loading. At ratios of dynamic load/effective static capacity lower than 3%, a prestressed anchor reached failure later than a similar anchor subjected only to cyclic loading. However, for anchors with a ratio of dynamic load /effective static capacity above of 3%, the anchor reached failure sooner and a deterioration of the pile strength was observed.
28	**Test 1:** Model-scale with shaft diameters of 0.24", 0.31", 0.39" and 0.47" and shaft depth of 8.6". Single helix diameters of 0.79", 1.05", 1.3" and 1.6" **Test 2:** Full-scale helical piles with: 4" shaft diameter,	**Test 1:** Initial monotonic tensile load followed by a **Cyclic** loading through centrifuge acceleration applied to the helix of the model anchor, different acceleration levels were used for each pile. **Test 2: Cyclic** full scale test: Four series of uplift loads, each one involving a monotonic load	**Test 1:** Dry Dense fine silica sand **Test 2:** Clayey sand overlying a layer of pebbles and then clayey sand	**Test 1:** Before cyclic loading, the helix bearing resistance was 82% of the total applied load. The degradation on shaft resistance was more evident during the first 100 cycles, which was represented by accumulation of permanent displacements. Helical anchor presented vertical displacements greater than 10% of the helix diameter (D) after 1000 cycles, nevertheless the post-cycle uplift capacity did not presented degradation until it reached 2000 cycles. On the other hand, under low mean load, the accumulated displacement was lower	**Test 1:** Scaling issues on modeling helical piles have not been investigated before; the proposed solution consisted of conducting different pullout-tests on model-scale piles using the centrifuge to select an anchor model. The identified scaling effects are valid for models with effective helical radius/average grain size ratios greater than 58. Under cyclic loadings, the anchor behavior and failure mechanism depends on the disturbance produced during installation. Sand disturbance is not uniform along the cylindrical zone above the helices.

Ref	Pile Type	Vertical Load Test description	Soil	Results	Recommendations/Conclusion
	depth 8.4" by 0.18" OD; P7,P8,P9 = embedded depth 11" by 0.24" OD) and 3 pipe piles (embedded depths of 5.7", 8.4" and 11" and O.D. of 0.12", 0.18" and 0.24" respectively) **2nd Test**: 8 Full scale helical piles: embedment depth of 32.8' by 2.87" OD with single, double and triple helices of varying diameters		**Second test:** sandy clay (26.25'depth) overlying a residual soil and then a layer of pebbles	and the sand penetrated 2 or 3 times is significant. The efficiencies of the second plates of the tested anchors decrease with the increase in helix diameter, therefore the effect of the helical pile installation is more significant with anchors with larger helices. Strong influence of sand density in uplift capacity and installation torques. An increase in pile size and number of helices causes increases in the uplift capacities and installation torque. Ratio of measured displacement at failure to the helix diameter was larger in dense sand models and was not affected by the number of helices. The torque correlation factor decreases with an increase in pile dimensions and also with sand friction angle (increase in density). **Second test:** The uplift capacity of an anchor with tapered helices (6"-8"-10") was around 8% greater than that of an anchor with the same average plate diameter (8"-8"-8"). However, to install the tapered helical pile it was necessary to apply 20% greater torque.	**Second test:** The contribution of the second helix to the total capacity is better for tapered configurations. The contribution of the third helix to the total capacity decreases with an increase in the third helix diameter, even for tapered piles. Further investigation is needed to confirm.